DOE/BC/15047-1
(DE98000545)

IMPROVED EFFICIENCY OF MISCIBLE CO_2 FLOODS AND ENHANCED PROSPECTS FOR CO_2 FLOODING HETEROGENEOUS RESERVOIRS

Annual Report
June 1, 1997 – May 31, 1998

By
Reid B. Grigg
David S. Schechter

July 1998

Performed Under Contract No. DE-FG26-97BC15047

New Mexico Institute of Mining and Technology
Socorro, New Mexico 87801

National Petroleum Technology Office
U. S. DEPARTMENT OF ENERGY
Tulsa, Oklahoma

DISCLAIMER

Portions of this document may be illegible in electronic image products. Images are produced from the best available original document.

DOE/BC/15047-1
Distribution Category UC-122

Improved Efficiency of Miscible CO_2 Floods and Enhanced Prospects for CO_2 Flooding Heterogeneous Reservoirs

By
Reid B. Grigg
David S. Schechter

July 1998

Work Performed Under Contract DE-FG26-97BC15047

Prepared for
U.S. Department of Energy
Assistant Secretary for Fossil Energy

Jerry F. Casteel, Project Manager
National Petroleum Technology Office
P.O. Box 3628
Tulsa, OK 74101

Prepared by:
New Mexico Petroleum Research Center
New Mexico Institute of Mining and Technology
Socorro, NM 87801

TABLE OF CONTENTS

LIST OF TABLES

LIST OF FIGURES

ABSTRACT

The goal of this project is to improve the efficiency of miscible CO_2 floods and enhance the prospects for flooding heterogeneous reservoirs. This report provides results of the first year of the three-year project that will be exploring three principle areas:

- Fluid and matrix interactions (understanding the problems): interfacial tension (IFT), phase behavior, miscibility, capillary number, injectivity, wettability, and gravity drainage.
- Conformance control/sweep efficiency (solving the problems): reduction of mobility using foam, diversion by selective mobility reduction (SMR) using foam, improved injectivity, alternating water and gas injection, and using horizontal wells.
- Reservoir simulation for improved oil recovery (predicting results): gravity drainage, SMR, CO_2-foam flooding, IFT, injectivity profile, horizontal wells, and naturally fractured reservoirs.

The study of the effect of oil saturation on foam showed that in a single, relatively homogeneous core, CO_2-foam improves CO_2 breakthrough time and oil recovery. In composite core samples with two permeability regions parallel to the flow direction, the CO_2-foam systems significantly improved the CO_2 sweep efficiency in the low permeability region compared with similar runs when CO_2 alone was used. When foam was used as a displacing agent, breakthrough time of CO_2 was substantially delayed in the high permeability region in both isolated and communicating composite core systems. During oil displacement, foam improved sweep efficiency by a diversion of CO_2 from the high permeability to the low permeability region. A foam flood is more effective in assisting oil recovery in an isolated coaxial core system than in a capillary contact core system.

Mixed surfactant foaming agents were tested to see if mixtures were detrimental or synergistic when analyzing foaming properties, and as a prelude to the search for effective, inexpensive sacrificial agents to be used to satisfy reservoir rock adsorption requirements. Mixed systems were found that demonstrated substantial mobility reduction and favorable selective mobility reduction when coinjected with CO_2. A mixture of an anionic alpha olefin sulfonate and an anionic ethoxylated alcohol sulfate was tested that generated a more stable foam than its individual components. One mixture of a nonionic and an anionic surfactant was found to have better foaming stability, mobility reduction and SMR than the anionic surfactant alone.

Studies of surfactant foam quality were performed during this first year. The effect of CO_2 fraction on the total mobility of CO_2-brine (non-surfactant system) was inconclusive, but had an apparent minimum between CO_2 fractions of 0.333 and 0.667 and increased with increasing flow rate. The total mobility of CO_2-surfactant solution decreased with increasing foam quality and increased with increasing flow rate. Thus, the foam resistance factor increased with increasing foam quality and decreased with increasing flow rate.

Simulation studies on a foam pilot area resulted in an acceptable history match model. The simulated results of the foam test simulation were consistent with the foam pilot test results. The foam model was found to be adequate for field scale CO_2-foam simulation. The results confirm that the communication path between the foam injection well and a production well had a strong impact on the production performance.

A laboratory study to aid in the development of a gravity drainage reservoir was undertaken on the Wellman Unit. Reservoir performance, slim tube, large-diameter tube and gravity-stable corefloods in Wellman Unit whole core at reservoir conditions demonstrate excellent displacement efficiency with S_{or} after less than 10% CO_2. The MMP of Wellman Unit oil is 1600+/- 50 psig over a range of GORs from 150 to 600 scf/bbl. Reducing the pressure from above the MMP to near the MMP and below the MMP does not reduce efficiency in laboratory coreflooding. The data suggests the bottomhole pressure could be reduced from the current level of above 2000 psig to near the MMP of 1600 psig with no reduction in displacement efficiency. The reduction in CO_2 purchases would be a positive benefit from this strategy. The reduction in reservoir pressure, however, is constrained by voidage replacement issues. Gravity-stable coreflooding results, from transition zone core taken from the Wellman Unit, demonstrate that oil not mobilized by water influx in the transition zone can be effectively mobilized with CO_2 over a range of injection pressures.

Experiments were begun meant to duplicate situations of injectivity loss in WAG flooding and identify factors affecting the injectivity loss. Initially, four cores were tested. The preliminary results indicate that for a given rock the injectivity loss depends on oil saturation in the core during WAG flooding. The injectivity loss is higher in cores with high in-situ oil saturations during WAG flooding. This effect is being verified by more experimental data.

EXECUTIVE SUMMARY

During this first year of the current three-year project we examined the effect of selective mobility reduction (SMR) and oil saturation on several types of core, mobility reduction synergism of mixed surfactant systems, foam flood parameters, foam pilot modeling, CO_2 use reduction on a current CO_2 flood, and the cause and effect of injectivity problems in water alternating gas floods.

In examining the effect of oil saturation on foam we found that in a single, relatively homogeneous core, CO_2-foam slows CO_2 breakthrough time and improves oil recovery. In composite core samples with two permeability regions parallel to the flow direction, CO_2-foam systems significantly improved the CO_2 sweep efficiency in the low permeability region. Breakthrough time of CO_2 was substantially delayed in the high permeability region in both isolated and communicating composite core systems. Foam improved sweep efficiency by the diversion of CO_2 from the high permeability to the low permeability region. Finally, we found that a foam flood is more effective in assisting oil recovery in an isolated coaxial core system than in a capillary-contact core system.

Mixed surfactant foaming agents were tested to see if mixtures were detrimental or synergistic when analyzing foaming properties, and as a prelude to the search for effective, inexpensive sacrificial agents to be used to satisfy reservoir rock adsorption requirements. We found several promising systems. Systems were found that demonstrated substantial mobility reduction and favorable selective mobility reduction when coinjected with CO_2. A mixture of an anionic alpha olefin sulfonate and an anionic ethoxylated alcohol sulfate generated more stable foam than did its individual components. One mixture of a nonionic and an anionic surfactant was found to have better foaming stability, mobility reduction and SMR than the anionic surfactant alone.

The parameter of surfactant foam quality was studied during the first year. The effect of CO_2 fraction on the total mobility of CO_2-brine (non-surfactant system) had an apparent minimum and increased with increasing flow rate, but had much less of an effect than CO_2-surfactant. The system mobility of CO_2-surfactant solution decreased with increasing foam quality and increased with increasing flow rate. These effects have been incorporated into our foam model.

We feel confident that we can now predict foam behavior using reservoir simulation. Simulation studies on a foam pilot area resulted in an acceptable history match model. The simulated results of the foam test simulation were consistent with the foam pilot test results.

To determine the optimum flooding conditions and to predict the effect of flooding the water/oil transition region, a laboratory study to aid in the development of a gravity drainage reservoir was undertaken on the Wellman Unit. Reservoir performance, slim tube, large-diameter tube and gravity-stable corefloods in Wellman Unit whole core at reservoir conditions demonstrate excellent displacement efficiency with S_{or} after less than 10% CO_2 was injected. The data suggests current bottomhole pressure could be reduced from the current level of above 2000 psig to near the MMP of 1600 psig with no reduction in displacement efficiency. The reduction in CO_2 purchases would be a positive benefit from this strategy. The reduction in reservoir pressure, however, is constrained by voidage replacement issues. Gravity-stable coreflooding results, from transition zone core taken from the Wellman Unit, demonstrate that oil not mobilized by water influx in the transition zone can be effectively mobilized with CO_2 over a range of injection pressures.

Experiments were begun meant to duplicate situations of injectivity loss in the WAG flooding and identify factors affecting the injectivity loss. Initially, four cores have been tested. The preliminary results indicate that for a given rock the injectivity loss depends on oil saturation in the core during the WAG flooding. The injectivity loss is higher in cores with high in-situ oil saturations during WAG flooding. This effect is being verified by more experimental data.

BACKGROUND

The use of CO_2 as an injection fluid for oil recovery was initiated by the 1950s.[1,2] Today CO_2 flooding is considered one of the most promising techniques for improving oil recovery from oil reservoirs.[3-7] A number of research groups have studied mechanisms affecting performance of CO_2 injection, including phase behavior,[8-19] compositional effects,[20-24] and IFT.[24-32] However, it is unclear as to what constitutes the "optimum design" of CO_2 flooding. Thomas et al.[6] recently summarized the current situation of CO_2 miscible flooding as: "Depending upon where in the world one is implementing gas injection and to whom one is speaking, the post-mortem evaluations of 'miscible flooding' may vary from being very successful to 'miserable flooding'."

However, CO_2 injection has almost universally been a technical success. Now in the 90's, CO_2 injection in the U.S. is profitable in over 80% of the reported projects.[33,34] One reason that some CO_2 floods have underperformed is believed to be the lack of understanding of the mechanisms of CO_2-oil-rock interaction under flow conditions in oil reservoirs. Although CO_2 flooding has been studied for over forty years, most research has been focused on the effect of CO_2-oil phase behavior on oil recovery. It appears that there is a lack of understanding of the extent and the effect of heterogeneity in most oil reservoirs during the design of the CO_2 project. Therefore, it is unclear as to what constitutes the "optimum design" of CO_2 projects. This project is an investigation of how to effectively link theoretical and experimental aspects of heterogeneity to the performance of CO_2 floods.

Because of the importance of CO_2 flooding to future oil recovery in New Mexico and west Texas, the Petroleum Recovery Research Center (PRRC) maintains a vigorous experimental program in this area of research. The Department of Energy (DOE), the State of New Mexico, and a consortium of oil companies support this research.

This report summarizes work done during the first year of the second three-year project entitled "Improved Efficiency of Miscible CO_2 Floods and Enhanced Prospects for CO_2 Flooding Heterogeneous Reservoirs." The first three-year project[35-37] was based on encouraging results obtained from a previous laboratory project entitled "Improvement of CO_2 Flood Performance,"[38]

and a DOE-awarded grant for a CO_2-foam field demonstration that was a successful forerunner of DOE's Class I, II, and III Field Demonstration projects. This project was entitled "Field Verification of CO_2-Foam."[39]

Our studies in Selective Mobility Reduction (SMR) have progressed well. SMR is the property of CO_2-foam whereby mobility is reduced by a greater fraction in higher than in lower permeability zones and a property that promises to improve displacement efficiency in CO_2 floods by reducing the effects of reservoir heterogeneity.

We have been working on determining the optimum pressure for CO_2 flooding. A phase behavior database that concentrates on the effects of pressure, temperature, and fluid composition on the development of efficient CO_2 displacements under reservoir conditions is being developed. This information is being used directly to understand phase behavior in reservoir fluid CO_2 displacements and is also used to correlate IFT and capillary number under dynamic reservoir conditions. Phase behavior, IFT and capillary numbers are being used to predict miscibility and recovery in CO_2 displacement under reservoir conditions.

CO_2-foam coreflood tests continue and are being used to identify and quantify a number of variables in foam flooding; effects of flow rate, gas foam quality (gas volume fraction), and surfactant concentration. Foam and horizontal well models were developed, refined, and tested to verify the feature. The programming and testing of two reservoir simulators (MASTER -- Miscible Applied Simulation Techniques for Energy Recovery from the Department of Energy, and UTCOMP -- provided by the University of Texas at Austin) and the testing on a reservoir scale for the foam option were completed.

Multiphase flow behavior in fractured reservoirs is being investigated. Understanding the relationship of fluid flow and reservoir heterogeneity in fractured reservoirs is the key factor in developing a strategy of improving oil recovery in these reservoirs. A pendant drop apparatus for measuring IFT at reservoir conditions has been designed, built, modified, and tested. A new method, based on a static force balance on the lower half of the pendant drop used to calculate low IFT, has been developed and shown to work at low IFT.

A new mathematical model was developed to describe free-fall gravity drainage with equilibrium and non-equilibrium fluids based on Darcy's law and film flow theory. The new model

shows better accuracy than existing models for the 20 sets of experimental data examined. The ability to measure and predict IFT under reservoir conditions and to describe gravity drainage are necessary developments toward the goal of improving oil recovery in naturally fractured systems that previously have not been seriously considered for CO_2 flooding.

Finally, we have been aggressive in publication and dissemination of the results of our research. This has included quarterly reports and a number of publications during the first year[34,40-46] related to this project. Also, several papers have been accepted for presentation and publication in upcoming international meetings. In addition, we organized the second CO_2-Oil Recovery Forum that was held October 29-30, 1997. The two-day forum had 112 participants, representing 43 organizations.

We are pleased with the progress we have made. Even with the relatively low oil prices in recent years, most CO_2 field projects are considered economic successes,[33,34,47] with current projects and engineering for future projects commencing each year in the west Texas -- New Mexico area. In fact, CO_2 suppliers are drilling new CO_2 production wells, to increase available CO_2 for delivery, and plans are under way to increase current pipeline capacities. Also, other areas in North America, such as the Wyoming-to-Canada corridor and the Mississippi region, continue to consider extending the current pipeline networks to encompass wider areas. In the United States, CO_2 injection is the only significant improved oil recovery method that has resulted in increased yearly oil production, despite thirteen years of depressed oil prices.[47] CO_2 is a proven means to improve oil recovery and must be exploited to the fullest extent to increase national and individual company recoverable reserves.

There are many reservoirs that are not being considered for CO_2 or any type of improved oil recovery because of a low fracture pressure, poor injectivity, extreme heterogeneity, or fractures. In some CO_2 floods, sections are often shut in early because of gas channeling. It is more crucial than ever, that research organizations interact with operators concerning IOR techniques such as CO_2 injection to maximize domestic resources. Thus, the developments from our present project and the proposed extension of our project are an asset to the economic and strategic future of the United States of America.

PROGRAM OBJECTIVE AND STATEMENT OF WORK

The present project consists of an experimental research effort aimed at improving the effectiveness of CO_2 flooding in heterogeneous reservoirs. The intent is to investigate new concepts that can be applied by field operators within the next two to five years. The proposed activities will consist of experimental research in three closely related areas:

- Fluid and matrix interactions (understanding the problems): interfacial tension (IFT), phase behavior, development of miscibility, capillary number (Nc), wettability, gravity drainage, etc.
- Conformance control/sweep efficiency (solving the problems): reduction of mobility using foam, diversion by selective mobility reduction (SMR) using foam, improved injectivity, WAG, horizontal wells, etc.
- Reservoir simulation for improved oil recovery (predicting results): gravity drainage, SMR, CO_2-foam flooding, IFT, injectivity profile, horizontal wells, and naturally fractured reservoirs.

CO_2 FOAM AND SELECTIVE MOBILITY REDUCTION

Foam has a great potential for mobility control application for gaseous phases in heterogeneous reservoirs. Using carbon dioxide (CO_2)-foam for oil displacement can reduce or eliminate the frontal irregularities and minimize early breakthrough of CO_2 due to fingering or channeling phenomena. As a result, the displacement efficiency and ultimate oil recovery can be improved. In an earlier project, it was demonstrated that foam delayed gas breakthrough in a high permeability layer of a composite core when oil is not present. Last year, experiments were conducted with two types of composite cores, with and without capillary contact, in the presence of crude oil. The objective of this laboratory study was to demonstrate the foam impact on delaying gas breakthrough and improving oil recovery. CO_2-foam significantly improved CO_2 sweep efficiency in systems with and without capillary contact, in the presence of crude oil. The improvement was more pronounced in the system without capillary contact between parallel permeability regions.

In addition to this test, other laboratory tests were conducted to study the possibility of using mixed surfactants at low concentration to improve mobility control in CO_2 flooding. We examined various mixed surfactant systems, such as alpha olefin sulfonate and ethoxylated alcohol sulfate, through foam durability and flowing tests. Our preliminary results show that some mixed surfactants exhibit either comparable or better foam stability than the foam generated from the individual surfactants. In some cases, a substantial mobility reduction of CO_2 was observed when foam was generated with mixed surfactants at very low concentration. Other results in composite coreflood experiments indicated that foam improved oil recovery by reducing CO_2 in the higher permeability region. Detailed results are discussed in the following sections and some have been reported in recent conferences.[40-42]

CO_2-Foam Coreflooding Experiments

Introduction.

Viscous fingering, gravity override, and reservoir heterogeneity have long been known to be major problems in gas injection processes.[7,12,48,49] In a CO_2 flood, the large viscosity contrast

between the reservoir and injected fluids (dense CO_2 has a viscosity in a range of 0.03 to 0.08 cp) induces an unfavorable mobility ratio that results in early breakthrough and consequently decreases reservoir sweep efficiency. Several processes such as the injection of water alternating with gas (WAG),[50] direct CO_2 thickeners,[51] and surfactant solution alternating with gas (SAG)[52,53] are used to mitigate the sweep deficiency of CO_2 floods. Surfactant solution used at low concentrations (0.05wt% to 0.5wt%), in conjunction with CO_2, forms a foamy solution in porous media that reduces the mobility of the gaseous phase. This mobility reduction in heterogeneous rock can improve sweep efficiency, as reported by several investigators.[54-56]

Surfactant-based mobility control in CO_2 flooding is an effective way to mitigate problems normally associated with the miscible gas recovery processes. Earlier laboratory results[57,58] indicated that changes in flow and displacement behavior of CO_2-foam reduce the mobility of CO_2 and increase the displacement efficiency. CO_2-foam mobility measurements taken by several researchers[56,59-65] indicated that some surfactants generate smart foams, that is to say that the foam selectively reduces the mobility of CO_2 by a greater fraction in higher than in lower permeability cores. Since most occurrences of the selective mobility reduction (SMR) were observed in relatively homogeneous core samples, the question was raised whether this behavior also occurs in heterogeneous porous media, which would more closely simulate heterogeneity in reservoir formations.

Recent experiments conducted in our laboratory[41,54,60,66] confirmed that SMR indeed exists in composite core samples with two known regions of differing permeability in capillary contact. Where the differing permeability regions are parallel and in capillary contact, corefloods using the smart foam that has SMR properties demonstrated a substantial delay in CO_2 breakthrough in the higher permeability region. This delay in breakthrough time corrected the nonuniformity of the displacement front. However, these experiments were all conducted in core samples without oil present. To examine the effectiveness of foam in displacing oil in heterogeneous porous media, we conducted experiments on two composite core systems with a known heterogeneity. The first composite core system consisted of two coaxial permeability layers in capillary contact, as reported previously,[66] which allowed the crossflow of fluid between the two permeability regions. The second composite core system had the same configuration as the first one except that a barrier was embedded between two differing permeability regions. This barrier prevented flow communication between two

parallel zones, and therefore, simulated a layered-reservoir formation without the crossflow.

Experiments with relatively homogeneous permeability cores have shown the effect of foam on the reduction of mobility with and without oil present.[67,68] The presence of oil in porous media can be detrimental to foam formation and durability.[68-70] Surfactant properties play an important role on foam durability, especially when oil is present. A series of experiments in which foam is examined for its mobility reduction and effective oil recovery has been conducted both in a relatively homogeneous single core and composite core systems of two regions of differing permeability.

Laboratory experiments were conducted to examine the effect of foam with various fluid saturations in a single fired Berea sandstone core with relatively homogeneous permeability and two heterogeneous composite core systems (one with and one without capillary contact). This study indicates that foam could delay CO_2 breakthrough time and improve oil recovery efficiency in both single core and composite core experiments. Our results demonstrate that smart foam is useful in correcting nonuniform frontal displacement due to the heterogeneity of a reservoir formation. Smart foam is also very effective in displacing the oil—a benefit frequently overlooked by researchers testing the foam aspects of mobility control.

Experimental Description

A high-pressure coreflood apparatus was designed to conduct CO_2-foam experiments. The schematic diagram of the coreflood apparatus is shown in Fig. 1. The major components of the apparatus are two metering pumps, three Temco floating-piston accumulators, a wet test meter, a strip chart recorder, and a data acquisition system. A detailed description of the apparatus has been given in previous publications.[69,71,73] As indicated in Table 1, three different porous systems were used in these experiments. The fired Berea cores were epoxied and cast in stainless steel sleeves.

Two composite core systems were fabricated to simulate the heterogeneity of a reservoir formation. To simulate a communicating-layered formation system, a coaxial composite core was prepared. As described previously,[66] this core contained two different permeability zones that were in capillary contact. A 2.64 in. (6.7 cm) long, 1.4 in. (3.56 cm) diameter fired Berea sandstone core was coated with epoxy and cast in a stainless steel sleeve. A 0.625 in. (1.6 cm) central hole was then drilled end-to-end and filled with relatively uniform silica sand particles.

In the single core system, a downstream outlet conducts the fluids through a backpressure regulator (BPR), while in the composite system a special dual outlet end cap was designed to collect the effluent fluid separately from the center and annulus sections of the composite core. The composite core holder assembly has been previously described in detail.[71]

To simulate a noncommunicating-layered formation system, the annulus portion of core was first fabricated following the same procedure as in the first composite core system. A 0.875-in. (2.22-cm) central hole was then drilled end-to-end. An annular brass pipe (0.875 in. OD, 0.563 in. ID) was cast inside the annulus core as a barrier. Finally, another fired Berea sandstone core was coated with epoxy and cast in the center of the annular brass pipe.

During each experiment, the aqueous phase and high pressure CO_2 phase were injected into the system from floating-piston accumulators driven by distilled water, via a Temco injection pump and a Milton Roy pump, respectively. The input fluids were uniformly distributed to the inlet surfaces of two different permeability regions. The output flows from the two regions were separated by a circular barrier of the same diameter as the central zone of the composite core. Each of the two output regions had their own exit plumbing, each leading into a modified Temco BPR-50 backpressure regulator (BPR) in which the dome pressure was maintained at the test pressure (2100 psi). The two low-pressure liquid outputs from the BPRs flow into receiving flasks (low pressure separator), from which a gas stream at atmospheric pressure flow through a gas meter for volumetric measurements.

Tests are normally performed with a constant injection rate for either CO_2 alone, CO_2-brine (4:1 ratio), or CO_2-surfactant (4:1 ratio) at a typical Permian basin reservoir pressure and temperature (101°F and 2100 psig). Experiments were divided into two phases. In the first phase of experiments, the core samples were saturated with either brine or surfactant solution prior to injection of CO_2. In the second phase of experiments, the cores were saturated with crude oil to the residual water saturation prior to injection of CO_2. The crude oil was filtered Sulimar Queen dead oil with a density of 0.83 g/cc and viscosity of 2.9 cp at the test condition of 101°F and 2100 psi. Brine was a synthetic solution with a composition of 1.5 wt% NaCl and 0.5 wt% $CaCl_2$ in distilled water. The surfactant solution was prepared using the 2 wt% brine with Chase™ CD1045 surfactant at concentrations of either 500 ppm or 2500 ppm. The CD1045 was identified as one of the best mobility control foaming

agents in several other studies.[53,56,67] All the tests were conducted at a constant total injection rate for either CO_2 alone, CO_2-brine, or CO_2-surfactant with a volumetric ratio of 4:1 for the latter two. The brine permeability was measured prior to each run and followed by constant fluid injection of CO_2, CO_2-brine or CO_2-surfactant. CO_2 breakthrough time and incremental recovery were recorded for each run. The properties of the aqueous fluids are presented in Table 2.

Results and Discussion

The main objective in this study is to show the effect of foam on delaying CO_2 breakthrough time and its impact on the oil recovery. We have shown in our previous work[69,71] that CO_2-foam improves CO_2 breakthrough in composite cores with two permeability zones in capillary contact when oil is present. The detrimental effect of oil on foam has been reported by others.[68,70-75] However, to our knowledge, this adverse effect has never been examined in a heterogeneous system. In foam flooding, the presence of oil in the porous system may decrease the sweep efficiency or the fluid recovery if the mobility ratio between the displacing fluid and displaced fluid becomes more unfavorable. Since the viscosity of crude oil is generally greater than dense CO_2 or the combination of CO_2 and brine, foam is one means of alleviating such a problem. However, the stability of foam may decrease substantially when it comes into contact with oil. Two surfactant concentrations were used (500 ppm and 2500 ppm), one below and one well above the critical micelle concentration (e.g., CMC of the Chase™ CD1045 is about 700 ppm), to examine the stability of foam during the flooding experiment.

Experimental tests were conducted in three different core systems. The first system was a single, relatively homogeneous core, while the second and third systems were heterogeneous coaxial layers. The second was in isolation and the third was in capillary contact. Results from these experiments are presented in the following sections.

Single Core Test Results

A series of coreflood experiments were conducted in a single, relatively homogeneous core. The description of this core is given in Table 1. A summary of these experiments is tabulated in Table 3. A comparison of CO_2 breakthrough time, as pore volume (PV) injected, and oil recovery,

fraction of initial oil in place, have been made between runs of injected CO_2, CO_2-brine, or CO_2-surfactant, each with and without oil present.

The breakthrough times in several bar plots are presented, based on the time (or PV) that CO_2 emerged at the effluent. Figure 2 shows a comparison of the CO_2 breakthrough times among the four runs when crude oil was not present. In the first run, the core was saturated with brine solution and displaced with CO_2 at a constant rate of 16.00 cc/hr (1.2 ft/d). The breakthrough occurred after about 0.35 PV of CO_2 injected. In the next run, the core was resaturated with the brine solution and displaced with CO_2-brine (4:1 ratio) at a total constant rate of 16.45 cc/hr (1.3ft/d). The CO_2 breakthrough time was delayed about 2.5 min or about 4% PV injected. In the third tests, a 500-ppm CD1045 solution was used to resaturate the core. The core was flooded with CO_2 in this run at a constant rate of 16.00 cc/hr (1.2 ft/d). The pressure drop increased as foam formed in the core and the CO_2 breakthrough time was increased by a factor of more than two after 0.79 PV injected fluid. A similar result has been observed in our earlier work.[71] In the fourth run, the breakthrough was delayed even further, to 1.29 PV of total fluid injection, when CO_2-surfactant was used. The fourth and last experiments in this series indicated that the injection of surfactant solution and CO_2 into the surfactant saturated core maintained the foam. Notice that about 1.29 CO_2-surfactant PV injected before breakthrough occurred (80% CO_2 by volume was), while in the third run where CO_2 alone was injected, foam quality increased to the level that the foam bubbles collapsed and could not be reformed. The pressure drop profile in the third run indicated that the foam was destroyed after several PV of CO_2 was injected.

Figure 3 shows the second series of experiments conducted in the single core, runs 5 through 8 in Table 3. In this series, prior to each run, the core was saturated with the crude oil to near irreducible water saturation. The first run was a typical CO_2 core flood. The core was saturated with oil and displaced with CO_2 at the constant rate of 16.00 cc/hr (1.2 ft/d). CO_2 breakthrough occurred after about 17 min or 0.29 PV of CO_2 injected. In the second run, breakthrough time was increased about to 0.44 PV when CO_2-brine were coinjected, a 50% increase in breakthrough time. The breakthrough time was delayed further in the next two runs when surfactant solution was coinjected. The lower surfactant concentration (500 ppm) performed slightly better than the 2500 ppm solution. Figure 4 summarizes the two series of experiments with and without oil present. This bar plot

compares the breakthrough time in three sets of tests and clearly indicates the adverse effect of oil in CO_2 breakthrough time. The presence of oil enhanced the fingering phenomenon, whereas the WAG or SAG systems improved the CO_2 breakthrough time. This observation demonstrates the potential value that foam has for improving oil sweep efficiency.

Figures 5 and 6 are the plots of pore volume injected versus incremental recovery for the two series of runs with and without the presence of oil, respectively. The recovery curves for the surfactant solutions show an improvement in the liquid phase displaced from the core. Figure 5 shows that CO_2 had a poor recovery of 41% after about 0.82 PV of CO_2 injected. The system with the later breakthrough is an indication that the core was more efficiently swept. At about 2 PV fluid injected, CO_2 recovered over 76% of the oil while at the same PV injected, CO_2-brine and CO_2-surfactant at 500 ppm and 2500 ppm recovered 82%, 86%, and 85%, respectively. CO_2-surfactant at both concentrations (Fig. 6) shows a pistonlike displacement with oil present. Most of the oil was recovered after about three PV of CO_2-surfactant was injected. The recovery for CO_2-surfactant at 500 ppm and 2500 ppm concentrations were 95% and 90%, respectively (Fig. 6). We also observed in these tests (Figs 5 and 6) that CO_2 alone recovered more oil than CO_2-brine solution in runs 1 and 5 (Table 3).

The properties of the two composite core systems are tabulated in Table 1. The capillary contact core system simulates a communicating-layered formation, whereas the isolated coaxial core system simulates a noncommunicating-layered formation. The results and discussion in the following sections are based on the two types of composite core systems.

Isolated Coaxial Core System

Each experimental setup was first conducted in the core system without the presence of oil. Prior to the injection of CO_2, the core was either saturated with brine or surfactant solution. When CO_2, CO_2-brine or CO_2-surfactant was injected into the core, the breakthrough time of CO_2 in both regions were recorded and the results summarized in Table 4. In cases where no oil was present in the core, the unfavorable mobility ratio between CO_2 and the displaced fluid, accompanied by the heterogeneity, caused CO_2 to channel through the higher permeability region.

Breakthrough of CO_2 occurred earlier at 0.63 PV in the high permeability zone (annulus) than

at 1.13 PV in the low permeability zone (center) when CO_2 alone was used as a displacing agent. Coinjection of CO_2 and brine, simulating a quick and short cycle of WAG in the field, delayed CO_2 breakthrough only slightly to 0.64 PV in the high permeability region and 1.17 PV in the low permeability region. When surfactant was added to the brine, foam displacement significantly delayed CO_2 production in both regions. The breakthrough of CO_2 occurred at 1.12 PV in the high permeability region and 1.86 PV in the low permeability region. This successful use of surfactant to delay the production of CO_2 in the isolated coaxial composite core supports tests results reported previously for a capillary contact composite core.[12] The remaining question is, to what extent foam can assist CO_2 floods in the oil recovery processes. In a layered model theoretical study,[18] we demonstrated that the breakthrough time of the high permeability layer is delayed and the sweep efficiency of the model is improved if the mobility of the injected fluid is reduced.

To experimentally demonstrate the benefits of using foam in an oil recovery process, the three tests were rerun with a core that was saturated with crude oil to irreducible water prior to the injection of CO_2, CO_2-brine or CO_2-surfactant. The breakthrough times of CO_2 for both regions of the composite core in each run are summarized in Table 4. The results are generally in agreement with those obtained previously in cases where the core was not saturated with oil. In other words, when core was saturated with oil and displaced by CO_2 alone, a very early breakthrough of CO_2 occurred in the high permeability region (annulus) at 0.24 PV. As the mobility of the injected fluid was reduced by using CO_2-brine, the production of CO_2 in the annulus was not observed until 0.74 PV of total fluid was injected. In addition, no breakthrough of CO_2 was observed in the low permeability (center) region in these two cases before the end of the experiment, 15 PV of total fluid having been injected. CO_2 breakthrough occurred much earlier in the high permeability region, as compared with the case where brine was displaced instead of oil. This result indicates that unfavorable mobility ratio between CO_2 and oil causes a severe fingering or channeling of CO_2 in the high permeability region. When surfactant was added to the brine and coinjected with CO_2 into the core, production of CO_2 from the high permeability region was observed at 0.88 PV while substantial CO_2 production from the low permeability region started at 2.56 PV. The further delay of CO_2 breakthrough in the high permeability (annulus) region and production of CO_2 in the low permeability (center) region indicated that foam diverted part of the injected CO_2 from the high to the low

permeability region. Further evidence to support this assertion is presented in Fig. 7 where the cumulative gas oil ratio is plotted as a function of total pore volume of the fluid injected. In this plot, the highest cumulative GOR occurs in the high permeability (annulus) region when CO_2 is the only displacing agent. The cumulative GOR in the high permeability (annulus) region is reduced as brine is coinjected with CO_2.

When surfactant was coinjected with CO_2, foam was displaced through the core, substantially reducing the GOR in the annulus while detectable CO_2 was produced from the low permeability center region. This illustrates how foam reduces CO_2 channeling in a heterogeneous core and corrects the problem of nonuniformity in a displacement associated with the rock heterogeneity.

Oil production history from both regions of the composite core supports the fact that foam improves the displacement efficiency in each region and, as a consequence, foam displacement improves the total sweep efficiency. In Fig. 8, the oil recovery represents the amount of oil produced from the annulus as a fraction of the initial oil in place in that region. It is evident that the displacement efficiency in this region is improved, from 62% for CO_2 injection to 80% for CO_2-brine injection, and 95% for CO_2-foam injection after 15 PV of fluid was injected. Similar results are also presented in Fig. 9 where the final oil recovery increased in the low permeability center region 40%, 80%, and 95%, and the PV of CO_2, CO_2-brine and CO_2-foam injected to reach final recovery decreased to 8, 10, and 4 PV, respectively. The total oil recovery history presented in Fig. 10 summarizes the sweep efficiency of this composite core that was improved from 60% for CO_2 injection to 80% for CO_2-brine injection and 95% for CO_2-foam injection.

Communicating Coaxial Composite Core System

A summary of the composite core properties is given in Table 1. A series of CO_2, CO_2-brine, and CO_2-foam experiments were conducted in a composite coaxial system having two regions of differing permeability. These runs are summarized in Table 5. The first series (two tests) were performed with no oil present. The crude oil was introduced in the second series of these runs, tests 3 through 5. The importance of the composite system is that the effect of heterogeneity on the foam performance can be examined along with other parameters. Experiments with composite core samples provide information that cannot be acquired from individual single cores of relatively uniform

permeability.[69,76]

Figures 11 through 13 show CO_2 breakthrough times as the function of PV injected in the form of bar plots for the two permeability regions, high (annulus) and low (center). Figure 11 shows the two runs in the absence of oil (CO_2-brine and CO_2-surfactant). The surfactant solution used in these tests had a concentration of 2500 ppm. In the first run, CO_2 breakthrough occurred in the higher permeability region (annulus) after 0.42 PV of CO_2-brine was injected and in the lower permeability region after 0.62 PV. In the second run, as indicated in Fig. 11, CO_2-foam improved the breakthrough time significantly in the high permeability region. In this run, breakthrough occurred in the high and low permeability regions at 0.66 and 0.61 PV of CO_2-surfactant injected, respectively. This shows that selective mobility reduction (SMR) occurred and effectively reduced CO_2 mobility. SMR could have a great impact on improving oil recovery efficiency if it occurs in a reservoir. In Fig. 12, each bar represents the CO_2 breakthrough as a function of PV injected for either the high permeability (annulus) or the low permeability (center) regions. Prior to each run, the composite core was saturated with Sulimar Queen crude oil until brine production stopped. In the first experiment, CO_2 displaced the oil from both regions of high and low permeability. Breakthrough occurred about three minutes earlier (or 0.06 less PV injected) in the high permeability zone. Breakthrough time increased in the next run when CO_2-brine was used as the displacing fluid. The final run, using CO_2-foam, improved the breakthrough time in the high permeability region significantly. This foam behavior indicates of a favorable mobility reduction in which the mobility of CO_2 was reduced more in the high than in the low permeability zone. Figure 13 compares the five runs and shows the variations of PV injected in each run. This plot shows that CO_2-foam improved the breakthrough time more in the high permeability region.

The incremental oil recovery for the three composite core runs (run # 3, 4, and 5) are plotted in Figs. 14 and 15 as a function of total PV injected in both high (annulus) and low (center) permeability regions. Oil recoveries in the plots are in terms of the amount of oil produced in each region as fraction of the total original oil in the system. Figure 14 compares the oil recovery for the CO_2, CO_2-brine, and CO_2-foam runs in the high permeability region (annulus). The CO_2 and CO_2-brine curves show a better recovery efficiency than the recovery curve for the CO_2-foam. The CO_2-foam in this plot shows a recovery of about 22% from the high permeability region at almost 4 PV

(e.g., total PV for the composite core) of the CO_2-foam injected. The oil recovery for the CO_2 and CO_2-brine at the same injected PV, were about 38% and 68%, respectively. When foam was injected, oil recovery from the low permeability center region shows a significant improvement (summarized Fig. 15). This result indicates that foam recovered much more oil compared with the recovery curve, at 2 PV of injecting only CO_2. The oil recovery also improved over CO_2 only injection when CO_2-brine (run # 4) was injected. The 70% oil recovery from the center for the CO_2-foam was more than the original oil in the center. This indicates foam in the high permeability region had cross-flow, diverting oil into the low permeability region.

Figures 16 through 20 show the oil recovery curves as the function of total PV injected for both high and low permeability regions in each individual run. The two curves in Figs. 16 and 17 compare the water (brine and surfactant solution) recovery in both regions at a given PV injected. In Fig. 18, the oil recoveries for the high and low permeability regions at two PV of CO_2 injected are 13% and 31%, respectively. Similarly, in Fig. 19 the oil recoveries for the high and low permeability regions at two PV of CO_2-brine injected are 22% and 60%, respectively. Compared to the CO_2 curves in Fig. 18, the curves in Fig. 19 show significant increases for the low and high permeability regions, respectively. In the CO_2-foam run (Fig. 20), the oil recovery from the low permeability region is about 70% at two PV of CO_2-surfactant injected. A comparison of these curves with the CO_2 recovery curves (Fig. 18) indicates an increase of over five times the amount of oil recovered from the low permeability region. In fact, there was more oil recovered from the center than was originally in place in the center volume. The center of the core amounted to about 18% of the pore volume of the system. At the same time, there was a decrease in oil recovery from the high permeability region to only about 20% of the oil. This would have to be expected if 70% of the oil was produced through the center, leaving only 30% maximum that could be produced through the annulus.

Total oil recovery from the high and low permeability regions are plotted in Fig. 21. These curves compare the total oil recovery between runs 3 through 5. Breakthrough values are found in Table 5. In the plots shown in Fig. 21, CO_2-brine and CO_2 -foam curves show a better recovery efficiency than CO_2 alone. The significant increase in oil recovery from the low permeability zone shows that foam is capable of diverting displacing fluid from a high to a low permeability region to

recover oil. A similar test study in a longer core sample, in which the residual oil will be displaced with CO_2-foam, is underway. More tests will be conducted to help understand how surfactants behave and under what conditions they are most effective.

Using these composite core systems allowed us to evaluate the effects of heterogeneity on the flow behavior of CO_2, CO_2-brine, and CO_2-foam. In addition, when oil was present in the core system, we observed that CO_2 breakthrough and oil recovery efficiency were improved by using smart foam. The breakthrough times of CO_2 from each region of the composite core are summarized in Table 6. The first two tests were performed with no oil present inside the core. When CO_2 and brine were coinjected into the core, production of CO_2 started at 0.42 PV in the high permeability (annulus) region and 0.62 PV in the low permeability (center) region. When surfactant was used to generate foam in the next test, no production of CO_2 in the annulus was observed until 0.66 PV of total fluid was injected. The production of CO_2 in the low permeability region, however, occurs slightly earlier at 0.61 PV. The flowing behavior of CO_2 in these two zones indicates a possible effect of selective mobility reduction as a result of foam displacement. In fact, mobility of displacing fluid in the low permeability region was reduced from 123 to 12.7 md/cp and it was reduced from 287 to 1.7 md/cp in the high permeability region. A significant selective mobility reduction (SMR) behavior was observed in this case.

To examine the effectiveness of foam on oil recovery, three tests were performed on a core that was saturated with the crude oil. The first test was performed using CO_2 as the displacing agent. As expected, the CO_2 breakthrough occurred earlier in the annulus region at 0.44 PV than in the center region at 0.50 PV. Using CO_2-brine to displace the oil resulted in a slight delay of CO_2 breakthrough in both regions. However, when foam was used to displace the oil, a significant delay in breakthrough time in the annulus region and an earlier breakthrough in the center region were observed. As shown in Fig. 22, the cumulative GOR increases substantially in the center region when foam is used as a displacing agent. This indicates that foam assists in correcting the nonuniform displacement normally associated with heterogeneity.

The oil production history plotted in Fig. 23 shows that after 4 PV of total fluid was injected, the sweep efficiency was improved from 49% for CO_2 injection to 92% for CO_2-brine injection and a lower 88% for CO_2-foam injection. Using foam is less effective in improving sweep efficiency, as

compared with CO_2-brine. This was probably because most of the displaced fluid was diverted into the center region, which had a much smaller pore volume containing a small portion of recoverable oil. The performance of foam in oil recovery should have improved if the target (low permeability) zone contained most of the original oil in place, or the high permeability zone was swept before introducing foam. In other words, if we conducted the experiments on a composite core that has a low permeability region with a high portion of recoverable oil, high recovery would be expected as a result of using foam in the oil displacement.

The results presented here are based on our preliminary study. We plan to continue similar experiments by changing parameters such as permeability contrast between two zones, the layout of the different permeability zones, core length, and oil saturation. Nevertheless, our preliminary results show that the delay of CO_2 breakthrough in the high permeability region is a favorable indication that suggests that, when surfactant solution is used with CO_2 to form CO_2-foam, oil displacement is more efficient. Substantial reduction of CO_2 mobility in higher permeability regions or diversion of CO_2 from high permeability to low permeability regions helps improve the sweep efficiency. At the tested conditions, although the results show that foam is more effective in assisting oil recovery in the isolated coaxial core system than in the capillary contact core system, results from both systems indicate the potential of using foam for improvement of oil recovery in heterogeneous porous media.

Use of Mixed Surfactants in CO_2 Foam Experiments

Introduction

The use of a single surfactant system to reduce CO_2 mobility was reported in a number of publications.[53,56,61,63-65,77-81] Reported surfactants include ethoxylated alcohols, sulfate and sulfonate esters of ethoxylated linear alcohols, alkyphenol ethoxylates, and low molecular weight ethylene oxide-propylene oxide copolymers. At concentrations of less than 0.1 wt%, most surfactants lower the mobility of miscible gas, though high surfactant concentrations are usually preferred in foam application to assure the stability of the foam during displacement. To stabilize the foam bubbles, some researchers have proposed using a mixed surfactant system to enhance foaming properties. Sharma *et al.*[82] found that mixed surfactants affect the surface properties of the surfactant, and that when two components of the surfactant system had the same chain length, the performance of foam

in displacement was optimized. In experiments described by Llave *et al.*,[83] foam generated by a mixed surfactant formulation was reported to exhibit a comparable or better stability than the foams generated using an individual surfactant. Although synergetic mechanisms of using mixed surfactant to enhance foam properties are not well understood, both reports suggest a possibility of using mixed surfactants at lower concentrations to stabilize the foam.

Using low concentrations of mixed surfactants to generate foam has at least two benefits in foam application: it can reduce the cost of surfactant and minimize possible injectivity problems associated with the foam injection. To explore the possibility of using low concentration of surfactants in foam application, we extend our previous study[54] to assess mixed surfactant systems for mobility control. The evaluation procedures include tests on foaming ability and stability in foam durability tests, and mobility measurements of CO_2 with mixed surfactants in foam flowing tests. A composite core system is used in these foam flowing tests. The results are examined to investigate the dependence of mobility reduction on rock permeability or selective mobility reduction (SMR), which is an important characteristic of foam to preserve the uniform displacement in a heterogeneous porous media.

Foam Durability Test

A schematic of the foam durability test apparatus is shown in Fig. 24. This high-pressure foam durability test apparatus was used to determine the properties of individual surfactant, mixed surfactants (such as the interfacial tension between surfactant and dense CO_2), and properties of foam generated by these surfactants (such as the foaming ability and stability). The apparatus consists of a CO_2 source tank, a visual cell made from a transparent sapphire tube, a buffer solution cylinder, and a Ruska pump. A major part of this system, the CO_2 tank and the sapphire tube high-pressure cell, is contained in a temperature-controlled water bath. The buffer solution cylinder as well as the Ruska pump are installed outside the water bath, and their temperatures are maintained at the test temperature through another temperature control system.

During operation, the sapphire visual cell is first filled with the solution to be tested. Once the system is brought to the desired pressure by means of the Ruska pump, the dense CO_2 is introduced through a needle at the lower end of the cell. The CO_2 is drawn upward inside the cell when the

Ruska pump is in a withdrawing process. Because of the density difference between dense CO_2 and tested solution, CO_2 bubbles are formed and collected at the upper end of the cell. Depending on the effectiveness of the surfactant, these bubbles will then either form a layer of foamlike dispersion at the top of the sapphire tube or coalesce into a clear layer of dense CO_2. After a standard volume of CO_2 (1.75 cc) has been introduced into the sapphire tube, the pump is stopped and the volume of foam versus time it is measured.

Surfactants tested with this apparatus are described in Table 7. Different batches of individual surfactant solution (each at 0.05 wt% active component) were prepared by dissolving the surfactant as received from the suppliers into a brine system consisting of 5.6 wt% NaCl and 1.4 wt% $CaCl_2$. The mixed surfactant solutions were subsequently prepared by mixing two of the surfactants listed in the Table 7, each at an equal amount, to make a final total concentration of 0.05 wt%. The screening tests on four individuals and six mixed surfactant systems were then conducted at 77 °F and 2000 psig.

Results and Discussion.

Table 8 summarized the results of interfacial tension (IFT) between CO_2 and different surfactant systems. In the single surfactant systems, the IFTs decrease with the surfactant concentration. In the mixed surfactant systems, the IFTs show no significant reduction as a result of mixing between two individual surfactants. However, some of the mixed surfactants perform better in foaming and stabilizing the bubbles than the individual foaming agents.

Figure 25 presents the results of static decay of the CO_2-foam using either single surfactant or mixed surfactant systems. The percentage of foam in the graph indicates the persistence of foam remaining inside the sapphire cell after a standard volume of CO_2 has been bubbled through the surfactant solution. Of single surfactant systems tested, the bubbles formed by surfactants Dowfax 8390 and CD1040 coalesced in less than a minute, whereas bubbles formed by surfactants CD128 and CD1050 lasted 30 and over 90 minutes, respectively. Of mixed surfactant systems tested, bubbles formed by CS4090 (CD1040+Dowfax 8390) coalesced in less than a minute while bubbles formed by other mixed systems lasted at least five minutes. The effectiveness of surfactant in stabilizing the foam bubbles as determined by this method demonstrated that, at 0.05 wt%, Chaser™ CD1050

generates the most stable foams, followed by mixed surfactants CS4050 (CD1040+CD1050), CS2850 (CD128+CD1050), CS2840 (CD128+CD1040), Alipa® CD128, CS5090 (CD1050+Dowfax 8390), CS2890 (CD128+Dowfax 8390), CS4090 (CD1040+Dowfax 8390), Chaser™ CD1040, and Dowfax™ 8390. For these results, mixtures of nonionic and anionic surfactant performed better than each individual anionic surfactant, but slightly worse than the nonionic surfactant alone. When two anionic surfactants were mixed, however, only a mixture of alpha olefin sulfonate (CD1040) and ethoxylated alcohol sulfate (CD128) performs better than either surfactant alone.

Foam Mobility Test

To assess flowing foam properties in a heterogeneous porous media, core systems containing well defined high and low permeability regions were constructed and arranged in series in the flow system. The composite core system in this study consists of two cores of 0.5 in. diameter, each about 3 in. long. The two abutting end faces of the cores are carefully cut perpendicular to their axes and are ground flat prior to mounting them end-to-end. In such an assembly, the unavoidable space between the two core faces is filled with fine sand. Three pairs of pressure taps are mounted along the core-holder, defining three segments of the composite rock. The experiment yields records of three pressure differences, between each pair of successive pressure taps. A sketch of such a composite core is presented in the bottom of Fig. 26.

A schematic of the high-pressure mobility measurement system is also presented in Fig. 26. In this flow system, the fluids flowing into a foam generator and the composite core are injected by two pumps (a Ruska positive displacement pump for the CO_2 and an ISCO piston pump for brine or surfactant solution). System pressure is maintained almost constant by leading the output fluids into a backwards-running ISCO pump, which takes in the output at the total rates of the other two pumps. When the experimental conditions reach steady state, pressure drops in each segment of core are recorded as a function of time. The mobility of injected fluid, defined as the ratio of Darcy or superficial velocity of the fluid to the average pressure gradient along each segment of core, is calculated and compared at different injection rates.

As a standard procedure, the foam generator and core sample were first flushed with at least 50 PV of synthetic brine before starting the brine permeability measurements. The heterogeneity of

the series composite core was determined by measuring the brine permeabilities for three different sections along the core. Following the permeability measurements, dense CO_2 and brine were simultaneously injected into the core sample. The mobility of this two-phase mixture was measured for each core section and used as a reference for later comparison. After establishing the baseline, foam experiments were performed. The surfactant adsorption requirement was satisfied by displacing 50 PV of surfactant solution through the core. Then CO_2 and surfactant solution were coinjected into the core until steady state was reached and foam mobility was measured. Finally the core was flushed with another 50 PV of brine. During the coinjection of CO_2 and brine or CO_2 and surfactant solution, the ratio of the volumetric flow rate of CO_2 to aqueous phase was maintained at 4:1. The total injection rate, however, was varied from 5.0 cc/hr to 15 cc/hr, which corresponds to Darcy velocities of 3.1 ft/D to 9.4 ft/D. All the mobility measurements were conducted at 77°F and 2000 psig. The composite core used in the experiments had permeabilities ranging from 550 md to 270 md.

Results and Discussion.

A typical pressure drop profile during foam flowing tests is presented in Fig. 27. In this graph, the pressure drop increases as the foam front passes through each segment of core. The pressure drop normally becomes stable by 2 PV of injected foam when the single-surfactant system is used. With mixed surfactant systems, the pressure drop usually stabilized by 3 PV of injected fluid (see Figs. 28 and 29). When using a mixed surfactant system, multiple foam fronts were sometime observed during foam displacement. Figure 29 presents such a case, of two distinct foam fronts that were found to propagate through the whole core during the flowing test. It is not clear whether this behavior is related to propagation of surfactant or is simply a synergetic mechanism for this mixed surfactant system.

Normally, after about 5 PV of total injected fluid, the steady state was well established; 100 pressure-drop data points in each segment of core were recorded and the average value was used to estimate the mobility of injected fluid. Mobility data of the single-surfactant and mixed-surfactant systems are tabulated in Tables 9 and 10, respectively. Also included in these tables are slope values that indicate how favorable the SMR is in each case. The interpretation of these slope values will be discussed later. Comparison of the mobility data in the tables shows that adding surfactant effectively

reduces the mobility of CO_2-brine. The extent of this mobility reduction varies with the surfactant system and flow conditions. When the performance of mixed-surfactant systems is examined, again, as with the single-surfactant system, mobility reduction is related to the foam stability of mixed surfactants. In other words, the flowing properties of foam correlate well with the properties of static foam in foam durability tests. Mobility reduction is enhanced as foam stability increases.

When the mobility dependence on rock permeability is examined, SMR is found to exist in mixed-surfactant systems. The results of mobility dependence on rock permeability in a series composite core are presented in Fig. 30. On this log-log scale plot, the mobility of CO_2-brine or CO_2-foam is plotted against the sectional permeability. Also included in this plot are values determined by regression based on each set of data points. The numerical value, representing the slope of each line of each set of data, is used to indicate how favorable the mobility dependence of fluid is to the permeability of porous media. A slope of one indicates that the mobility of the fluid is proportional to the rock permeability as described in Darcy's law. A value of less than one shows a favorable SMR, which will lead to a more uniform displacement front when the fluid is flowing through heterogeneous porous media. We observed that the slope of CO_2-brine data is greater than one, indicating that unfavorable mobility dependence occurs when CO_2 and brine are flowing in a heterogeneous porous media. The results in the same graph also show that foam can correct this problem by reducing the mobility of CO_2 and by changing the mobility more at higher permeability (*i.e.*, when surfactant is added to brine and generates foam, the slope of foam mobility versus rock permeability data becomes less than that of CO_2-brine, and preferably less than one).

Of the six mixed surfactants tested, the slope values vary considerably: 1.16 for CS4090, 1.12 for CS 2890, 0.98 for CS5090, 0.86 for CS2840, 0.64 for CS4050 and 0.58 for CS2850. Although some of the slope values are greater than one, the values are less than the 1.24 found for CO_2-brine for this system, indicating that foam has corrected the dependence of CO_2 on rock permeability in a favorable direction. This favorable trend is also tied in with how effectively the mixed surfactant stabilized the foam. When we compared the effectiveness of using a mixed-surfactant system with that of using a single surfactant alone in foam displacement, we found mixed nonionic and anionic surfactants perform better than an anionic surfactant alone. Figure 31 presents some of the mobility data by using nonionic surfactant CD1050, anionic surfactant CD128 and the mixture, CS2850. As shown on this

graph, the mobility of using CS2850 at 0.05 wt% is comparable to that of using CD1050 alone and much lower than that of using CD128 alone at the same concentration. Furthermore, more favorable SMR, 0.58, is also observed with CS2850 compared to 0.80 for CD128 and 0.59 for CD1050, respectively.

The favorable results in flowing tests lead us to believe that low concentrations of mixed-surfactant systems can be used to improve the CO_2 mobility. In addition, foam can correct the nonuniform flow of CO_2 and brine in a porous system consisting of differing permeabilities. The noticeable effect of using mixed nonionic and anionic surfactant in mobility improvement provides an alternates in selecting surfactants for foam application in different types of reservoirs. Since an anionic surfactant normally has less adsorption in a sandstone reservoir than in a carbonate reservoir, careful selection of a suitable mixed-surfactant system for a particular reservoir can minimize surfactant loss and preserve the effectiveness of foam for mobility control.

Conclusions

1. In a single, relatively homogeneous core, CO_2-foam (CD1045 at 500 ppm and 2500 ppm concentration) improves CO_2 breakthrough time and oil recovery.
2. The experimental results from composite core samples with two permeability regions parallel to the flow direction led to the following observations and conclusions:
   a. The CO_2-foam systems significantly improved the CO_2 sweep efficiency in the low permeability region compared with similar runs when CO_2 alone was used.
   b. Breakthrough time of CO_2 was substantially delayed in the high permeability region in both composite core systems (isolated and communicating cores) when foam was used as a displacing agent.
   c. Foam improved sweep efficiency during oil displacement. This improved efficiency results either from a more substantial reduction of CO_2 in the higher permeability region or a diversion of CO_2 from the high permeability to the low permeability region.
   d. A foam flood is more effective in assisting oil recovery in an isolated coaxial core system than in a capillary contact core system.

3. The experimental results from composite core samples having two permeability regions in series with respect to the flow direction, and from testing mixed surfactant systems as foaming agents led to the following observations and conclusions:

   a. Substantial mobility reduction and favorable selective mobility reduction are observed when mixed surfactants are coinjected with CO_2.

   b. The effectiveness of mixed surfactant systems in stabilizing foam affects its performance in mobility reduction and mobility dependence on rock permeability.

   c. A mixture of an anionic alpha olefin sulfonate and an anionic ethoxylated alcohol sulfate generated more stable foam than its individual components.

   d. A mixture of nonionic and anionic surfactants in this study, however, shows better foaming stability, mobility reduction and SMR than that generated by an anionic surfactant alone.

Future Plans

Our plan for this year is to continue conducting experiments to improve CO_2 mobility control and oil recovery efficiency in heterogeneous porous media. We have designed coreflood experiments to examine CO_2-foam ability to recover residual crude oil from the heterogeneous core system both in isolation and in capillary contact. The core dimensions in these experiments will be increased in order to have measurable amount of residual oil to recover from these core systems. These experiments will be more representative of reservoir EOR processes. In addition to these experiments, we will continue our research to find suitable surfactants with the SMR property for fluid diversion and improved CO_2 mobility control. Our research study will also be continued to identify a suitable sacrificial agent in order to decrease the amount of surfactant adsorption that normally dissipates onto the rock surface during foam processes.

TESTS DETERMINING FOAM COREFLOOD PARAMETERS

Introduction

CO_2 flooding processes frequently have experienced poor sweep efficiency despite the favorable characteristics of CO_2 in displacing oil. The mobility of CO_2 is usually high relative to that of other reservoir fluids, and the resulting unfavorable mobility ratio enhances channeling that initially results from reservoir heterogeneity or gravity override. To improve the efficiency of CO_2 displacement, researchers have been studying on foam processes that consist of the injection of CO_2 with a surfactant solution (an aqueous solution of a surfactant). When gas is dispersed within a surfactant solution forming a foam,[84] the mobility of gas flowing through a porous medium is lowered. Foam is defined as a dispersion of gas in a liquid so that the water phase is continuous and part of the gas phase is made discontinuous by lamellae.[85] In the case of high-pressure CO_2, the CO_2 is still often referred to as a gas even though CO_2 is actually a high-density supercritical fluid or a liquid. CO_2 is the noncontinuous phase, as is the gas in conventional foam. Since CO_2 is a gas at ambient conditions it is often inappropriately referred to as a gas at high pressure. Extensive laboratory evaluations on the use of CO_2-foam in CO_2 mobility control have been reported.[56,57,62,65,67,72,86-88]

Laboratory foam experiments are usually performed by coinjecting CO_2 and surfactant solution into a core saturated either with surfactant solution or brine at an imposed gas-liquid volumetric injection ratio and a fixed total injection rate. The surfactant solution is prepared by mixing a surfactant with brine at a specified surfactant concentration. Note that a foam quality of 80% (a CO_2 fraction of 0.8) corresponds to a foam test with a gas-liquid (CO_2-aqueous) volumetric injection ratio of 4:1. When a steady-state pressure drop across the core is achieved, the total mobility of CO_2-surfactant solution can be calculated for the corresponding foam quality (CO_2 fraction), total flow rate, and surfactant concentration. The foam resistance factor[66,89] is an expression commonly used to assess the magnitude of the mobility reduction in laboratory foam tests. It is defined as the total mobility of CO_2-brine divided by the total mobility of CO_2-surfactant solution (foam mobility), where both mobility measurements are conducted at the same gas-liquid volumetric injection ratio. If foam

is not generated, the total mobility of CO_2-surfactant solution is about the same as the total mobility of CO_2-brine and the resistance factor is unity. If foam is generated, the value of the resistance factor quantifies the effect of the presence of foam. It is important to note that the total mobility of CO_2-surfactant solutions, which is often referred to as the foam mobility,[62,72,89,90] are different from the mobility of CO_2 in the presence of foam. The total mobility of CO_2-surfactant solution is calculated as a single fluid and is defined as the ratio of the combined (gas and liquid) flow rate per unit superficial area to the pressure gradient required for simultaneous flow of CO_2 and brine-surfactant through the core.[62]

Recent field tests[91,92] using high-pressure CO_2-foam indicate that field application of CO_2-foam is a technically viable process for improved oil recovery (IOR). Efficient application and evaluation of candidate reservoirs for CO_2-foam processes requires information on CO_2-foam behavior at various foam test conditions. Many parameters (e.g., surfactant concentration, foam quality, and flow rate) have been evaluated to study their effects on foam flow behavior. However, some of the information available in the literature is inconclusive and incomplete. Comparing the results of various authors is difficult because experimental conditions were different and foam properties depend on these conditions.

Foam quality is one the most controversial parameters affecting foam flow behavior. For example, Marsden and Khan[93] and Patton *et al.*[94] found that foam mobility decreases with increasing foam quality. On the other hand, Lee and Heller[67] reported that foam mobility decreases with decreasing foam quality. In addition to the contradictory results, the foam-flow behavior in the lower range of foam quality (below 50%) has never been reported. This information is required for foam models used in modeling foam flow behavior, such as those developed by Chang and Grigg.[8]

Flow rate is another important parameter affecting foam flow behavior. Persoff *et al.*[95] found that, at a fixed gas velocity, foam mobility decreases with increasing liquid velocity. On the other hand, Huh and Handy[96] reported foam mobility increases with increasing liquid velocity. The results by Lee *et al.*[62] demonstrated that foam mobility increases as the combined (liquid and gas) flow rate is raised. It is important to note, in the study of Persoff *et al.*,[95] that because the gas velocity was fixed, the foam quality changed each time the liquid velocity varied. Therefore, their finding is a combined effect from flow rate and foam quality. Since foam quality is one of the most important

parameters affecting foam flow behavior, their finding is not valid if related only to liquid velocity without considering the effect of foam quality.

Obviously, more experimental work is needed to expand knowledge in the above areas and to illuminate some of these discrepancies. The objectives of this study are to further examine the inconsistent information on CO_2-foam behavior and to explore the information in the lower range of foam quality.

Experimental Descriptions

A schematic diagram of the test apparatus is shown in Fig. 32. Brine, surfactant solution (SS), and CO_2 were loaded into floating piston accumulators and then displaced into the system by using pumps filled with distilled water. The pressure drop across the core was measured by a Honeywell differential pressure transducer (DPT) and by two Sensotec pressure transducers (PT) located upstream and downstream of the core, respectively. System pressure was controlled to the desired run pressure by using a Temco backpressure regulator (BPR). The test apparatus was housed in an oven to maintain a constant temperature. A wet test meter outside the oven was used to monitor gas production. Either both CO_2 and brine or both CO_2 and surfactant solution could be coinjected into the system by turning their corresponding pumps on simultaneously. For the purpose of this study, oil was not injected into the core and a filter upstream to the core was used to prevent particles from going to the core.

Foam tests were conducted on a fritted, glass bead cores at conditions of 101°F and 2100 psig. As a standard foam test procedure, the core was first saturated with brine by injecting brine overnight at a flow rate of 5 cc/hr. Then the brine permeability was determined by regression based on several brine injection rates varying from 5 to 40 cc/hr. Next, baseline experiments were performed at various flow rates by coinjecting CO_2 and brine into the core at various gas-liquid volumetric injection ratios. Note that a gas-liquid volumetric injection ratio of 4:1 corresponds to a CO_2 fraction of 0.8. Each baseline experiment lasted until a steady-state pressure drop across the core was achieved. After the baseline experiments, the core was flushed with brine to displace CO_2 and then the brine permeability was determined again.

To bring the surfactant adsorption level to a constant value, the core was saturated with

surfactant solution at a surfactant concentration of 2500 ppm. The surfactant-solution permeability was determined by varying the flow rate. The foam experiments were then performed at various flow rates by coinjecting CO_2 and surfactant solution at various CO_2 fractions similar to that of the baseline experiments. Note that a CO_2 fraction of 0.8 is corresponds to a foam quality of 80%. Each foam experiment lasted until a steady-state pressure drop across the core was achieved. After the last foam experiment, the core was depressurized to ambient pressure and flushed with brine to completely displace CO_2 and surfactant solution. The core was then pressurized and saturated with brine for a final brine permeability determination. The brine permeability was used to determine whether the conditions of the core had been significantly altered during the foam tests. The total mobility of CO_2-surfactant solution (foam mobility) in the core is the ratio of the Darcy or superficial velocity of the foam (treating it as a single fluid for the calculation) to the average pressure gradient along the core. It is calculated from measured values of the pressure drop, total flow rate, and the dimension of the core. The unit of mobility is millidarcy per centipose (md/cp).

In all the tests, the synthetic brine with the composition shown in Table 10 was used. The surfactant used in this study was Chevron Chaser CD1045. The surfactant solution at a concentration of 2500 ppm was prepared by mixing CD1045 in the synthetic brine. Information on fritted, glass bead cores used in the tests is listed in Table 11.

Results and Discussion

The results of the baseline experiments are summarized in Table 12 for total flow rates of 4.2, 8.4, and 16.8 cc/hr and CO_2 fractions of 0.2, 0.333, 0.5, 0.667, and 0.8. The experimental conditions, total flow rate and CO_2 fraction, are listed in the second and third columns. Pressure drop across the core, total mobility of CO_2-brine, and the corresponding total interstitial velocity are listed in the last three columns. The results of the foam experiments are summarized in Table 13 for total flow rates of 4.2, 8.4, and 16.8 cc/hr and foam qualities of 20%, 50%, and 80% (CO_2 fractions of 0.2, 0.5, and 0.8). The experimental conditions, total flow rate and foam quality, are listed in the second and third columns. Pressure drop across the core, total mobility of CO_2-surfactant solution (foam mobility) and the corresponding total interstitial velocity are listed in the fourth to sixth columns. WAG mobility (total mobility of CO_2-brine determined by regression based on all tested flow rates in the baseline

experiments) and resistance factor are listed in the last two columns.

Test Series I

In this test series, core E was used. The initial brine permeability of the core was 110.1 md. Since this is the first time a fritted, glass bead core was used in our study, our primary focus is on the effects of CO_2, brine, surfactant solution, and foam on the condition of the core. To examine the effect of CO_2 on the core, CO_2 was injected into the core for about 50 cc. After the CO_2 injection, the brine permeability was determined to be 148.2 md indicating some effect of CO_2 on the core. Three baseline experiments were then performed at 4.2 cc/hr for CO_2 fractions of 0.2, 0.5, and 0.8. The results of the baseline experiments are summarized in Table 12. The total mobility of CO_2-brine decreased with increasing CO_2 fraction, as clearly shown in Fig. 33. After the baseline experiments, the brine permeability was determined to be 186.9 md, indicating some effect of CO_2-brine on the core.

Foam experiments were then conducted at 4.2 cc/hr for various foam qualities. Note that a foam quality of 50% in a foam experiment corresponds to a CO_2 fraction of 0.5. The results of the foam experiments are summarized in Table 13 for foam qualities of 20%, 50%, and 80% (CO_2 fractions of 0.2, 0.5, and 0.8) and plotted in Fig. 34. The total mobility of CO_2-surfactant solution (foam mobility) decreased with increasing foam quality (CO_2 fraction), as shown in Fig. 32.

After the foam experiments, the brine permeability was determined to be 178.9 md (slightly decreased from 186.9 md), indicating little effect of foam on the core. To examine the effect of CO_2 on the core, CO_2 was injected into the core for about 50 cc. After the CO_2 injection, the brine permeability was determined to be 174.6 md, indicating little effect of CO_2 on the core. These two brine permeability measurements together indicate that the condition of the core was stable and was not affected either by the injection of CO_2 or the coinjection of surfactant solution and CO_2.

To examine the effect of CO_2 fraction on the total mobility of CO_2-brine, a set of experiments were performed for CO_2 fractions of 1.0 (pure CO_2), 0.8, 0.667, 0.5, 0.333, 0.2 and 0.0 (pure brine). These experiments were all performed at 16.8 cc/hr, as shown in Table 12, and they were divided into two groups: group A is in decreasing order of CO_2 fraction and group B is in reverse order. When the CO_2 fraction was decreased from 0.8 to pure brine and then increased back to 0.8, the pressure

drop was greater than that was obtained previously (2.44 vs. 3.36 psid), see Table 12. The reason for this irreversible behavior is not clear. The brine permeability of the core was restored (184.3 md) after the experiments indicating the core was not altered due to the coinjection of CO_2 and brine. This suggests that the reason for the irreversible behavior might be due to the trapping of CO_2 in the core. The trapped CO_2 was displaced by brine after the depressurization of the core to the ambient pressure such that the brine permeability of the core was restored. The effect of CO_2 fraction on the total mobility of CO_2-brine was inconclusive, as shown in Fig. 33. However, it is clear that the total mobility of CO_2-brine increased with increasing flow rate.

Test Series II

In this series of experiments, core F was used. The initial brine permeability of the core was 184.3 md. Four baseline experiments were performed at CO_2 fraction of 0.5 for flow rates of 4.2, 8.4, and 16.8 cc/hr. The results of the baseline experiments are summarized in Table 12. The total mobility of CO_2-brine increased with increasing flow rate, as shown in Fig. 35. After the baseline experiments, the brine permeability was determined to be 188.5 md, indicating little effect of CO_2-brine on the core.

The results of the foam experiments are summarized in Table 13 for total flow rates of 4.2, 8.4, and 16.8 cc/hr and foam qualities of 20%, 50%, and 80% (CO_2 fractions of 0.2, 0.5, and 0.8). The total mobility of CO_2-surfactant solution (foam mobility) decreased with increasing CO_2 fraction, as shown in Fig. 36. When examining the effect of flow rate, the total mobility of CO_2-surfactant solution (foam mobility) increased with increasing flow rate, as clearly shown in Fig. 37. After the foam experiments, the brine permeability was determined to be 116.2 md. Even though the core could not be restored to the original permeability, baseline experiments were performed at CO_2 fractions of 0.2, 0.333, 0.667, and 0.8 for flow rates of 4.2, 8.4, and 16.8 cc/hr. The results of the baseline experiments are also summarized in Table 12. The total mobility of CO_2-brine increased with increasing flow rate, as shown in Fig. 38. This is consistent with that of CO_2 fraction of 0.5 (see Fig. 35). The effect of CO_2 fraction on the total mobility of CO_2-brine was inconclusive, however, and there appeared to be a minimum mobility between CO_2 injection fractions of 0.333 and 0.667, as shown in Fig. 39. When comparing foam resistance factors for the tested foam quality range (Fig. 40),

the foam resistance factor increased with increasing foam quality. It is also clear that the foam resistance factor decreased with increasing flow rate.

Conclusions

1. The effect of CO_2 fraction on the total mobility of CO_2-brine was inconclusive; there appeared a minimum mobility reached between CO_2 fractions of 0.333 and 0.667.
2. The total mobility of CO_2-brine increased with increasing flow rate.
3. The foam mobility (total mobility of CO_2-surfactant solution) decreased with increasing foam quality.
4. The foam mobility increased with increasing flow rate.
5. The foam resistance factor increased with increasing foam quality.
6. The foam resistance factor decreased with increasing flow rate.

FOAM SIMULATION

Introduction

Despite the favorable characteristics of CO_2 in recovering oil,[12] CO_2 floods frequently produce poor sweep efficiency. The mobility of CO_2 is usually high relative to that of other reservoir fluids, and the resulting unfavorable mobility ratio enhances channeling that initially results from reservoir heterogeneity or gravity override. To improve the efficiency of CO_2 displacements, researchers have been studying foam processes that consist of the injection of CO_2 with a suitable surfactant solution (an aqueous solution of a surfactant). The mobility of CO_2 is lowered when CO_2 is dispersed within a surfactant solution forming a foam.[84] Extensive laboratory evaluations on the use of CO_2-foam in mobility control of CO_2 have been reported.[56,57,62,67,86,88,97] Recent field trials[92,98] using CO_2-foam indicate that field application of CO_2-foam is a technically viable process for improved oil recovery (IOR). Clearly, a foam predictive model is required for efficient application and evaluation of candidate reservoirs for CO_2-foam injection processes.

Foam resistance factor[66,99] defined in the last section, is a measurement commonly used to assess the magnitude of the mobility reduction in laboratory foam tests. Based on the foam resistance factor,[100] a foam model was developed and incorporated into an existing pseudomiscible reservoir simulator, MASTER (Miscible Applied Simulation Techniques for Energy Recovery).[101]

MASTER, which is supplied by the U.S. Department of Energy, is an extension of the so-called black-oil model and uses the mixing-rule approach to calculate the effective fluid density and viscosity. The readers are referred to the original report of Ammer *et al.*[101] for the detailed descriptions of MASTER. To incorporate the foam features into MASTER, major modifications were made to MASTER. These modifications include: (1) the addition of a surfactant conservation equation including the adsorption isotherm, (2) the addition of lookup tables for the foam resistance data, and (3) the addition of an algorithm to calculate the gas mobility in the presence of foam. Validation simulations have been performed to assess the adequacy of the included foam features in MASTER. The readers are referred to the original paper of Chang and Grigg[100] for the detailed descriptions of the foam model and the newly developed pseudo-miscible foam simulator.

EVGSAU Development History

The East Vacuum Grayburg San Andres Unit (EVGSAU), operated by Phillips Petroleum Company, is the site of the first full-scale miscible CO_2 injection project in the state of New Mexico. The Vacuum field, about 15 miles northwest of Hobbs in Lea County, New Mexico, is on the Artesia-Lovington uplift along the northern limit of the Delaware basin. The EVGSAU covers 7025 acres on the eastern side of the Vacuum field. The unitized interval includes the Grayburg and San Andres formations. The EVGSAU was formed in December 1978. At that time, the unit comprised 169 producing wells drilled on 40-acre spacing. Beginning in 1979, the unit was infill drilled to 20-acre spacing and was converted to an 80-acre inverted nine-spot-pattern waterflood development by 1982.

Operation of the CO_2 project began in September 1985 with a 2:1 water-alternating-gas (WAG) ratio.[91] The CO_2 project area, which covers 5000 acres of the EVGSAU, was divided into three WAG injection areas with each area receiving four months of CO_2 injection followed by eight months of water injection. The readers are referred to the original paper of Brownlee and Sugg[102] for the summary of the development and initial results of CO_2 project. In September 1991, operation of the CO_2-foam pilot test began at the pilot area in the center of the unit, as shown in Fig. 41. Specifically, the prime directive of the foam field trial was to prove that foam could be generated and that it could aid in suppressing the rapid CO_2 breakthrough by reducing the mobility of CO_2 in the reservoir. Operation of the foam field trial ended in 1993. The response from the foam field trial was very positive, successfully demonstrating[91] that strong foam could be formed *in situ* at reservoir conditions and that the diversion of CO_2 to previously bypassed zones/areas due to foam resulted in increased oil production and dramatically decreased CO_2 production. The readers are referred to the original paper of Martin *et al.*[91] for the details of the CO_2-foam pilot test.

This report presents the most recent history match results of the CO_2-foam pilot area at EVGSAU based on the newly developed pseudomiscible foam simulator,[100] MASTER. The objective was to match the producer fluid rates as closely as practical. The ultimate purpose was to establish a foam predictive model for CO_2-foam field applications.

History Match Model

The foam pilot area is an inverted nine-spot pattern with eight producers (indicated by the solid circles) and one injection well in the center (indicated by the solid triangle), as shown in Fig. 41. Well 3332-001, located at the center of the pattern, was the foam injection well. Well 3332-32 was the so-called "offending" production well, which consistently flowed very strongly after each period of CO_2 injection and produced more than 80% of the CO_2 injected into the pattern. The foam pilot area of nine wells and the surrounding 16 wells (eight injectors and eight producers outside the pilot area) were included in the history match model. The layout of the wells is shown in Fig. 42 with solid circles as producers and solid triangles as injectors.

The history match model consisted of a 16 × 16 grid (as shown in Fig. 42) in seven separate layers for a total of 1792 grid blocks. These seven layers were chosen based on the type-log zonation (C-3, C-2, C-1, D, E, G, and H) employed by Hoefner and Evans.[91] Injection rates and bottomhole pressures were specified as well constraints in the history model. The surrounding producers outside the pilot area were opened to flow at a bottomhole pressure of 150 psi from 1959 to 1979 and 1500 psi from 1980 to 1992. However, rate control was used for the eight producers in the pilot area based on the oil production data. Case runs were conducted to examine the effects of several model parameters (e.g. absolute permeabilities, end points and curvature of relative permeability curves). These parameters were gradually modified until the total cumulative production for gas and water for the pilot area (sum of the eight producers) were satisfactorily matched.

History Match Simulations

The history match simulations involved three phases of simulations: (1) primary depletion from 1959 to 1979, (2) waterflood from 1980 to 1985, and (3) CO_2-flood (WAG injection) from 1985 to 1992. Fig. 43 compares simulated and field data of the total cumulative production for oil, gas, and water (Oil(S)/Gas(S)/Water(S) vs. Oil(F)/Gas(F)/Water(F)) from 1959 to 1985 for the pilot area. The match was good until about 1984 when the simulation results deviated significantly. The instantaneous gas-oil ratio (GOR) behavior was achieved for the pilot area, as shown in Fig. 44. For the eight producers in the pilot area, most matches were of good quality with a few of the producers showing only a fair match of historical production. Fig. 45 compares simulated and field data of the

cumulative production data for oil, gas, and water from 1959 to 1985 for the offending well (3332-32 at the pilot area). As shown in the figure, the match of the cumulative gas production was very good and the cumulative water production was less than the field data, although the breakthrough of water was virtually identical.

The initial simulation of the CO_2-flood (WAG injection) from 1985 to 1992 showed a poor match of field performance, with some wells producing little or no CO_2 and others producing much more than the field data. In order to match this period's field performance, additional modifications were made to interwell permeabilities, especially between the foam injection well and the offending well. Fig. 46 compares simulated and field data of the total cumulative production for oil, gas, and water from 1985 to 1992 for the pilot area. The match for cumulative gas production was good, with some deviation initially. The match for cumulative water production was satisfactory with some lag for the simulated cumulative water production. For the offending well, the match for cumulative gas production was satisfactory with higher gas production initially, as shown in Fig. 47. The match for cumulative water production was also satisfactory.

Foam Test Simulation

From the history match simulations, an acceptable history match model was obtained. A foam test simulation was performed based on the history match model. The foam test simulation was performed using exactly the same EVGSAU injection schedule from January 1985 to November 1991 for all the injection wells shown in Fig. 42 except the foam injection well 3332-032. The injection schedule for the foam injection well during the foam test was modified as following:

1. Surfactant was introduced into the pilot through water injection from August to October 1988 without changing the injection schedule. This kind of water injection is referred to as a "surfactant solution injection." The surfactant concentration was 2500 ppm active.
2. Five rapid cycles of alternating injection of surfactant solution and CO_2 (SAG) were performed for a total of 75 days. Each SAG cycle consisted of three days of surfactant solution injection and 12 days of CO_2 injection. The surfactant solution injection rate was 1703.53 STB/D and the CO_2 injection rate was 3862.05 MSCF/D. These rates were obtained by averaging the rates of the 75-day period so that the whole material balance in the pilot area

could be maintained.

In order to evaluate the foam test, a base case that was needed. The injection schedule of the base case was identical with that of the foam test, except surfactant was not introduced into the pilot.

Figure 48 shows the oil rate history of the offending production well from the initiation of the surfactant solution injection (3.6 years of simulation, August 1988) for the foam test and the base case. The oil rate for the foam test was reduced during the time period between 3.9 to 4.3 years into the simulation but was increased later between the period 4.8 to 5.3 years into the simulation as compared to the base case. The reduction of the gas rate of the offending production well for the foam test was clearly shown in Fig. 49 at 3.9 years of simulation and lasted almost one year as compared to the base case. The reduction of both the oil and gas rates at 3.9 years of simulation indicated that foam was generated at the "path" from the foam injection well to the offending well. Continued reduction of the gas rate until 4.8 years of simulation indicated CO_2 was diverted away from the "path" and resulted in the higher oil rate from 4.8 to 5.3 years of the simulation. The increased oil recovery from the offending well was about 1.7 MSTB at 5.3 years of simulation. Note that the total increased oil recovery of the foam pilot area was about 9 MSTB as shown in Fig. 50. This indicated that the CO_2-foam process increased the oil production for some if not all of the production wells in the pilot area, not just the offending production well. Therefore, the presence of the foam improved the CO_2 sweep in the pilot area and thus resulted in higher oil production. The corresponding reduction in instantaneous gas-oil ratio and cumulative gas production can be clearly observed in Figs. 51 and 52.

Conclusions

1. An acceptable history match model was obtained for the foam pilot area at EVGSAU.
2. The simulated results of the foam test simulation were consistent with the foam pilot test results.
3. The foam model was found to be adequate for field scale CO_2-foam simulation.
4. The results confirm that the communication path between the foam injection well and the offending well had a strong impact on the production performance.

WELLMAN UNIT CO_2 FLOOD: RESERVOIR PRESSURE REDUCTION AND FLOODING THE WATER/OIL TRANSITION ZONE

Summary

CO_2 injection is a proven technology.[34] Results from two decades of reservoir and economic performance prove that CO_2 can: 1) be transported over large distances via pipeline, 2) handled and injected easily at well-site facilities, and 3) recover oil that water injection could not mobilize. This has been accomplished at cost levels that are profitable, provided enough HCPV (hydrocarbon pore volume) of CO_2 is injected into the reservoir and sweep and displacement efficiency are sufficient.

The most recent challenge involves optimizing efficiency of CO_2 flooding, i.e. maximizing oil recovery while at the same time reducing operating expenses. A useful method to attain the goal of CO_2 flood optimization is careful performance review of better-performing CO_2 floods. The Wellman Unit CO_2 flood has a long history. This CO_2 flood is one of the most successful CO_2 floods documented in terms of CO_2 utilization, i.e. MCF of CO_2 required to recover one barrel of oil. This section explores the role of laboratory experimentation for improvement of performance of a mature CO_2 flood.

In this section, the history of the Wellman Unit CO_2 flood is reviewed and two possibilities are examined that are to optimize reservoir performance: 1) reducing CO_2 injection pressure, thereby reducing the volume of purchased CO_2 while at the same time maintaining miscibility (optimum displacement efficiency); and 2) exploring the possibility of mobilizing reserves in the water-oil transition zone below the original oil-water contact.

Introduction

The Wellman Unit has an extensive history, yielding papers addressing assessment of reservoir performance,[103] simulation of reservoir performance[104] and re-completion strategies.[105] A schematic of the history of reservoir depletion was presented earlier by Bangla *el.al.*[103] Currently, the reservoir is 20-40 ft. of net pay. A CO_2 gas cap overlies the reservoir zone and the original water-oil contact and transition zone below the reservoir. This is a gravity-stable process as the gas cap expands and

displaces oil towards perforations in the oil-saturated interval. Figure 53 shows the structure of the Wellman Unit. Figures 54 (a) and (b) show the reservoir prior to CO_2 injection and the current state of the reservoir after 15 years of CO_2 injection. Table 15 provides the reservoir parameters.

Our goal is to optimize a mature CO_2 flood. Two important questions arise as the thickness of the oil column diminishes and the CO_2 flood front reaches the current water-oil contact:

1. Can the watered-out intervals and underlying transition zone contain waterflood residual oil that could be mobilized by CO_2?
2. Is it possible the pressure in the reservoir can be reduced while still maintaining displacement efficiency, thereby reducing CO_2 purchases?

This section addresses the laboratory measures taken to assess these questions.

Part of this study was designed to assess the effect of solution gas on the minimum miscibility pressure (MMP) of CO_2 with Wellman reservoir oil and the effect of pressure on the displacement efficiency of a gravity-stable displacement of CO_2. Contrary to the findings reported in the literature,[12,13,22,107,108] earlier Wellman fluid tests indicate that there were significant--several hundred psi--effects on the MMP due to the changing in the solution gas.[109] Correlations that take the solution gas into account to determine CO_2 MMP predict the effect to be in the order of 50 psi, going from a dead oil to one with a GOR of about 600.[110] Also, most correlations ignore the solution gas because the authors, upon examining a number of systems, had concluded the low molecular weight hydrocarbon gases had little or no effect on CO_2 miscibility. The intermediate hydrocarbons (C_5 to C_{30}, with the most effect from C_5 to about C_{13}) are primarily responsible for the development of miscibility; for CO_2 injection, the light hydrocarbons (C_1 to C_4) have much less effect on the development of miscibility. It is not uncommon to find exception to a rule of thumb; thus, we considered it important to reexamine this system versus GOR.

Current Field Performance

The Wellman Unit CO_2 flood has produced 7.2 MMbbls of oil by CO_2 flooding in the last 15 years. Approximately 42 BCF of CO_2 has been injected since 1983. This CO_2 flood ranks as one of the most efficient floods on record. The utilization through 1993, before change in ownership, was 7.85 MCF CO_2/bbl IOR oil. Reduction in CO_2 purchases since 1993 has resulted in a net utilization

of 2.25 MCF/bbl. Clearly, one of the primary reasons for the success of this flood is the excellent sweep efficiency apparent in the Wellman Unit. The reservoir is a thick, steeply dipping limestone reef with an extensive system of vugular porosity and vertical fractures. The Wellman Unit is characterized by good vertical permeability. Pervasive communication across the reservoir as a result of the fracture and vugular network is observed in the reservoir. Secondary porosity results in very little deviation of BHP (bottomhole pressure) in the Wellman Unit wells across the structure. Good lateral and vertical communication ensures that injected CO_2 moves to the top of the reservoir and displaces fluid downward. In this case of excellent lateral and vertical communication, the gas liquid interface is relatively flat. The development of miscibility near the MMP of the crude oil and CO_2 results in low interfacial tension (IFT) between the gas and oil phases. The combination of gravity stability at near miscible conditions, where the IFT is low, has been demonstrated to be a very efficient process.[32,111-114] Every aspect of response to CO_2 injection in the Wellman Unit confirms this observation.

Natural gas liquids (NGL) are removed through a series of scrubbers, chillers, membranes and an amine unit. Produced gas is typically 10% NGL; the CO_2 must be removed before NGL are transported to the sales line. Production of oil at the Wellman Unit, gas processing and re-injection of CO_2 after removal of the NGL is a finely tuned control operation. Oil production history, decline in BHP and CO_2 utilization plots are shown in Figs. 55,56 and 57.

CO_2 Recovery Mechanism – Gravity Drainage

Gravity drainage is known to be a dominant mechanism in the Wellman Unit CO_2 flood. The project was initially designed at pressures well above the MMP of the oil. We sought to optimize the pressure by performing experiments that take advantage of the gravity component above, near, and below the MMP. Optimization of the flood requires knowledge of reservoir pressure and recovery in the gravity drainage mode at pressures as near to the MMP as possible. Furthermore, continuation of injection as the gas-oil contact reaches the water-oil contact remains an imminent decision. Experiments were devised and performed to interpret performance and answer the questions concerning reduction in reservoir pressure and flooding the transition zone.

Experiments were performed with CO_2 to compare recovery results between slim tube, gravity-stable and unstable, large-diameter tube and gravity-stable injection into reservoir whole core at reservoir conditions. The purpose of this set of experiments was twofold:

1. The first objective was to examine the performance of recovery at or near the MMP with CO_2 in:
   a. standard slim tube analysis
   b. vertically-oriented, bead-packed large diameter tubes
   c. vertically-oriented reservoir cores at reservoir conditions
2. The second objective was to examine the possibility that residual oil existed below the original water-oil contact that could be mobilized by continuation of CO_2 injection.
3. Finally, an accurate knowledge of S_{or} after CO_2 improves uncertainty in ultimate recovery.

Experimental Tests

Wellman Unit Oil Characterization

Two separator gas samples and one separator oil sample were taken from the Wellman unit Well 5-12 on January 15, 1997. This well had been on the test separator for several days and was one of the few wells that had not had significant CO_2 breakthrough. The separator conditions were 126, 126, and 130 psig and 61, 61, and 60°F at the time of sampling for the gas and oil samples, respectively. Tables 16 and 17 are compositional analyses from separation and Gas Chromatograph of the separator gas and oil samples, respectively. Both analyses are in good agreement with the analysis done on samples taken in 1988,[109] considering the separator pressure difference. The average molecular weight of the separator oil was determined to be 147 g/mol. The separator oil had a solution gas GOR of 150 scf/bbl. Tests done on the separator oil at 100 °F and 1000 psig determined the density to be 0.8329 g/cc and the viscosity to be 2.956 cp. In tests where higher GOR oil was used Wellman separator gas was added to the separator oil. The separator gas had an average molecular weight of 24.18 g/mol. The composition of the sample recombined to a GOR of 400 scf/bbl is shown in Table 18 compares well with the 1988 calculated reservoir stream.[109] Finally, Table 19 is the composition of a higher, GOR oil recombined to a solution gas GOR of 600 scf/bbl. Additional separator samples were taken on May 2, 1997 to complete gravity-stable displacement tests. These

samples were similar to those taken earlier, except that CO_2 was starting to break through and the gas contained about 39 mol % CO_2. There was sufficient gas from the first sample to complete the tests.

Slim Tube Tests: MMP Determinations

The minimum miscibility pressure (MMP) of the oil was measured with a standard slim-tube configuration and found to be ~1600 psig at the reservoir temperature of 151°F. The interfacial tension, σ (IFT) at the MMP is about 1.5 mN/m as measured by the pendant drop method at reservoir conditions. The MMP is relatively low for a reservoir temperature of 151°F. There are at least two factors that contribute to the low MMP: 1) Wellman Unit oil is high gravity (42°API), and 2) the high intermediate hydrocarbon content in the C_5 to C_{13} range present in Wellman crude. All of these components are first-contact miscible at reservoir conditions.

Three MMP determinations using a slim tube apparatus were performed, one for each of three different samples. The intent was to cover a range of GORs. The three samples had GORs of about 150, 400, and 600 scf/bbl, with their compositions listed in Tables 17 through 19, respectively. The bubble point pressures at the reservoir temperature of 151°F were determined for the 400 and 600 GOR systems to be 1118 and 1480 psig, and the results of the PVT bubblepoint determinations are found in Tables 20 and 21, respectively. Six slim tube tests were performed for each sample. The results are compared in Figs. 58-60. In each case, the oil production at the time of CO_2 breakthrough, after 1.2 PV of CO_2 had been injected and at the end of the run, is plotted. The results are summarized in Tables 22a, 23a, and 24a. The results for these floods are found in Tables 22b through 22g, 23b through 23g, and 24b through 24g. From the estimated break point when plotting recovery versus pressure, the MMPs were determined to be about 1595, 1605, and 1625 psig for solution GORs of 150, 400, and 600 scf/bbl, respectively. The difference is only about 30 psi over the solution gas GOR range examined. The ultimate recovery numbers were used to make the MMP determinations, but the results would be similar if either of the other two recovery figures had been used. The commutative percent recovery (last column of each of Tables 22b through 22g, 23b through 23g, and 24b through 24g) was calculated from the volume of oil recovered at atmospheric

condition (second to last column in the same tables) times the formation volume factor (FVF). The FVF for the separator, medium GOR, and high GOR oils were 1.14, 1.30, and 1.35, respectively.

In the lower GOR system, a break in the recovery versus pressure curve can be justified at a pressure as low as 1550 psig. In the highest GOR system, the MMP could be as low as 1600 psig and as high as 1650 psig. The effect of the GOR on the MMP is shown to be, at most, 100 psi. Thus using an MMP of 1650 psig would be conservative and cover a wide range of GORs. Using only the MMP as a guide, the reservoir pressure can be as low as 1650 psig with the expectation that miscible displacement will occur.

The MMP value of 1650 psig is relatively low for a reservoir temperature of 151°F. There are at least two factors that attribute to this relatively low MMP. One is the relatively high gravity of the Wellman oil (40 to 42°API). The other is a high intermediate hydrocarbon content, especially in the C_5 to C_{13} carbon number range. About 68 mol % of the C_5 plus hydrocarbons have carbon numbers at or below C_{13}, these components are essentially 100% soluble in CO_2 under conditions found in many reservoirs, especially in the Permian Basin. This is the range that is essential to the development of miscibility.

Large-Diameter (Fat) Tube Tests: Gravity-Stable Displacements

The second series of tests was done in order to determine the effect of pressure on a gravity-stable flood. In many CO_2 floods the reservoir is in the range of 10 to 100 ft thick, but in the case of Wellman the interval is much thicker, with vertical permeability. Thus, the effects of a vertical flood combined with the recovery mechanisms of CO_2 were examined. In the laboratory, vertical floods in a glass bead pack were performed. The bead pack had a diameter large enough to permit that viscous fingering. The bead pack was a 27-in. cylinder with a 4.75-in. diameter, filled with 80-120 mesh glass beads. The porosity of the system was around 35% with permeability more than one Darcy.

The system was first filled with distilled water and then displaced with reservoir brine in order to determine the system volume. This information was used to determine if the system had good flow properties. Brine was then displaced with reservoir crude oil, leaving residual water saturation. Finally the oil was displaced with CO_2, with fluid flowing from the top to the bottom. Three tests were

performed using the 400 GOR solution at 1700 psig (above the MMP), 1550 psig (at or just below the MMP), and 1400 psig (well below the MMP). These are designated as Runs A through C. The results are plotted in Fig. 61 and found listed in Tables 25a through 25c. The results demonstrated that good recoveries were obtained in each case. The results show that below the MMP (1400 psig), excellent recovery continued.

In many CO_2 floods the pressure is maintained well above the MMP to avoid a pressure drop below the MMP in parts of the reservoir, thus causing poor recovery. Therefore, the expense of maintaining the reservoir pressure well above the MMP is accepted. The results of this work imply that in gravity-stable floods, miscibility is not the only mechanism and that lowering the pressure to or even below the MMP will not significantly effect the displacement efficiency. In fact, it will increase the efficiency because less CO_2 at the lower pressure will be required to fill the same reservoir volume. Note that these experiments were performed using a glass bead pack at much higher porosity and permeability values than those found in the reservoir. The work performed on reservoir core confirmed what has been found in this study and will be discussed in a later section.

For completeness and scientific curiosity, three additional floods were performed to help verify the effect of flooding orientation. In these last three tests, test separator oil was used. Run D was identical to Run C, except for using the low GOR separator oil. This test was run in the vertical position, flooding from top to bottom at 1400 psig (below the MMP) and 151°F. The results are plotted in Fig. 61 as Run D and listed in Table 25d. The results are similar to Runs A through C. The fifth run, Run E, was performed by injecting into the bottom of the vertical core, thus flowing from the bottom to the top. The sixth run, Run F, CO_2 displacement was performed with the core in the horizontal position. The last two runs are also plotted in Fig. 61 and summarized in Tables 25e and 25f. As expected, the core orientation to the flow direction had significant effects due to gravity override and viscous fingering.

Core From Wellman 5-10

The Wellman Unit 5-10 (shown in Fig. 53) was cored in the water-oil transition zone, above the original water-oil contact. A total of 30 ft of whole core was retrieved from the 9400-9430 ft interval. From this, 26 samples were subjected to standard core analysis while one 3 ft section of core

was preserved for gravity-stable CO_2 tests. Vugularity and vertical fracturing was observed in almost all of the samples. Helium porosities were measured from 2.4% up to 12.5% with an average porosity of 5.8% for the 26 samples. The average water saturation in this interval was 42%. Every core sampled was oil-saturated.

Gravity-Stable Coreflooding Results

A 4 in.-diameter whole core from an interval of 9403.6-9406.5 ft in Wellman Unit Well 5-10 was cut to 28 in. long to fit into a Hassler sleeve core holder. The core was taken from below the original water-oil contact. The intervals above and below this core were oil-saturated according to standard core analysis results. Pore volume (PV) was determined to be 390 cm^3 brine injection. Porosity was measured at 6.8%. Vertical permeability to brine was measured at 15.4 md. The core was mounted in the core holder and the entire cell was oriented vertically. The configuration is shown in Fig 62(a).

The procedure for establishing conditions similar to the current reservoir transition zone in the Wellman Unit Well 5-10 whole core is shown in Fig. 62(b), steps 1-4. After circulating brine for more than 10 PV at 151°F and 1900 psig, dead oil was introduced into the core. The dead oil was aged in the core for 10 days before separator oil was injected into the core. By circulating separator oil in the core, the initial water saturation was reduced to 23%. Recombined reservoir oil was then injected into the core. After aging, the recombined reservoir oil in the core for three days, brine was slowly injected into the core from the bottom to simulate bottom-up water drive in the reservoir. Water saturation of 53% was achieved with varying water injection rates. A water saturation of 53% agrees reasonably well with the average water saturation of 42%, determined by standard core analysis on 26 samples. The higher water saturation would render our experimental results pessimistic. It should be noted that the oil (47% PV) remaining in the core is a 400 GOR recombined reservoir oil with a formation factor of 1.33. This means that the initial saturation of the dead oil in the core is about 35% PV. After 5 PV of brine injection, virtually no oil was produced.

CO_2 was injected into the top of cell to represent a downward flood. CO_2 was injected into the core at a rate of 20 cm^3/hr. Currently, about 15 MMscf/D of CO_2 is injected into an area of 1250 acres. Reducing that injection rate to the coreflood scale would require more than one year to inject

a single pore volume. Thus, compared to the actual field rate of CO_2 injection, the advance rate of the CO_2 flood front is far greater in the experiments reported. The discrepancy in injection rate also would underestimate reservoir recovery in swept zones.

During CO_2 injection, the temperature was maintained at 151°F and the pressure at 1650 psig 1543 and 1320 psig for the three experiments. Water and oil production from the core during CO_2 injection is shown in Fig. 63 for the run at 1650 psig. This figure shows that oil and water were not produced proportionally. For the initial 150 cm^3 of CO_2 injection, the produced liquid was essentially water. After 200 cm^3 of CO_2 injection, water production gradually ceased and oil production increased rapidly. This indicates the formation of an oil bank at the CO_2 front during a gravity-stable CO_2 displacement. Figure 64 demonstrates back-calculated changes in water and oil saturation in the core during CO_2 injection. It shows that after 0.5 PV of CO_2 injection, essentially all the mobile water was removed from the core. It also demonstrates that about 10% PV of residual, live oil was left in the core after 1.3 PV CO_2 injection. This 10% PV live oil saturation is equivalent to 7.5% PV dead oil saturation. Figure 65 presents the oil recovery curve obtained from the experiment. Showing the final oil recovery as 79% OOIP, established after 1.3 PV of injected CO_2.

After 2.1 PV of CO_2 injection, flow through the core was stopped. The backpressure was increased to 1740 psig. After three days of CO_2 soak at an elevated pressure of 1740 psig and temperature of 151°F, 0.3 PV of CO_2 was injected into the core at a rate of 50 cm^3 per hour with a backpressure of 1650 psig. About 2% OOIP of additional oil was recovered resulting in a residual live oil saturation of 9% PV, or a dead oil saturation of 7% PV.

The core remained in the core holder at a pressure of 1650 psig and temperature of 151°F for nine days. Then, 4.3 PV of CO_2 was injected into the core at a rate of 5,000 cm^3/hr with a backpressure of 1650 psig. About 1.4% OOIP of additional oil was recovered, resulting in a residual live oil saturation of 7.5% PV, or a dead oil saturation of 5.7% PV.

To check the material balance, the core was cleaned by injection of methanol, chloroform, water and CO_2. After 2 PV of methanol injection at a rate of 1,000 cm^3/hr from the bottom, only one cm^3 of oil was extracted from the core. The backpressure was then reduced to atmospheric (bypassing the BPR) and 3 PV of chloroform was injected into the core from bottom at a rate of 1,000 cm^3/hr, followed by 4 PV of water injection at the same rate. A 1,000-cm^3 cylinder of CO_2 at a pressure of

950 psig and room temperature was heated to 150°F and flushed through the core from top to bottom to ensure the core was clean and dry. About 11 cm^3 of additional oil was extracted from the beginning of chloroform injection to the end of the CO_2 flush. This brought the final oil recovery to 93% OOIP. The final residual oil saturation is 3.3% PV of live oil, or 2.5% PV of dead oil.

For the second experiment, brine was again introduced into the core from the bottom at a lower pressure. The circulated brine was clean. The pore volume indicated by this brine injection was close to that determined by the brine injection before the first experiment. Confining pressure, injection pressure, and BPR dome pressure were 3400 psig, 3100 psig, and 3100 psig, respectively.

The second gravity-stable CO_2 displacement was conducted approximately 50 psig below the slim tube MMP. Results indicate that the final oil saturation is not significantly different from that obtained at a pressure 50 psig above the MMP. A third gravity stable experiment was conducted at a pressure 300 psig below the slim tube MMP. The final oil saturation is not very different from that obtained at a pressure 50 psig below the MMP. The oil recovery-pressure relationship from the CO_2 core floods is compared with that from slim tube and large-diameter tube tests and shown in Fig. 66. The results from all of the gravity drainage experiments are summarized in Table 26. Consistency is observed with an exception that oil recovery from core floods was lower than that from the slim tube and large-diameter tube tests. However, the final oil saturation in all the experiments was 10% or less. The experimental results indicate high efficiency of CO_2 flooding in the Wellman field, from where the core and oil samples were taken, both above and below the MMP.

It should be noted that this result was obtained from a high-water saturation core simulating the water-oil transition zone. The core was taken from above the transition zone and the experiments were performed at reservoir conditions.

Conclusions

1. The MMP of Wellman Unit oil is 1600+/- 50 psig over a range of GORs from 150 to 600 scf/bbl.
2. Reservoir performance, slim tube, large-diameter tube and gravity-stable corefloods in Wellman Unit whole core at reservoir conditions demonstrate excellent displacement efficiency with S_{or} after CO_2 less than 10%.

3. Reducing the pressure from above the MMP to near the MMP and below the MMP does not reduce efficiency in laboratory coreflooding. The data suggests that current BHP in the Wellman Unit could be reduced from the current level of 2000 psig to near the MMP of 1600 psig with no reduction in displacement efficiency. The reduction in CO_2 purchases would be a positive benefit from this strategy. The reduction in reservoir pressure, however, is constrained by voidage replacement issues.
4. Gravity-stable coreflooding results, from transition zone core taken from the Wellman Unit, demonstrates that oil not mobilized by water influx in the transition zone can be effectively mobilized with CO_2 over a range of injection pressures.
5. CO_2 flooding in the Wellman Unit has performed exceptionally well due to gravity-stable displacement above the miscibility pressure. This combination of factors results in excellent sweep and displacement efficiency. Over 42 Bcf of CO_2 has been injected, recovering 7.2 MMbbls of tertiary oil. The resulting utilization is 5.83 Mcf CO_2 injected per barrel of incremental oil.

PRELIMINARY IVESTIGATION ON INJECTIVITY LOSS IN WAG FLOODING

Introduction

Injectivity loss is one of the frequently reported problems in water-alternating-CO_2 (WAG) flooding.[115-125] We have conducted experimental investigations on injectivity loss using four cores during the past three months: the first two cores were Berea cores, the third core is a naturally fractured carbonate reservoir core, and the fourth core is a sandstone reservoir core. The purposes of the experiments were to duplicate situations of injectivity loss in the WAG flooding and identify factors affecting the injectivity loss. Our preliminary results indicate that for a given rock the injectivity loss depends on oil saturation in the core during the WAG flooding. The injectivity loss is higher in cores with high in-situ oil saturations. No injectivity loss was observed with the naturally fractured carbonate core. More experiments are being conducted using reservoir cores to identify factors affecting the injectivity loss.

Experimental Procedure.

The following procedure was followed in all the experiments:

1. Seal a cleaned core sample in a core holder with CERROTRU.
2. Inject water into the core sample until full saturation is reached. Determine core porosity and permeability to water. This step simulates the initial condition in the reservoir before oil accumulation.
3. Inject crude oil into the core until irreducible (initial) water saturation is established. Determine oil saturation in the core sample. This step simulates oil migration and accumulation in the reservoir.
4. Inject water into the core sample to reduce oil saturation to a desired level. This step simulates waterflooding process in the oil reservoir.
5. Inject CO_2 into the core at a pressure slightly higher than the minimum miscibility pressure

(MMP) of the oil until desired oil saturation is reached.

6. Inject water into the core until desired oil saturation is reached.
7. Repeat steps 5 and 6 to simulate WAG process.

Materials and Condition

The first two cores used in the experiments are Berea cores. The third core is a carbonate reservoir core with natural fractures. Petrophysical properties of the cores are summarized in Table 27. Distilled water was used after degassing. Separator oil with an MMP of 1,650 psig was used in the experiments. All the experiments were conducted at back pressures between 1661 psig and 1667 psig and temperatures ranging from 147°F to 149°F. Volumetric flow rate was kept constant in each experiment run.

Results

Figure 67 presents recorded pressure drops across core sample No. 1 (100-md Berea). The pressure drop was about 106 psi during the pre-CO_2 water flooding. The average pressure drop increased to 111 psi during the post-CO_2 water floods in the WAG period. This is equivalent to a 5% loss in water injectivity.

Figure 68 shows recorded pressure drop across core sample No. 2 (650 md Berea) on the first run with initial water saturation $S_{wi} = 0.23$. The pressure drop was about 12 psi during the pre-CO_2 water flooding. The average pressure drop increased to about 17 psi during the post-CO_2 water floods in the WAG period. This is equivalent to about 40% loss in water injectivity. Figure 69 demonstrates recorded pressure drop across core sample No. 2 (650 md Berea) on the second run with initial water saturation $S_{wi} = 0.14$. The pressure drop was about 15 psi during the pre-CO_2 water flooding. The average pressure drop increased to about 18 psi during the post-CO_2 water floods in the WAG period. This is equivalent to about 20% loss in water injectivity. The major difference between the two runs is that the residual oil saturation in the second run during WAG is significantly lower than that in the first run. It appears that the higher the residual oil saturation is, the higher the

injectivity loss is.

Figure 70 illustrates recorded pressure drop across core sample No. 3 (315 md fractured carbonate). The pressure drop was about 2 psi during the pre-CO_2 water flooding. The average pressure drop is slightly higher during the post-CO_2 water floods in the WAG period. Since the natural fracture provided a relatively large flow channel for fluids in the small core plug, the results should not be simply scaled up to the field level. A reservoir core without natural fractures is currently be tested to enable better data interpretation.

Figure 71 shows recorded pressure drop across core sample No. 4 (3.5 md reservoir sandstone). The pressure drop was about 24 psi during the pre-CO_2 water flooding. The initial pressure drops are 30 psia and 37 psia during the first two post-CO_2 water floods in the WAG period. This indicates an inectivity loss of about 40%.

Conclusion

In order to duplicate situations of injectivity loss in the WAG flooding and identify factors affecting the injectivity loss, we have conducted experimental investigations on injectivity loss using four cores during the past three months. Two of them are Berea cores and the other two are a naturally fractured carbonate reservoir core and a sandstone reservoir core. The preliminary results indicate that for a given rock the injectivity loss depends on oil saturation in the core during the WAG flooding. The injectivity loss is higher in cores with high in-situ oil saturations during WAG flooding. This effect is being verified by more experimental data.

ACKNOWLEDGMENTS

This work could not have been done without the financial support of the U.S. Department of Energy, the State of New Mexico, and various industrial contributors including Texaco, The Wiser Oil Company, Arch Petroleum, etc. Appreciation is extended to James McLemore, Robert Svec, Cletus Scharle, Ucok Siagian, and David Fritchman for their assistance in equipment design, construction, and operation. We would also like to express appreciation to Drs. Shih-Hsien Chang, Jyun-Syung Tsau, Boyun Guo, and Hossein Yaghoobi for their assistance in different areas of this project.

REFERENCES

1. Whorton, L.P., and Kieschnick, W.F.: "Oil Recovery by High Pressure Gas Injection," *OGJ*, (April 6, 1950) 78-84.
2. Whorton, L.P., Brownscombe, E.R., and Dyes, A.B.: "Method for Producing Oil by Means of Carbon Dioxide," U.S. Patent No. 2,623,596 (Dec. 30, 1952).
3. Holm, L.W.: "Carbon Dioxide Solvent Flooding for Increased Oil Recovery, *Trans.*, AIME (1959) **216**, 225–231.
4. Beeson, S.M., and Ortloff, G.D.: "Laboratory Investigations of the Water-Driven Carbon Dioxide Process for Oil Recovery," *Trans.*, AIME (1969) **216**, 388–391.
5. Holm, L.W.: "CO_2 Slug and Carbonated Water Oil Recovery Process," *Prod. Monthly*, (Sept. 1963) 6–9.
6. Thomas, F.B., Holowach, N., Zhou, X.L., Bennion, D.B., and Bennion, D.W.: "Miscible or Near-Miscible Gas Injection, Which is Better?" paper SPE/DOE 27811 presented at the 1994 SPE/DOE Symposium on Improved Oil Recovery, Tulsa, April 17-20.
7. Stalkup, F.I.: *Miscible Displacement*, SPE Monograph Series, Richardson, TX, SPE-AIME (1984).
8. Chang, S.-H. and Grigg, R.B.: "Foam Displacement Modeling in CO_2," paper SPE/DOE 35401 presented at the 1996 SPE/DOE Tenth Improved Oil Recovery Symposium, Tulsa, April 22–24.
9. Grigg, R.B., Gregory, M.D., and Purkaple, J.D.: "The Effect of Pressure on Improved Oilflood Recovery from Tertiary Gas Injection," *SPERE* (Aug. 1997) 179.
10. Chang, S.-H., Grigg, R.B., and Huang, T.C.: "Characterization and Multiphase Equilibrium Prediction of Crude Oil Heavy Components," *Fuel Science and Technology Int'l* (1996) **14**(1&2), 179–201.
11. Grigg, R.B.: "Dynamic Phase Composition, Density, and Viscosity Measurements During CO_2 Displacement of Reservoir Oil," paper SPE 28974 presented at the 1995 SPE International Symposium on Oilfield Chemistry, San Antonio, February 14–17.
12. Holm, L.W., and Josendal, V.A.: "Mechanisms of Oil Displacement by Carbon Dioxide,"

Trans., AIME (1974) **257**, 1427–1436.

13. Yellig, W.F., and Metcalfe, R.S.: "Determination and Prediction of CO_2 Minimum Miscibility Pressures," *JPT,* (Jan. 1980) 160–168.
14. Orr, F.M., Jr., Johns, R.T., and Dindoruk, B.: "Development of Miscibility in Four-Component CO_2 Floods," *SPERE* (May 1993) 135–142.
15. Christiansen, R.L., and Kim, H.: "Apparatus and Method for Determining the Minimum Miscibility Pressure of a Gas in a Liquid," Canadian Patent No. 1,253,358.
16. Simon, R., Rosman, A., and Zana, E: "Phase-Behavior Properties of CO_2-Reservoir Oil Systems," *SPEJ* (Feb. 1978) 20-26.
17. Novosad, Z.: "On the Aspects of Reservoir Fluids Phase Behavior Important in a Design of Miscible Gas Injection Process," IOR Symposium, Stavanger, Norway, May 21–23, 1991.
18. Thomas, F.B., Holowach, N., Zhou, X.L., Bennion, D.B., and Bennion, D.W.: "A Comparative Study of RBA, P-X, Multicontact and Slim Tube Results," *J. Can. Pet. Tech.*, **33**, No. 2, (Feb. 1994) 17–26.
19. Shyeh-Yung, G.J.: "Mechanisms of Miscible Oil Recovery: Effects of Pressure on Miscible and Near Miscible Displacements of Oil by Carbon Dioxide," paper SPE 22651 presented at the 1991 Annual Technical Conference and Exhibition, Denver, CO, Oct. 9–12.
20. Lange, E.A.: "Correlation and Prediction of Residual Oil Saturation for Gas Injection EOR Processes," paper SPE/DOE 35425 presented at the 1996 SPE/DOE Symposium on Improved Oil Recovery, Tulsa, OK, April 21–24.
21. Gupta, S.P., and Trushenski, S.P.: "Micelar Flooding—Compositional Effects on Oil Displacement," *SPEJ* (April 1979) 116–128.
22. Holm, L.W., and Josendal, V.A.: "Effect of Oil Composition on Miscible-Type Displacement by Carbon Dioxide," *SPEJ* (Feb. 1982) 87–98.
23. Hagedorn, K.D.: "Component Partitioning in Carbon Dioxide/Crude Oil Mixtures," PhD dissertation, Stanford U., Stanford, CA (1992).
24. Nagarajan, N., and Robinson, Jr., R.L.: "Equilibrium Phase Compositions, Phase Densities and Interfacial Tensions for CO_2 + Hydrocarbon Systems: 2. CO_2 + n-Decane," *J. Chem. and*

Eng. Data, 31, No. 2 (1986) 168–171.

25. Schechter, D.S. and Guo, B.: " Parachors Based on Modern Physics and Their Uses in IFT Prediction of Reservoir Fluids," paper SPE 30785 presented at the 1995 SPE Annual Technical Conference and Exhibition, Dallas, October 22–25.
26. Guo, B., and Schechter, D.S.: "A Simple and Accurate Method for Determining Low IFT from Pendant Drop Measurements," paper SPE 37216 to be presented at the 1997 SPE International Symposium on Oilfield Chemistry, Houston, February 18–21.
27. Morii, S., Yazawa, N., Inoue, S., and Arihara, N.: "Effects of Oil Composition on CO_2-Flood Displacement Performance," paper presented at the 1985 European Symposium on Enhanced Oil Recovery, April 1985.
28. Rosman, A., and Zana, E.: "Experimental Studies of Low IFT Displacement by CO_2 Injection," paper SPE 6723 presented at the 1977 SPE Annual Technical Conference and Exhibition, Denver, Oct. 9–12.
29. Moore, T.F., and Slobad, R.L.: "The Effect of Viscosity and Capillarity on the Displacement of Oil by Water," *Prod. Monthly* (Aug. 1956) 20–30.
30. Catchpole, G., and Fulford, G.: Dimensionless Groups," *Ind. and Eng. Chem.*, **58**, No. 3 (March 1966) 46–60.
31. Abrams, A.: "The Influence of Fluid Viscosity, Interfacial Tension, and Flow Velocity on Residual Oil Saturation Left by Water Flood," *SPEJ*, (Oct. 1975) 473–477.
32. Schechter, D.S., Zhon, D., and Orr, F.M., Jr.: "Low IFT Drainage and Imbibition," *J. Pet. Sci. Eng.*, 11 (1994) 283.
33. Taber, J.J.,Martin, F.D.,and Seright, R.S." EOR Screening Criteria Revisited," paper SPE 35385 presented at the 1996 SPE/DOE Symposium on Improved Oil Recovery, Tulsa, April 21–24.
34. Grigg, R.B. and Schechter, D.S.: "State of the Industry in CO_2 Floods," paper SPE 38849 presented at the 1997 SPE Annual Technical Conference and Exhibition, San Antonio, TX, Oct. 6-9, 1997.
35. Grigg, R.B., Heller, J.P., and Schechter, D.S.: "Improved Efficiency of Miscible CO_2 Floods and Enhanced Prospects of CO_2 Flooding Heterogeneous Reservoirs," Annual Report,

Contract No. DE-FG22-94BC14977, U.S. DOE (April 1995).

36. Grigg, R.B. and Schechter, D.S.: "Improved Efficiency of Miscible CO_2 Floods and Enhanced Prospects of CO_2 Flooding Heterogeneous Reservoirs," annual report, Contract No. DE-FG22-94BC14977, U.S. DOE, (April 1996).
37. Grigg, R.B. and Schechter, D.S.: "Improved Efficiency of Miscible CO_2 Floods and Enhanced Prospects of CO_2 Flooding Heterogeneous Reservoirs," Final Report, Contract No. DE-FG22-94BC14977, U.S. DOE, (FEB. 1998).
38. Heller, J.P. et.al.: "Improvement of CO_2 Flood Performance," Final Report, Contract No. FC21-84MC21136, U.S. DOE, (1991).
39. Martin, F.D. et.al.: "Field Verification of CO_2 Foam," Final Report, DE-FG21-89MC26031, U.S. DOE, (February 1996).
40. Tsau, J-S., Yaghoobi, H., and Grigg, R.B.: "Smart Foam to Improve Oil Recovery in Heterogeneous Porous Media," paper SPE 39677 presented at the 1998 SPE/DOE Improved Oil Recovery Symposium, Tulsa, 19-22 April.
41. Yaghoobi, H., Tsau, J-S., and Grigg R.B.: "Effect of Foam on CO2 Breakthrough: Is This Favorable to Oil Recovery?" paper SPE 39789 presented at the 1998 SPE Permian Basin Oil and Gas Recovery Conference, Midland, 25-27 March.
42. Tsau, J-S., Yaghoobi, H., and Grigg, R.B.: "Use of Mixed Surfactants to Improve Mobility Control in CO_2 Flooding," paper SPE 39792 presented at the 1998 SPE Permian Basin Oil and Gas Recovery Conference, Midland, 25-27 March.
43. Chang, S-H. and Grigg, R.B.: "History Matching and Modeling the CO_2-Foam Pilot Test at EVGSAU," paper SPE 39793 presented at the 1998 SPE Permian Basin Oil and Gas Recovery Conference, Midland, 25-27 March.
44. Chang, S-H. and Grigg, R.B.: "Effects of Foam Quality and Flow Rate on CO_2-Foam Behavior at Reservoir Conditions," paper SPE 39679 presented at the 1998 SPE/DOE Improved Oil Recovery Symposium, Tulsa, 19-22 April.
45. Siagian, U.W.R. and Grigg, R.B.: "The Extraction of Hydrocarbons from Crude Oil by High Pressure CO2," paper SPE 39684 presented at the 1998 SPE/DOE Improved Oil Recovery Symposium, Tulsa, 19-22 April.

46. Grigg, R.B. and Siagian, U.W.R.: "Understanding and Exploiting Four Phase Flow in Low Temperature CO2 Floods," paper SPE 39790 presented at the 1998 SPE Permian Basin Oil and Gas Recovery Conference, Midland, 25-27 March.
47. Taber, J.J.: "Environmental Improvements and Better Economics in EOR Operations," *In Situ* (1990) **14**(4), 345.
48. Benham, A. L., et al.: "Miscible Fluid Displacement-Prediction of Miscibility," *Trans.*, AIME (1960) 219, 229.
49. Bernard, G.G., and Holm, L. W.: "Effect of Foam on Permeability of Porous Media to Gas," *SPEJ* (Sep. 1968) 267.
50. Caudle, B. H., and Dyes, A. B.: "Improving Miscible Displacement by Gas-Water Injection," *Trans.*, AIME (1958) 213, 281.
51. Heller, J.P., et al.: "Direct Thickeners for Mobility Control in CO_2 Floods," paper SPE 11789 presented at the 1983 International Symposium on Oilfield and Geothermal Chemistry, Denver, June 1-3.
52. Bernard, G. G., and Holm, L. W.: "Effect of Foam on Permeability of Porous Media to Gas," *SPEJ* (Sept. 1964) 267.
53. Tsau, J. S. and Heller J. P.: "Evaluation of Surfactants for CO_2-Foam Mobility Control," paper SPE 24013 presented at the 1992 SPE Permian Basin Oil and Gas Recovery Conference, Midland, March 18-20.
54. Tsau, J.S. and Grigg, R.B.: "Assessment of Foam Properties and Effectiveness in Mobility Reduction for CO_2-Foam Floods," paper SPE 37221 presented at the 1997 International Symposium on Oilfield Chemistry, Houston, Feb. 18-21.
55. Albrecht, R. A., and Marsden, S. S.: "Foams as Blocking Agents in Porous Media," *SPEJ* (March, 1970) 51.
56. Yang, S.H., and Reed, R.L.: "Mobility Control Using CO_2-Foams," paper SPE 19689 presented at the 1989 Annual Technical Conference and Exhibition San Antonio, Oct. 8-11.
57. Bernard, G.G., Holm, L.W., and Harvey, C.P.: "Use of Surfactant to Reduce CO_2 Mobility in Oil Displacement," *SPEJ* (August 1980) 281.
58. Wellington, S.L. and Vinegar, H. L.: "CT Studies of Surfactant to Reduce CO_2 Mobility

Control," paper SPE 14393 presented at the 1985 SPE Annual Technical Conference, Las Vegas, September 22-25.

59. Moradi-Araghi, A., Johnston, E.L., Zornes, D.R., and Harpole, K.J.: "Laboratory Evaluation of Surfactants for CO_2-Foam Applications at the South Cowden," paper SPE 37218 presented at the 1997 SPE International Symposium on Oilfield Chemistry, Houston, February 18-21.
60. Tsau, J.S., and Heller, J.P.: "How Can Selective Mobility Reduction of CO_2-Foam Assist in Reservoir Floods," paper SPE 35168 presented at the 1996 Permian Basin Oil and Gas Recovery Conference, Midland, March 27-29.
61. Heller, J. P., Lien, C. L., and Kuntamukkula, M. S.: "Foamlike Dispersions for Mobility Control in CO_2 Floods," *SPEJ* (August 1985) 603.
62. Lee, H.O., Heller, J.P., and Hoefer, A.M.W.: "Change in Apparent Viscosity of CO_2 Foam with Rock Permeability," *SPERE* (November 1991) 421.
63. Yaghoobi, H. and Heller, J.P.: "Laboratory Investigation of Parameters Affecting CO_2-Foam Mobility in Sandstone at Reservoir Conditions," paper SPE 29168 presented at the 1994 Eastern Regional Conference and Exhibition, Charleston, November 8-10.
64. Preditis, J. and Paulett, G.S.: "CO_2-Foam Mobility Tests at Reservoir Conditions in San Andres Cores," Paper SPE 24178 presented at the 1992 SPE/DOE Symposium on Enhanced Oil Recovery, Tulsa, April 22-24.
65. Kuehne, D.L., Frazier, R.H., Cantor, J., and Horn, W. Jr.: "Evaluation of Surfactants for CO_2 Mobility in Dolomite Reservoirs," paper 24177 presented at the 1992 SPE/DOE Symposium on Enhanced Oil Recovery, Tulsa, April 22-24.
66. Yaghoobi, H. and Heller, J.P.: "Effect of Capillary Contact on CO_2-Foam Mobility in Heterogeneous Cores," paper SPE 35169 presented at the 1996 Permian Basin Oil and Gas Recovery Conference, Midland, March 27-29.
67. Lee, H. O., and Heller, J.P.:"Laboratory Measurements of CO_2-Foam Mobility," *SPERE* August (1990) 193.
68. Kuhlman, M. I., Falls, A. H., and Wellington, S. L.: "Gas/Oil Lamellae and Surfactant Propagation in the Oil in Carbon Dioxide Foam," paper SPE/DOE 27788 presented at the

1994 Symposium on Improved Oil Recovery, Tulsa, April 17-20.

69. Yaghoobi, H. and Heller, J.P.: "Effect of Capillary Contact on CO_2-Foam Mobility in Heterogeneous Cores," paper SPE 35169 presented at the 1996 Permian Basin Oil and Gas Recovery Conference, Midland, March 27-29.
70. Hanssen, J. E., and Dalland, M.: "Foams for Effective Gas Blockage in the Presence of Crude Oil," paper SPE/DOE 20193 presented at the 1990 EOR Symposium, Tulsa, 22-25 April.
71. Yaghoobi, H.: "Experimental Evaluation of CO_2-Foam Mobility in Heterogeneous Porous Systems," PhD Dissertation, New Mexico Institute of Mining and Technology, August 1995.
72. Yaghoobi, H. and Heller, P. J.: "Laboratory Investigation of Parameters Affecting CO_2-foam Mobility in Sandstone at Reservoir Conditions," paper SPE 29168, presented at the 1994 Eastern Regional Conference and Exhibition, Charleston, Nov. 8-10.
73. Kuhlman, M. I.: "Visualizing the Effect of Light Oil on CO_2 Foams," *JPT* (July, 1990) 902.
74. Nikolov, A. D., Wasan, D. T., Huang, D. W., and Edwards, D. A.: "The Effect of Oil on Foam Stability: Mechanisms and Implications for Oil Displacement by Foam in Porous Media," paper SPE 15443 presented at the 1986 Annual Technical Conference and Exhibition, New Orleans, Oct. 5-8.
75. Parra, M. G., and Scag, A.: "A Foam Pilot in a North Sea Oil Reservoir: Preparation for a Production Well Treatment," paper SPE 18599 presented at the 1994 Annual Technical Conference and Exhibition, New Orleans, LA, Sept. 25-28.
76. Rosen, W. R., and Lu, Q.:"Effect of Capillary Crossflow on Foam Improved Oil Recovery," paper SPE 38319 presented at the 1997 SPE Western Regional Meeting, Long Beach, June 25-27.
77. Heller, J.P.: "Reservoir Application of Mobility Control Foams in CO_2 Floods," paper SPE/DOE 12644 presented at the 1984 SPE/DOE Fourth Joint Symposium on Enhanced Oil Recovery, Tulsa, April 15-18.
78. Dellenger, S.E., Holbrook, S.T. and Patton, J.T.: "CO_2 Mobility Control," *SPEJ*, April 1984, 191.
79. Borchardt, J.K, *et.al.*, S.L.: "Surfactants for CO_2 Foam Flooding," paper SPE 14394 presented at the 1985 Annual Technical Conference and Exposition of the Society of

Petroleum Engineers, Las Vegas, September 22-25.

80. Suffridge, F.E., Raterman, K.T. and Russell, G.C.: "Foam Performance Under Reservoir Conditions," paper SPE 19691 presented at the 1989 Annual Technical Conference and Exposition of the Society of Petroleum Engineers, San Antonio, October 8-11.
81. Chou, S.I.: "Conditions for Generating Foam in Porous Media," paper SPE 22628 presented at the 1991 Annual Technical Conference and Exposition of the Society of Petroleum Engineers, Dallas, Oct. 6-9.
82. Sharma, M.K., Shah, D.O. and Brigham, W.E.: "Effect of Mixed-Chain-Length Surfactants on Fluid Displacement in Porous Media by In-Situ Foaming Process," *SPERE*, May 1986, 253-260.
83. Llave, F.M. and Olsen, D.K.: "Use of Mixed Surfactants to Generate Foams for Mobility Control in Chemical Flooding," paper SPE/DOE 20223 presented at the 1990 SPE/DOE Symposium on Enhanced Oil Recovery, Tulsa, April 22-25.
84. Bernard, G.G., Holm, L.W., and Jacobs, W.L.: "Effect of Foam on Trapped Gas Saturation and on Permeability of Porous Media to Water," *SPEJ* (Dec. 1965) 295.
85. Falls, A.H., *et.al.*: "Development of a Mechanistic Foam Simulator: The Population Balance and Generation by Snap-Off," *SPERE* (Aug. 1988) 884.
86. Casteel, J.F. and Djabbarah, N.F.: "Sweep Improvement in CO_2-Flooding by Use of Foaming Agents," *SPERE* (Nov. 1988) 1186.
87. Lee, H.O. and Heller, J.P.: "Mobility of Foam in Porous Rocks," *Oilfield Chemistry: Enhanced Recovery and Production Stimulation*, J.K. Borchardt and T.F. Yen (Eds.), ACS Symposium Series No. 396 (1989) Chap. 27.
88. Kuhlman, M.I., *et.al.*: "CO_2 Foam with Surfactants Used Below Their Critical Micelle Concentrations," *SPERE* (Nov. 1992) 445.
89. Chang, S.-H. and Grigg, R.B.: "Laboratory Flow Tests Used to Determine Reservoir Simulator Foam Parameters," paper SPE 27675 presented at the 1994 SPE Permian Basin Oil and Gas Recovery Conference, Midland, March 16-18.
90. Tsau, J.S., *et.al.*: "CO_2-Foam Field Verification Pilot Test at EVGSAU: Phase IIIA - Surfactant Performance Characterization and Quality Assurance," paper SPE 27785

presented at the 1994 SPE/DOE Symposium on Improved Oil Recovery, Tulsa, April 17-20.

91. Martin, F.D., Stevens, J.E., and Harpole, K.J.: "CO_2-Foam Field Test at the East Vacuum Grayburg/San Andres Unit," *SPERE* (Nov. 1995) 266.
92. Hoefner, M.L. and Evans, E.M.: "CO_2 Foam: Results from Four Developmental Field Trials," *SPERE* (Nov. 1995) 273.
93. Marsden, S.S. and Khan, S.A.: "The Flow of Foam Through Short Porous Media and Apparent Viscosity Measurements," *SPEJ* (March 1966) 17.
94. Patton, J.T., Holbrook, S.T., and Hsu, W.: "Rheology of Mobility-Control Foams," *SPEJ* (June 1983) 456.
95. Persoff, P., *et. al.*: "A Laboratory Investigation of Foam Flow in Sandstone at Elevated Pressure," *SPERE* (Aug. 1991) 365.
96. Huh, D.G. and Handy, L.L.: "Comparison of Steady- and Unsteady-State Flow of Gas and Foaming Solution in Porous Media," *SPERE* (Feb. 1989) 77.
97. Lee, H.O. and Heller, J.P.: "Mobility of Foam in Porous Rocks," *Oilfield Chemistry: Enhanced Recovery and Production Stimulation*, J.K. Borchardt and T.F. Yen (Eds.), ACS Symposium Series No. 396 (1989) Chap. 27.
98. Hoefner, M.L. and Evans, E.M.: "CO_2 Foam: Results from Four Developmental Field Trials," *SPERE* (Nov. 1995) 273.
99. Chang, S.-H. and Grigg, R.B.: "Laboratory Flow Tests Used to Determine Reservoir Simulator Foam Parameters," paper SPE 27675 presented at the 1994 SPE Permian Basin Oil and Gas Recovery Conference, Midland, March 16-18.
100. Chang, S.-H. and Grigg, R.B.: "Foam Displacement Modeling in CO_2 Flooding Processes," paper SPE/DOE 35401 presented at the 1996 SPE/DOE Symposium on Improved Oil Recovery, Tulsa, April 21-24.
101. Ammer, J.R., Brummert, A.C., and Sams, W.N.: "Miscible Applied Simulation Techniques for Energy Recovery–Version 2.0," Report to U.S. Department of Energy, Contract No. DOE/BC-91/2/SP (February 1991).
102. Brownlee, M.H. and Sugg, L.A.: "East Vacuum Grayburg-San Andres Unit CO_2 Injection Project: Development and Results to Date," paper SPE 16721 presented at the 1987 SPE

Annual Technical Conference and Exhibition, Dallas, Sept. 27-30.

103. Bangla, V.K., Yau, F.F. and Hendricks, G.R.: "Reservoir Performance of a Gravity-Stable, Vertical CO_2 Miscible Flood: Wolfcamp Reef Reservoir, Wellman Unit," SPE Reservoir Engineering, Nov. 1993.

104. Nagai, R.B. and Redmond, G.W.: "Numerical Simulation of a Gravity-Stable, Miscible CO_2 Injection Project in a West Texas Carbonate Reef," paper SPE 11129 presented at the 1993 Middle East Oil Technical Conference, Manama, Bahrain, March 14-17.

105. Schneider, B.D., Hogan, G.P. and Holt, W.N., Jr.: "Using Pulsed Neutron Decay-Spectrum Data and Multi-Inflatable Packer Plugdown Assemblies Improve Oil Production Rates in a Mature CO_2 Flood," paper SPE 35165 presented at the 1996 Permian Basin Oil and Gas Recovery, Midland, March 27-29.

106. Mungan, M.: "Carbon Dioxide Flooding - Fundamentals," *JCPT* (Jan. - March 1981) 87.

107. Yellig, W.F. and Metcalfe, R.S., "Determination and Prediction of CO_2 Minimum Miscibility Pressure," *JPT* (January 1980) 160.

108. Orr, F.M. Jr. and Jensen, C.M.: "Interpretation of Pressure-Composition Phase Diagrams for CO_2/Crude-Oil Systems," *SPEJ* (October 1984) 485.

109. ERCO Petroleum Services, Inc.: "Miscible - PVT Analysis, Union Texas Petroleum, Wellman Field, Terry County, Texas." & Core Laboratory Inc.: "Packed Column Displacement Study, Union Texas Petroleum, Wellman Field, Terry County, Texas," RFL 880266, September 13, 1988.

110. Glaso, O.: "Generalized Minimum Miscibility Pressure Correlation," *SPEJ* (December 1985) 927.

111. Beliveau, D., Payne, D.A., and Mundry, M.: "Waterflood and CO_2 Flood of the Fractured Midale Field," *JPT* (Sept. 1993) 881.

112. Schechter, D.S., McDonald, P., Sheffield, T., and Baker, R.: "Reservoir Characterization and CO_2 Pilot Design in the Naturally Fractured Spraberry Trend Area," paper SPE 35469 presented at the 1996 Permian Basin Oil & Gas Recovery Conference, Midland, March 27–29.

113. Schechter, D.S.: "Advanced Reservoir Characterization and Evaluation of CO_2 Gravity

Drainage in the Naturally Fractured Spraberry Trend Area," First Annual Technical Progress Report, U.S. DOE Contract No. DE-FC22-95BC14942, (Dec 1996).

114. Schechter, D.S. and Guo, B.: "Mathematical Modeling of Gravity Drainage After Gas Injection Into Fractured Reservoirs," paper SPE 35170 presented at the 1996 Improved Oil Recovery Symposium, Tulsa, April 22–24.
115. Pontious, S.B. and Tham, M.J.: "North Cross (Devonian) Unit CO_2 Flood – Review of Flood Performance and Numerical Simulation Model, " paper SPE 6390 presented at the 1977 SPE-AIME Permian Basin Oil and Gas Recovery Conference, Midland, March 10-11.
116. Greenwalt, W.A., Vela, S., Christian, L.D. and Shirer, J.A.: "A Field Test of Nitrogen WAG Injectivity," paper SPE 8816 presented at the 1980 SPE/DOE Symposium on Enhanced Oil Recovery, Tulsa, April 20-23.
117. Henry, R.L., Feather, G.L., Smith, L.R. and Fussell, D.D.: "Utilization of Composition Observation Wells in a West Texas CO_2 Pilot Flood," paper SPE 9786 presented at the 1981 SPE/DOE Symposium on Oil Recovery, Tulsa, April 5-8.
118. Rowe, H.G., Yor, S.D., and Ader, J.C.: "Slaughter Estate Unit Tertiary Pilot Performance," *JPT* (March 1982), 613-620.
119. Hopkins, C.W., Wu, C.H. and Poston, S.W.: "A Simple Segregated Flow Model for a WAG Process," paper SPE 15016 presented at the 1986 SPE Permian Basin Oil & Gas Recovery Conference, Midland, March 13-14.
120. Pittaway, K.R., Albright, J.C., and Hoover, J.W.: "The Maljamar Carbon Dioxide Pilot: Review and Results," paper SPE/DOE 14940 presented at the 1986 SPE/DOE Symposium on Enhanced Oil Recovery, Tulsa, April 20-23.
121. Champion, J.H. and Sheldon, J.B.: "An Immiscible WAG Injection Project in the Kuparuk River Unit," paper SPE 16719 presented at the 62nd SPE Annual Technical Conference and Exhibition, Dallas, September 27-30.
122. Christman, P.G. and Gorell, S.B.: "Comparison of Laboratory- and Field-Observed CO_2 Tertiary Injectivity," *JPT* (Feb. 1990), 226-233.
123. Prieditis, J., Wolle, C.R., and Notz, P.K.: "A Laboratory and Field Injectivity Study: CO_2 WAG in the San Andres Formation of West Texas," paper SPE 22653 presented at the 65th

SPE Annual Technical Conference and Exhibition, Dallas, October 6-9.

124. Roper, Jr., M.K., Cheng, C.T., Varnon, J.E., and Pope, G.A.: "Interpretation of a CO_2 WAG Injectivity Test in the San Andres Formation Using a Compositional Simulator," paper SPE 24163 presented at the 1992 SPE/DOE Symposium on Enhanced Oil Recovery, Tulsa, April 22-24.

125. Tanner, C.S., Baxley, P.T., Crump, J.G. and Miller, W.C.: "Production Performance of the Wasson Denver Unit CO_2 Flood," paper SPE 24156 presented at the 1992 SPE/DOE Symposium on Enhanced Oil Recovery, April 22-24.

Table 1. Properties of Composite and Single Cores

Composite core sample	Center Region				Annulus Region			
	Type	**K (md)**	**φ**	**Area (cm^2)**	**Type**	**K (md)**	**φ**	**Area (cm^2)**
Isolated	Fired Berea sandstone	120	0.19	1.27	Fired Berea Sandstone	590	0.23	7.58
Capillary contact	Fired Silica sand	450	0.19	2.01	Fired Berea Sandstone	1250	0.22	7.94

Length of the isolated coaxial core = 6.0 cm
Length of the capillary contact core = 6.7 cm

Core sample	Type	K (md)	φ	Area (cm^2)
Single	Fired Berea sandstone	840	0.23	10.64

Length of the single core = 6.5cm
Pore volume= 15.62 cm^3

Table 2. Surfactant and Brine Properties

Surfactant	Conc. (PPM)	pH	Type	Active (%)	Formula
Chase™ CD1045	500	6.05	Anionic	46.7	(Not available) Manufactured by Chase International
	2500	5.88			
Brine	20000	5.75	----------	100	1.5 Wt % NaCl & 0.5 Wt % $CaCl_2$

Table 3. Summary of Single Core Experiments

Run #	Description	Q_t (cc/hr)/(ft/d)	Ratio	Breakthrough (PV)
1	CO_2 displaced brine	16.00 / 1.2	1	0.35
2	CO_2/Brine displaced brine	16.45 / 1.3	4:1	0.38
3	CO_2 displaced surf. (500 ppm)	16.00 / 1.2	1	0.79
4	CO_2/Surf. displaced surf. (500 ppm)	16.45 / 1.3	4:1	1.29
5	CO_2 displaced oil	16.00 / 1.2	1	0.29
6	CO_2/Brine displaced oil	16.45 / 1.3	4:1	0.44
7	CO_2/Surf displaced oil @ 500 ppm	16.45 / 1.3	4:1	0.51
8	CO_2/Surf displaced oil @ 2500 ppm	16.45 / 1.3	4:1	0.50

Table 4. Summary of Isolated Coaxial Composite Core Experiments

Run #	Description	Q_t (cc/hr)/(ft/d)	Ratio	Breakthrough in annulus region (PV)	Breakthrough in center region (PV)
1	CO_2 displaced brine	16.45/1.3	4:1	0.63	1.13
2	CO_2/brine displaced brine	16.45/1.3	4:1	0.64	1.17
3	CO_2-foam displaced surf.	16.00/1.2	1	1.12	1.86
4	CO_2 displaced oil	16.45/1.3	4:1	0.24	N/A
5	CO_2/brine displaced oil	16.45/1.3	4:1	0.74	N/A
6	CO_2-foam displaced oil	16.45/1.3	4:1	0.88	2.56

N/A: no breakthrough was observed

Table 5. Summary of Composite Core Experiments

Run #	Description	Q_t (cc/hr)/ (ft/d)	Ratio	Breakthrough in Annulus region (PV)	Breakthrough in center region (PV)
1	CO_2/brine displaced brine	16.45/1.3	4:1	0.42	0.62
2	CO_2/Surf. displaced surf. @ 2500 ppm	16.45/1.3	4:1	0.66	0.61
3	CO_2 displaced oil	16.00/1.2	1	0.44	0.50
4	CO_2/brine displaced oil	16.45/1.3	4:1	0.46	0.61
5	CO_2/surf displaced oil @ 2500 ppm	16.45/1.3	4:1	0.86	0.34

Table 6. Summary of Capillary Contact Composite Core Experiments

Run #	Description	Q_t (cc/hr)/ (ft/d)	Ratio	Breakthrough in Annulus region (PV)	Breakthrough in center region (PV)
1	CO_2/brine displaced brine	16.45/1.3	4:1	0.42	0.62
2	CO_2-foam displaced surf.	16.45/1.3	4:1	0.66	0.61
3	CO_2 displaced oil	16.00/1.2	1	0.44	0.50
4	CO_2/brine displaced oil	16.45/1.3	4:1	0.46	0.61
5	CO_2-foam displaced oil	16.45/1.3	4:1	0.86	0.34

Table 7. Foaming Agents Tested

Surfactant	Type	Active wt%	Formula	Manufacture
Chaser™ CD1040	Anionic	40.0	Alpha Olefin Sulfonate	Chaser International
Chaser™CD1050	Nonionic	70.0	Alkyl Phenol Ethoxylate	Chaser International
Alipa®CD128	Anionic	58.0	Ethoxylated alcohol sulfate	GAF
Dowfax™ 8390	Anionic	35.0	C16-diphenylether disulfonate	Dow Chemical

Table 8. Interfacial Tension Between CO_2 and Aqueous Phase

Aqueous phase	Surfactant concentration	IFT (dyne/cm)
Brine	0 wt%	23.03
8390	0.025 wt%	12.24
8390	0.05 wt%	9.78
CD1040	0.025 wt%	6.55
CD1040	0.05 wt%	3.83
CD1050	0.025 wt%	4.96
CD1050	0.05 wt%	4.35
CD128	0.025 wt%	3.74
CD128	0.05 wt%	3.29
CD1040+8390	0.05 wt%	9.30
CD128+8390	0.05 wt%	6.89
CD1050+8390	0.05 wt%	6.06
CD1040+CD1050	0.05 wt%	4.48
CD128+CD1050	0.05 wt%	3.61
CD128+CD1040	0.05 wt%	3.48

Table 9. Mobility Data in Composite Core with Single Surfactant System				
Fluid Injected	**Injection rate (cc/hr)**	**Mobility in Section #1 (md/cp)**	**Mobility in Section #2 (md/cp)**	**Mobility in Section #3 (md/cp)**
Brine	15	550	345	270
Brine/CO2	15	470.5	264.8	195.7
	10	449.0	254.5	182.9
	5	420.2	237.9	173.1
0.05 wt % CD1050/CO2	15	5.6	4.2	3.7
	10	4.4	3.5	3.1
	5	3.5	2.9	2.6
0.05 wt% CD128/CO2	15	23.3	16.0	13.3
	10	19.9	14.3	12.1
	5	17.9	13.0	11.0
0.05 wt% 8390/CO2	15	310.6	186.8	143.0
	10	308.3	183.7	140.0
	5	246.0	237.9	175.1
0.05 wt% CD1040/CO2	15	211.1	129.4	100.0
	10	175.8	109.7	85.7
	5	135.6	87.5	69.5
0.025 wt % CD1050/CO2	15	32.0	21.5	17.5
	10	26.5	18.1	14.8
	5	23.4	16.1	13.2
0.025 wt% CD128/CO2	15	75.0	48.6	38.6
	10	58.5	38.5	30.9
	5	45.4	30.5	24.7
0.025 wt% 8390/CO2	15	407.0	233.0	173.0
	10	388.6	222.0	165.5
	5	359.6	207.4	155.3
0.025 wt% CD1040/CO2	15	289.0	173.0	132.0
	10	269.0	160.9	122.9
	5	255.1	155.2	120.0

Table 10. Mobility Data in Composite Core with 0.05 wt% of Mixed Surfactant System

Fluid Injected	Injection rate (cc/hr)	Mobility in Section #1 (md/cp)	Mobility in Section #2 (md/cp)	Mobility in Section #3 (md/cp)	SMR (slope value)
CS4090/CO2	15	300.6	175.0	132.2	1.16
	10	288.9	165.7	123.9	1.19
	5	249.8	237.9	173.1	1.13
CS2890/CO2	15	223.8	131.2	101.3	1.12
	10	198.4	118.6	90.8	1.10
	5	170.7	106.2	82.4	1.03
CS5090/CO2	15	77.9	49.2	38.9	0.98
	10	50.7	33.7	25.4	0.96
	5	40.3	26.4	21.1	0.91
CS2840/CO2	15	36.4	24.4	19.7	0.86
	10	31.8	21.7	17.7	0.83
	5	23.9	16.2	13.1	0.85
CS4050/CO2	15	8.5	6.4	5.4	0.64
	10	7.1	5.3	4.6	0.61
	5	5.7	4.3	3.7	0.61
CS2850/CO2	15	6.2	4.7	4.1	0.58
	10	5.6	4.4	3.7	0.57
	5	4.2	3.3	2.9	0.52

CS4090: CD1040 + 8390, CS2890: CD128 + 8390, CS5090: CD1050 + 8390, CS2840: CD128 + CD1040, CS4050: CD1040 + CD1050, and CS2850: CD128 + CD1050

Table 11. Composition of Synthetic Brine

Component	Weight* (g)
NaCl	61.26
KCl	0.58
$CaCl_2\ 2H_2O$	10.86
$MgCl_2\ 6H_2O$	5.19
Na_2SO_4	5.91
H_2O	1916.20

* Based on 2000 g brine solution

Table 12. Core Properties

Core	Length (cm)	Diameter (cm)	Porosity	Pore Volume (cc)	Initial Brine Perm. (md)
E	3.51	1.27	0.25	1.10	110.1
F	2.79	1.27	0.25	0.87	184.3

Table 13. Summary of Baseline Experiments

Core #	Total Flow Rate (cc/hr)	CO_2 Fraction	Pressure Drop (psid)	Total Mobility (md/cp)	Total Interstitial Velocity (ft/day)
E	4.2	0.200	1.34	35.40	10.57
	4.2	0.500	3.72	12.75	10.57
	4.2	0.800	4.91	9.66	10.57
Group A	16.8	1.000	1.45	130.87	42.28
	16.8	0.800	2.44	77.77	42.28
	16.8	0.667	3.24	58.57	42.28
	16.8	0.500	3.53	53.76	42.28
	16.8	0.333	2.49	76.21	42.28
	16.8	0.200	2.07	91.67	42.28
	16.8	0.000	1.03	184.24	42.28
Group B	16.8	0.200	2.67	71.07	42.28
	16.8	0.333	3.14	60.44	42.28
	16.8	0.500	3.34	56.82	42.28
	16.8	0.667	3.35	56.65	42.28
	16.8	0.800	3.36	56.48	42.28
	16.8	1.000	3.09	61.41	42.28
F	4.2	0.500	0.83	45.56	10.57
	8.4	0.500	1.37	55.21	21.14
	16.8	0.500	2.70	56.02	42.28
	4.2	0.500	0.80	47.27	10.57
	4.2	0.800	1.66	22.78	10.57
	8.4	0.800	2.34	32.32	21.14
	16.8	0.800	3.71	40.77	42.28
	4.2	0.200	1.31	28.87	10.57
	8.4	0.200	2.59	29.20	21.14
	8.4	0.800	3.30	22.92	21.14
	4.2	0.200	1.82	20.78	10.57
	8.4	0.200	3.12	24.24	21.14
	4.2	0.667	2.37	15.96	10.57
	8.4	0.667	3.46	21.86	21.14
	16.8	0.667	6.04	25.04	42.28
	16.8	0.333	6.28	24.09	42.28
	8.4	0.333	3.81	19.85	21.14
	4.2	0.333	2.65	14.27	10.57

Table 14. Summary of Foam Experiments

Core #	Total Flow Rate (cc/hr)	Foam Quality (%)	Pressure Drop (psid)	Total Mobility (md/cp)	Total Interstitial Velocity (ft/day)	WAG Mobility (md/cp)	Resistance Factor
E	4.2	20	106.6	0.45	10.57	35.40	79.52
	4.2	50	105.1	0.45	10.57	12.75	28.26
	4.2	80	134.8	0.35	10.57	9.66	27.45
F	4.2	50	78.9	0.48	10.57	22.67	47.28
	8.4	50	88.2	0.86	21.14	22.67	26.45
	16.8	50	101.7	1.49	42.28	22.67	15.24
	4.2	50	79.0	0.48	10.57	22.67	47.35
	4.2	20	79.1	0.48	10.57	25.63	53.62
	8.4	20	78.5	0.96	21.14	25.63	26.61
	16.8	20	86.8	1.74	42.28	25.63	14.70
	4.2	80	81.8	0.46	10.57	36.41	78.78
	8.4	80	101.6	0.74	21.14	36.41	48.90
	16.8	80	131.3	1.15	42.28	36.41	31.60

Table 15. Wellman Unit Reservoir Characteristics

Geologic Age	Permian
Producing Formation	Wolfcamp
Lithology	Limestone, Vugular dense to coarsely granular dolomite, extensive vertical fracturing
Initial Oil-Water Contact, ft ss	6680
Average Porosity, %	8.5
Average Permeability, md	135
Initial Reservoir Pressure, psia	4115 @ - 6300 ft
Current Reservoir Pressure (08/96), psia	2050 @ - 6300 ft
Reservoir Temperature, °F	151
Initial Gross Oil Column, ft	824
Reservoir Drive Mechanism	Water Drive
Primary Recovery, MMSTBO	41.8
Primary Recovery, %	34.3
Secondary Recovery, MMSTBO	23.9
Secondary Recovery, %	19.5
Tertiary Recovery @7-1-97, MMSTBO	7.2
Tertiary Recovery @7-1-97, %	6
CO_2 Utilization through 10-93, MCF/STBO	7.85
CO_2 Utilization from 11-93 through 7-1-97, MCF/STBO	2.25
API Gravity of Oil	43.5
Bubble Point Pressure, psia	1248
Solution GOR, SCF/STB	503
Oil Viscosity @2000 psi, cp	0.4
Original Oil FVF	1.302
Oil FVF @2000psi, RB/STB	1.330
HC Gas FVF @2000 psi, RB/MSCF	1.142
CO_2 Gas FVF @2000 psi, RB/MSCF	0.6
Water Viscosity, cp	0.7
Water Compressibility, psi^{-1}	3×10^{-6}
Rock Compressibility, psi^{-1}	5×10^{-6}
Formation Water Density, lb/ft^3	62
Residual Oil Saturation to Water	0.32
Residual Oil Saturation to CO_2	0.15
Critical Gas Saturation	0.05
Irreducible Water Saturation	0.2
Minimum Miscibility Pressure, psia	1600

Table 16. Composition of Separator Gas

— COMPONENT —	— Assigned Values — Density g./cm^3 @60 F	Molecular Weight	Mol Percent	Weight Percent
Hydrogen Sulfide	0.801	34	0.00	0.00
Carbon Dioxide	0.817	44	3.41	6.20
Nitrogen	0.809	28	6.25	7.23
Methane	0.300	16	63.60	42.19
Ethane	0.356	30	12.64	15.72
Propane	0.507	44	10.24	18.68
Butanes	0.573	58	2.88	6.92
Pentanes	0.627	72	0.71	2.12
Hexanes	0.690	84	0.27	0.93
Heptanes	0.727	96	0.00	0.00
Octanes	0.749	107	0.00	0.00
Nonanes	0.768	121	0.00	0.00
Decanes	0.782	134	0.00	0.00
			100.00	100.00
Properties of Separator Gas				
Molecular Weight		24.18		

Table 17. Composition of Separator Oil: GOR = 150

	--- Assigned Values ---			
	Density	Molecular	Mol	Weight
--- COMPONENT ---	g./cm^3 @60 F	Weight	Percent	Percent
Hydrogen Sulfide	0.801	34	0.00	0.00
Carbon Dioxide	0.817	44	0.34	0.10
Nitrogen	0.809	28	0.08	0.02
Methane	0.300	16	2.67	0.29
Ethane	0.356	30	3.44	0.70
Propane	0.507	44	8.29	2.48
Butanes	0.573	58	7.58	2.99
Pentanes	0.627	72	6.67	3.27
Hexanes	0.690	84	8.18	4.66
Heptanes	0.727	96	12.42	8.09
Octanes	0.749	107	7.73	5.61
Nonanes	0.768	121	5.34	4.39
Decanes	0.782	134	4.60	4.18
Undecanes	0.793	147	3.51	3.50
Dodecanes	0.804	161	2.96	3.24
Tridecanes	0.815	175	2.75	3.26
Tetradecanes	0.826	190	2.11	2.73
Pentadecanes	0.836	206	1.65	2.31
Hexadecanes	0.843	222	1.62	2.43
Heptadecanes	0.851	237	1.67	2.68
Octadecanes	0.856	251	1.20	2.04
Nonadecanes	0.861	263	1.22	2.17
Eicosanes	0.866	275	0.88	1.65
Heneicosane	0.871	291	0.81	1.59
Docosane	0.876	300	0.77	1.57
Tricosanes	0.881	312	0.49	1.03
Tetracosanes	0.885	324	0.65	1.43
Pentacosanes	0.888	337	0.64	1.45
Hexacosanes	0.892	349	0.41	0.98
Heptacosanes	0.896	360	0.63	1.54
Octacosanes	0.899	372	0.42	1.07
Nonacosanes	0.902	382	0.67	1.74
Triacontanes	0.905	394	0.45	1.21
Hentriacontane	0.909	404	0.47	1.29
Dotriacontane	0.912	415	0.48	1.35
Tritriacontanes	0.915	426	0.79	2.27
Tetratricontanes	0.917	437	0.58	1.71
Pentatricontanes	0.920	445	0.62	1.87
Hexatricontanes	0.922	456	0.64	1.97
Heptatricontanes Plus	0.940	539	3.59	13.15
Properties of the Heavy Fractions, estimated from GC Simulated Distillation				
Heptanes plus	0.840	201	62.75	85.49
Undecanes Plus	0.877	285	32.66	63.22
Pentadecanes plus	0.897	349	21.33	50.49
Eicosanes plus	0.912	410	13.98	38.86

Properties of Separator Oil	
Molecular Weight calculated from GC results	147 g/mole
Density, gm/cc @ 75 F and 1000 psig (measured)	0.831 g/cc
Density, gm/cc @ 138 F and 1000 psig (measured)	0.809 g/cc

Table 18. Composition of Recombined Reservoir Oil: GOR=400

	— Assigned Values —			
— COMPONENT —	Density g./cm^3 @60 F	Molecular Weight	Mol Percent	Weight Percent
Hydrogen Sulfide	0.801	34	0.00	0.00
Carbon Dioxide	0.817	44	1.07	0.40
Nitrogen	0.809	28	1.55	0.37
Methane	0.300	16	17.13	2.33
Ethane	0.356	30	5.62	1.43
Propane	0.507	44	8.75	3.27
Butanes	0.573	58	6.47	3.18
Pentanes	0.627	72	5.26	3.21
Hexanes	0.690	84	6.30	4.48
Heptanes	0.727	96	9.47	7.70
Octanes	0.749	107	5.90	5.34
Nonanes	0.768	121	4.07	4.17
Decanes	0.782	134	3.50	3.98
Undecanes	0.793	147	2.68	3.33
Dodecanes	0.804	161	2.26	3.08
Tridecanes	0.815	175	2.10	3.11
Tetradecanes	0.826	190	1.61	2.59
Pentadecanes	0.836	206	1.26	2.20
Hexadecanes	0.843	222	1.23	2.32
Heptadecanes	0.851	237	1.27	2.55
Octadecanes	0.856	251	0.91	1.94
Nonadecanes	0.861	263	0.93	2.06
Eicosanes	0.866	275	0.67	1.57
Heneicosane	0.871	291	0.62	1.52
Docosane	0.876	300	0.59	1.49
Tricosanes	0.881	312	0.37	0.98
Tetracosanes	0.885	324	0.50	1.36
Pentacosanes	0.888	337	0.48	1.38
Hexacosanes	0.892	349	0.32	0.93
Heptacosanes	0.896	360	0.48	1.46
Octacosanes	0.899	372	0.32	1.01
Nonacosanes	0.902	382	0.51	1.65
Triacontanes	0.905	394	0.34	1.15
Hentriacontane	0.909	404	0.36	1.23
Dotriacontane	0.912	415	0.37	1.28
Tritriacontanes	0.915	426	0.60	2.16
Tetratricontanes	0.917	437	0.44	1.62
Pentatricontanes	0.920	445	0.47	1.78
Hexatricontanes	0.922	456	0.49	1.88
Heptatricontanes Plus	0.940	539	2.74	12.51
Properties of the Heavy Fractions, estimated from GC Simulated Distillation				
Heptanes plus	0.840	201	47.86	81.34
Undecanes Plus	0.877	285	24.91	60.15
Pentadecanes plus	0.897	349	16.27	48.04
Eicosanes plus	0.912	410	10.66	36.98

Properties of Reservoir Oil	
Molecular Weight calculated from GC results	118 g/mole
Density, gm/cc @ 151 F and Bubble point pressure (1118 psi)	0.7569 g/cc

Table 19. Composition of Recombined Reservoir Oil: GOR=600

	--- Assigned Values ---			
	Density	Molecular	Mol	Weight
— COMPONENT —	g./cm^3 @60 F	Weight	Percent	Percent
Hydrogen Sulfide	0.801	34	0.00	0.00
Carbon Dioxide	0.817	44	1.32	0.54
Nitrogen	0.809	28	2.04	0.53
Methane	0.300	16	22.06	3.27
Ethane	0.356	30	6.37	1.77
Propane	0.507	44	8.91	3.63
Butanes	0.573	58	6.09	3.27
Pentanes	0.627	72	4.78	3.19
Hexanes	0.690	84	5.66	4.40
Heptanes	0.727	96	8.47	7.52
Octanes	0.749	107	5.27	5.21
Nonanes	0.768	121	3.64	4.07
Decanes	0.782	134	3.13	3.88
Undecanes	0.793	147	2.39	3.25
Dodecanes	0.804	161	2.02	3.01
Tridecanes	0.815	175	1.87	3.03
Tetradecanes	0.826	190	1.44	2.53
Pentadecanes	0.836	206	1.13	2.15
Hexadecanes	0.843	222	1.10	2.26
Heptadecanes	0.851	237	1.14	2.49
Octadecanes	0.856	251	0.82	1.89
Nonadecanes	0.861	263	0.83	2.02
Eicosanes	0.866	275	0.60	1.53
Heneicosane	0.871	291	0.55	1.48
Docosane	0.876	300	0.52	1.45
Tricosanes	0.881	312	0.33	0.96
Tetracosanes	0.885	324	0.44	1.33
Pentacosanes	0.888	337	0.43	1.35
Hexacosanes	0.892	349	0.28	0.91
Heptacosanes	0.896	360	0.43	1.43
Octacosanes	0.899	372	0.29	0.99
Nonacosanes	0.902	382	0.46	1.61
Triacontanes	0.905	394	0.31	1.12
Hentriacontane	0.909	404	0.32	1.20
Dotriacontane	0.912	415	0.33	1.25
Tritriacontanes	0.915	426	0.54	2.11
Tetratricontanes	0.917	437	0.39	1.59
Pentatricontanes	0.920	445	0.42	1.73
Hexatricontanes	0.922	456	0.43	1.83
Heptatricontanes Plus	0.940	539	2.45	12.21
Properties of the Heavy Fractions, estimated from GC Simulated Distillation				
Heptanes plus	0.840	201	42.78	79.41
Undecanes Plus	0.877	285	22.27	58.72
Pentadecanes plus	0.897	349	14.54	46.90
Eicosanes plus	0.912	410	9.53	36.10
Properties of Reservoir Oil				
Molecular Weight calculated from GC results			108 g/mole	

Table 20. Pressure-Volume Relations at 151°F: GOR=400

Pressure Psig		Relative Volume(1)	Y Function(2)	Density gm/cc
3257		0.951		0.796
2617		0.963		0.786
2020		0.976		0.776
1508		0.988		0.766
1118	Bubble Pt	1.000		0.757
1114		1.001	3.36	
1109		1.002	3.37	
1068		1.014	3.24	
1032		1.028	2.99	
1005		1.041	2.72	
953		1.067	2.54	
910		1.094	2.40	
834		1.147	2.28	
774		1.200	2.19	
722		1.253	2.13	
627		1.386	1.99	
555		1.518	1.91	
502		1.651	1.84	

(1) Relative Volume: V/Vsat is barrels at indicated pressure per barrel at saturation
(2) Y Function: (Psat-P)/((Pabs)*((V/Vsat)-1))

Table 21. Pressure-Volume Relations at 151°F: GOR=600

Pressure Psig		Relative Volume(1)
2970		0.972
2481		0.980
2064		0.988
1693		0.995
1683		0.997
1539		0.997
1484		0.998
1480	Bubble Pt.	1.000
1470		1.003
1451		1.007
1370		1.030
1277		1.063
1205		1.096
1146		1.130
1048		1.196
949		1.263
903		1.312
845		1.362

(1) Relative Volume: V/Vsat, barrels at indicated pressure barrels at saturation pressure.

Table 22a. 150 GOR Oil Recovery vs. Pressure Slim Tube Tests Summary

Press	@BT	1.2 PV	ULT.
1400	67.63%	68.97%	69.07%
1500	79.03%	80.57%	80.57%
1550	86.12%	88.42%	88.42%
1600	86.12%	89.95%	90.05%
1700	89.76%	94.46%	94.55%
1800	87.27%	94.74%	94.84%

Table 22b. 150 GOR Oil Slim Tube Data at 1400 psig. FVF: 1.14

Time Min.	CO_2 injected cm^3	%PV	ΔP	Recovery cum. %	
10	5.0	4%	33	2.9%	
15	7.5	6%	28	8.6%	
30	15.0	13%	22	13.4%	
45	22.5	19%	22	15.3%	
60	30.0	25%	18	22.0%	
80	40.0	34%	21	30.5%	
100	50.0	42%	20	36.2%	
120	60.0	50%	16	40.8%	
140	70.0	59%	11	43.6%	
160	80.0	67%	9	48.9%	
180	90.0	76%	13	55.0%	
200	100.0	84%	5	60.9%	
220	110.0	92%	3	67.6%	
240	120.0	101%	3	68.8%	
260	130.0	109%	4	68.9%	
280	140.0	118%	2	69.0%	
300	150.0	126%	1	69.1%	
330	165.0	139%	2	69.1%	
360	180.0	151%	2	69.1%	

Gas rate: Before breakthrough = 0.77 l/hr;
After breakthrough = 6.29 l/hr

Table 22c. 150 GOR Oil Slim Tube Data at 1500 psig. FVF: 1.14

Time Min.	CO_2 injected Cm^3	%PV	ΔP	Recovery cum. %	
10	5.0	4%	28	2.9%	
15	7.5	6%	29	6.3%	
30	15.0	13%	24	10.4%	
45	22.5	19%	21	14.5%	
60	30.0	25%	20	17.9%	
80	40.0	34%	18	24.7%	
100	50.0	42%	18	30.7%	
120	60.0	50%	14	37.3%	
140	70.0	59%	16	44.0%	
160	80.0	67%	12	52.4%	
180	90.0	76%	9	60.4%	
200	100.0	84%	8	67.3%	
220	110.0	92%	4	75.2%	
240	120.0	101%	3	79.0%	BT
260	130.0	109%	3	80.3%	
280	140.0	118%	2	80.6%	
360	180.0	151%	3	80.6%	

Gas rate: Before breakthrough = 0.77 l/hr;
After breakthrough = 6.54 l/hr

Table 22d. 150 GOR Oil Slim Tube Data at 1550 psig. FVF: 1.14

Time Min.	CO_2 injected cm^3	%PV	ΔP	Recovery Cum. %	
10	5.0	4%	32	2.9%	
15	7.5	6%	30	4.7%	
30	15.0	13%	24	10.5%	
45	22.5	19%	22	17.0%	
60	30.0	25%	17	22.6%	
80	40.0	34%	18	31.1%	
120	60.0	50%	15	50.7%	
140	70.0	59%	16	57.1%	
160	80.0	67%	10	61.9%	
180	90.0	76%	9	67.5%	
200	100.0	84%	7	76.0%	
220	110.0	92%	4	80.9%	
230	115.0	97%	5	86.1%	BT
240	120.0	101%	4	87.2%	
260	130.0	109%	3	88.3%	
280	140.0	118%	3	88.4%	
360	180	151%	4	88.4%	

Gas rate: Before breakthrough = 0.88 l/hr;
After breakthrough = 6.71 l/hr

Table 22e. 150 GOR Oil Slim Tube Data at 1600 psig. FVF: 1.14

Time min.	CO_2 injected cm^3	%PV	ΔP	Recovery cum. %	
10	5.0	4%	35	3.1%	
15	7.5	6%	32	5.7%	
30	15.0	13%	35	14.5%	
45	22.5	19%	32	22.4%	
60	30.0	25%	28	30.5%	
80	40.0	34%	22	37.9%	
100	50.0	42%	18	42.9%	
120	60.0	50%	13	50.2%	
140	70.0	59%	15	55.9%	
160	80.0	67%	12	63.9%	
180	90.0	76%	8	73.2%	
200	100.0	84%	4	78.8%	
220	110.0	92%	4	86.1%	BT
240	120.0	101%	3	88.9%	
260	130.0	109%	5	89.8%	
280	140.0	118%	6	90.0%	
300	150.0	126%	4	90.1%	
360	180.0	151%	4	90.1%	

Gas rate: Before breakthrough = 1.02 l/hr;
After breakthrough = 7.6 l/hr

Table 22f. 150 GOR Oil Slim Tube Data at 1700 psig. FVF: 1.14

Time Min.	CO_2 injected cm^3	%PV	ΔP	Recovery cum. %	
10	5.0	4%	44	8.6%	
15	7.5	6%	42	11.5%	
30	15.0	13%	38	19.9%	
45	22.5	19%	39	26.1%	
60	30.0	25%	33	33.1%	
80	40.0	34%	29	40.8%	
100	50.0	42%	28	46.0%	
120	60.0	50%	18	56.7%	
140	70.0	59%	14	65.7%	
160	80.0	67%	9	72.0%	
180	90.0	76%	7	78.0%	
200	100.0	84%	6	83.0%	
210	105.0	88%	9	89.8%	BT
220	110.0	92%	3	92.8%	
240	120.0	101%	4	93.9%	
260	130.0	109%	2	94.4%	
280	140.0	118%	5	94.5%	
300	150.0	126%	4	94.6%	
360	180.0	151%	5	94.6%	

Gas rate: Before breakthrough = 1.08 l/hr;
After breakthrough = 7.5 l/hr

Table 22g. 150 GOR Oil Slim Tube Data at 1800 psig. FVF: 1.14

Time Min.	CO_2 injected cm^3	%PV	ΔP	Recovery Cum. %	
10	5.0	4%	69	8.6%	
15	7.5	6%	65	14.7%	
30	15.0	13%	42	20.1%	
45	22.5	19%	33	29.7%	
60	30.0	25%	26	34.0%	
80	40.0	34%	20	41.2%	
100	50.0	42%	18	49.8%	
120	60.0	50%	12	52.9%	
140	70.0	59%	14	61.0%	
160	80.0	67%	11	69.7%	
180	90.0	76%	9	78.5%	
200	100.0	84%	5	87.3%	BT
220	110.0	92%	2	91.6%	
240	120.0	101%	5	93.7%	
260	130.0	109%	3	94.6%	
280	140.0	118%	4	94.7%	
300	150.0	126%	2	94.8%	
360	180.0	151%	5	94.8%	

Gas rate: Before breakthrough = 0.98 l/hr;
After breakthrough = 7.7 l/hr

Table 23a. 400 GOR Oil Recovery vs. Pressure Slim Tube Tests Summary

Press	%@ BT	%1.2 PV	%ULT
1400	64.34	64.56	64.67
1500	80.08	80.40	80.40
1550	85.97	86.85	87.07
1600	88.49	92.53	92.64
1630	89.36	93.84	93.84
1800	89.25	93.29	93.40

Table 23b. 400 GOR Oil Slim Tube Data at 1400 psig. FVF: 1.3

Time min.	CO_2 injected cm^3	%PV	ΔP	Recovery cum. %	
10	5.00	4%	53	3.4%	
15	7.50	6%	35	6.0%	
30	15.00	13%	25	8.6%	
45	22.50	19%	15	14.1%	
60	30.00	25%	11	20.6%	
80	40.00	34%	10	26.1%	
100	50.00	42%	13	34.6%	
120	60.00	50%	10	41.1%	
140	70.00	59%	8	44.2%	
160	80.00	67%	6	50.3%	
180	90.00	76%	7	57.2%	
200	100.00	84%	6	63.8%	BT
220	110.00	92%	5	64.2%	
240	120.00	101%	5	64.3%	
260	130.00	109%	4	64.6%	
280	140.00	118%	3	64.6%	
300	150.00	126%	3	64.7%	
330	165.00	139%	3	64.7%	
360	180.00	151%	3	64.7%	

Gas rate: Before breakthrough = 2.66 l/hr;
After breakthrough = 6.2 l/hr

Table 23c. 400 GOR Oil Slim Tube Data at 1500 psig. FVF: 1.3

Time min.	CO_2 injected cm^3	%PV	ΔP	Recovery Cum. %	
10	5.00	4%	26	3.3%	
15	7.50	6%	24	6.6%	
30	15.00	13%	17	12.2%	
45	22.50	19%	19	21.5%	
60	30.00	25%	10	28.1%	
80	40.00	34%	16	33.5%	
100	50.00	42%	11	40.1%	
120	60.00	50%	9	46.8%	
140	70.00	59%	7	52.8%	
160	80.00	67%	6	62.1%	
180	90.00	76%	8	70.9%	
200	100.00	84%	4	77.5%	
220	110.00	92%	3	80.1%	BT
240	120.00	101%	2	80.3%	
260	130.00	109%	3	80.3%	
280	140.00	118%	2	80.4%	
300	150.00	126%	1	80.4%	
320	160.00	134%	3	80.4%	

Gas rate: Before breakthrough = 2.17 l/hr;
After breakthrough = 6.88 l/hr

Table 23d. 400 GOR Oil Slim Tube Data at 1550 psig. FVF: 1.3

Time Min.	CO_2 injected cm^3	%PV	ΔP	Recovery cum. %	
10	5.00	4%	21	3.3%	
15	7.50	6%	20	4.9%	
30	15.00	13%	22	8.2%	
45	22.50	19%	17	12.6%	
60	30.00	25%	12	17.9%	
80	40.00	34%	12	24.5%	
100	50.00	42%	11	34.2%	
120	60.00	50%	14	42.8%	
140	70.00	59%	9	52.0%	
160	80.00	67%	8	59.1%	
180	90.00	76%	5	64.6%	
200	100.00	84%	7	71.2%	
220	110.00	92%	3	75.1%	
240	120.00	101%	5	81.1%	
260	130.00	109%	3	86.0%	BT
280	140.00	118%	2	86.8%	
300	150.00	126%	2	87.0%	
320	160.00	134%	2	87.1%	
330	165.00	139%	2	87.1%	

Gas rate: Before breakthrough = 2.79 l/hr;
After breakthrough = 9.17 l/hr

Table 23e. 400 GOR Oil Slim Tube Data at 1600 psig. FVF: 1.3

Time Min.	CO_2 injected cm^3	%PV	ΔP	Recovery cum. %	
15	7.50	6%	55	6.8%	
30	15.00	13%	45	12.3%	
45	22.50	19%	32	18.9%	
60	30.00	25%	21	24.3%	
80	40.00	34%	14	33.0%	
100	50.00	42%	15	37.5%	
120	60.00	50%	9	46.8%	
140	70.00	59%	13	51.7%	
160	80.00	67%	8	61.5%	
180	90.00	76%	7	71.2%	
200	100.00	84%	9	80.2%	
220	110.00	92%	5	84.2%	
240	120.00	101%	4	88.5%	BT
260	130.00	109%	3	91.5%	
280	140.00	118%	4	92.5%	
300	150.00	126%	2	92.6%	
330	165.00	139%	3	92.6%	

Gas rate: Before breakthrough = 2.61 l/hr;
After breakthrough = 8.25 l/hr

Table 23f. 400 GOR Oil Slim Tube Data at 1630 psig. FVF: 1.3

Time min.	CO_2 injected cm^3	%PV	ΔP	Recovery cum. %	
10	5.00	4%	29	4.6%	
15	7.50	6%	31	7.0%	
30	15.00	13%	20	15.9%	
45	22.50	19%	22	21.5%	
60	30.00	25%	19	28.6%	
80	40.00	34%	16	35.5%	
100	50.00	42%	13	41.9%	
120	60.00	50%	9	49.8%	
140	70.00	59%	13	58.4%	
160	80.00	67%	9	67.1%	
180	90.00	76%	7	75.6%	
200	100.00	84%	6	82.0%	
220	110.00	92%	4	89.4%	BT
240	120.00	101%	3	91.5%	
260	130.00	109%	4	93.2%	
280	140.00	118%	2	93.8%	
300	150.00	126%	3	93.8%	
320	160.00	134%	1	93.8%	

Gas rate: Before breakthrough = 2.4 l/hr;
After breakthrough = 7.85 l/hr

Table 23g. 400 GOR Oil Slim Tube Data at 1800 psig. FVF: 1.3

Time Min.	CO_2 injected cm^3	%PV	ΔP	Recovery cum. %	
10	5.00	4%	41	3.5%	
15	7.50	6%	33	7.4%	
30	15.00	13%	21	12.8%	
45	22.50	19%	26	16.6%	
60	30.00	25%	19	25.9%	
80	40.00	34%	16	33.3%	
100	50.00	42%	17	43.8%	
120	60.00	50%	14	50.1%	
140	70.00	59%	14	60.7%	
160	80.00	67%	9	71.4%	
180	90.00	76%	13	77.8%	
200	100.00	84%	8	86.0%	
220	110.00	92%	8	89.3%	BT
240	120.00	101%	4	92.1%	
260	130.00	109%	5	93.2%	
280	140.00	118%	6	93.3%	
300	150.00	126%	2	93.4%	
320	160.00	134%	4	93.4%	

Gas rate: Before breakthrough = 2.43 l/hr;
After breakthrough = 8.08 l/h

Table 24a. 600 GOR Oil Slim Tube Recovery vs. Pressure

Pressure Psig	@BT	1.2 PV	ULT.
1500	75.0%	75.6%	76.6%
1600	83.0%	87.0%	87.6%
1623	85.2%	88.0%	89.7%
1650	85.7%	89.1%	90.0%
1700	88.4%	90.6%	91.2%
1800	90.9%	95.0%	95.5%

Table 24b. 600 GOR Oil Slim Tube Data at 1500 psig. FVF: 1.35

Time min.	CO_2 injected cm^3	%PV	ΔP	Recovery Cum. %	
10	5.0	4.2%	11	3.5%	
30	15.0	12.6%	12	7.4%	
40	20.0	16.8%	12	14.2%	
60	30.0	25.2%	12	17.6%	
80	40.0	33.6%	11	22.1%	
100	50.0	42.0%	11	31.2%	
120	60.0	50.4%	10	34.8%	
140	70.0	58.8%	9	44.0%	
160	80.0	67.2%	8	49.0%	
180	90.0	75.6%	7	53.0%	
200	100.0	84.0%	5	57.0%	
220	110.0	92.4%	6	63.9%	
240	120.0	100.8%	5	68.5%	
260	130.0	109.2%	3	72.4%	
270	135.0	113.4%	2	75.0%	BT
280	140.0	117.6%	3	75.6%	
300	150.0	126.1%	4	76.1%	
330	165.0	138.7%	4	76.6%	
360	180.0	151.3%	5	76.6%	

Gas rate: Before breakthrough = 2.43 l/hr;
After breakthrough = 6.82 l/hr

Table 24c. 600 GOR Oil Slim Tube Data at 1600 psig. FVF: 1.35

Time Min.	CO_2 injected cm^3	%PV	ΔP	Recovery cum. %	
10	5.0	4.2%	22	3.4%	
30	15.0	12.6%	9	6.8%	
60	30.0	25.2%	11	11.3%	
75	37.5	31.5%	11	13.6%	
95	47.5	39.9%	8	21.6%	
110	55.0	46.2%	10	28.2%	
120	60.0	50.4%	10	35.1%	
140	70.0	58.8%	10	40.2%	
160	80.0	67.2%	7	44.0%	
180	90.0	75.6%	8	50.3%	
210	105.0	88.2%	8	57.1%	
224	112.0	94.1%	2	66.1%	
230	115.0	96.6%	5	75.8%	
245	122.5	102.9%	2	81.6%	
260	130.0	109.2%	2	83.0%	BT
280	140.0	117.6%	1	87.0%	
300	150.0	126.1%	1	87.4%	
360	180.0	151.3%	2	87.6%	

Gas rate: Before breakthrough = 3.00 l/hr;
After breakthrough = 6.32 l/hr

Table 24d. 600 GOR Oil Slim Tube Data at 1623 psig. FVF: 1.35

Time min.	CO_2 injected cm^3	%PV	ΔP	Recovery cum. %	
10	5.0	4.2%	19	3.4%	
15	7.5	6.3%	13	5.7%	
30	15.0	12.6%	12	9.1%	
40	20.0	16.8%	11	12.7%	
60	30.0	25.2%	11	19.5%	
95	47.5	39.9%	10	30.3%	
115	57.5	48.3%	10	37.1%	
150	75.0	63.0%	9	49.0%	
165	82.5	69.3%	7	54.5%	
185	92.5	77.7%	7	61.5%	
200	100.0	84.0%	7	66.6%	
220	110.0	92.4%	4	73.1%	
240	120.0	100.8%	4	80.4%	
250	125.0	105.0%	4	85.2%	BT
260	130.0	109.2%	0	87.5%	
280	140.0	117.6%	1	88.0%	
300	150.0	126.1%	1	89.7%	
330	165.0	138.7%	1	90.4%	
360	180.0	151.3%	1	90.4%	

Gas rate: Before breakthrough = 2.61 l/hr;
After breakthrough = 7.21 l/hr

Table 24e. 600 GOR Oil Slim Tube Data at 1650 psig. FVF: 1.35

Time min.	CO_2 injected cm^3	%PV	ΔP	Recovery Cum. %	
10	5.0	4.2%	19	3.4%	
20	10.0	8.4%	14	5.1%	
40	20.0	16.8%	12	6.2%	
50	25.0	21.0%	12	9.6%	
60	30.0	25.2%	6	15.3%	
65	32.5	27.3%	10	21.6%	
95	47.5	39.9%	10	31.8%	
115	57.5	48.3%	11	38.0%	
135	67.5	56.7%	9	44.8%	
155	77.5	65.1%	7	51.6%	
175	87.5	73.5%	6	59.6%	
180	90.0	75.6%	7	60.7%	
190	95.0	79.8%	6	64.7%	
210	105.0	88.2%	5	72.6%	
220	110.0	92.4%	10	76.0%	
230	115.0	96.6%	1	80.5%	
240	120.0	100.8%	2	83.4%	
245	122.5	102.9%	2	85.7%	BT
275	137.5	115.5%	1	87.9%	
290	145.0	121.8%	2	89.1%	
320	160.0	134.5%	2	90.0%	
360	180.0	151.3%	2	90.0%	

Gas rate: Before breakthrough = 2.65 l/hr;
After breakthrough = 7.79 l/hr

Table 24f. 600 GOR Oil Slim Tube Data at 1700 psig. FVF: 1.35

Time min.	CO_2 injected cm^3	%PV	ΔP	Recovery Cum. %	
10	5.0	4.2%	15	3.4%	
20	10.0	8.4%	15	5.3%	
50	25.0	21.0%	13	16.1%	
70	35.0	29.4%	14	22.1%	
90	45.0	37.8%	12	31.8%	
110	55.0	46.2%	10	35.2%	
120	60.0	50.4%	10	40.8%	
140	70.0	58.8%	8	47.1%	
150	75.0	63.0%	8	51.2%	
180	90.0	75.6%	6	63.1%	
210	105.0	88.2%	3	71.9%	
225	112.5	94.5%	3	78.7%	
240	120.0	100.8%	3	88.4%	BT
250	125.0	105.0%	2	89.5%	
280	140.0	117.6%	2	90.6%	
300	150.0	126.1%	3	90.9%	
360	180.0	151.3%	2	91.2%	

Gas rate: Before breakthrough = 2.8 l/hr;
After breakthrough = 8.8 l/hr

Table 24g. 600 GOR Oil Slim Tube Data at 1800 psig. FVF: 1.35

Time Min.	CO_2 injected cm^3	%PV	ΔP	Recovery Cum. %	
10	5.0	4.2%	34	3.6%	
15	7.5	6.3%	23	4.7%	
30	15.0	12.6%	15	9.4%	
60	30.0	25.2%	15	19.9%	
80	40.0	33.6%	15	28.9%	
90	45.0	37.8%	14	33.1%	
130	65.0	54.6%	11	49.1%	
150	75.0	63.0%	10	55.9%	
160	80.0	67.2%	8	60.4%	
180	90.0	75.6%	8	68.3%	
190	95.0	79.8%	7	74.0%	
220	110.0	92.4%	6	85.2%	
230	115.0	96.6%	3	90.9%	BT
245	122.5	102.9%	2	93.7%	
260	130.0	109.2%	2	94.8%	
285	142.5	119.7%	2	95.0%	
300	150.0	126.1%	2	95.5%	
330	165.0	138.7%	1	95.5%	
360	180.0	151.3%	2	95.5%	

Gas rate: Before breakthrough = 3.1 l/hr;
After breakthrough = 10.5 l/hr

Table 25a. Vertical Large-Diameter Tube Data: Gravity-Stable, 400 GOR, 1700 psig

Run Time, hr	CO_2 inj., HC PV	Oil Prod., HC PV
0.0	0.0%	0.0%
8.0	12.0%	13.0%
18.0	26.0%	24.0%
18.0	27.0%	25.0%
24.0	36.0%	34.0%
32.0	47.0%	42.0%
32.0	47.0%	43.0%
42.0	62.0%	53.0%
42.0	62.0%	54.0%
50.8	74.9%	65.8%
51.1	75.4%	66.2%
56.1	82.8%	71.3%
66.7	98.4%	81.8%
73.3	108.2%	89.9%
73.7	108.7%	90.2%
77.6	114.5%	93.8%
80.6	119.0%	94.4%
83.8	123.6%	95.2%
97.6	144.0%	95.8%
100.7	148.5%	95.9%

Table 25b. Vertical Large-Diameter Tube Data: Gravity-Stable, 400 GOR, 1550 psig

Run Time, hr	CO_2 inj., HC PV	Oil Prod., HC PV
0.0	0.0%	0.0%
0.0	0.0%	0.0%
10.6	16.9%	12.9%
18.1	28.9%	21.8%
22.5	35.8%	26.5%
22.8	36.3%	26.9%
26.1	41.6%	30.6%
26.5	42.2%	31.0%
34.0	54.3%	40.2%
34.4	54.8%	40.6%
44.2	70.5%	51.2%
44.6	71.2%	51.6%
51.0	81.2%	58.4%
58.3	92.9%	67.4%
58.7	93.6%	67.8%
68.3	108.9%	77.7%
75.2	120.0%	85.0%
82.6	131.7%	91.3%
83.6	133.3%	91.3%
88.1	140.5%	91.9%
89.3	142.4%	92.1%
91.6	146.1%	92.4%
92.5	147.6%	92.4%

Table 25c. Vertical Large-Diameter Tube Data: Gravity-Stable, 400 GOR, 1400 psig

Run Time, hr	CO_2 inj., HC PV	Oil Prod., HC PV
0.0	0.0%	0.0%
6.1	10.3%	11.4%
6.5	10.9%	11.8%
18.1	22.7%	20.5%
18.7	23.8%	20.9%
26.2	36.4%	30.8%
29.2	41.4%	36.1%
33.8	49.2%	43.1%
42.1	63.2%	54.5%
42.5	63.9%	55.2%
45.9	69.5%	57.7%
50.3	77.0%	63.3%
55.6	86.0%	71.0%
56.3	87.1%	72.0%
66.2	103.9%	82.9%
73.3	115.9%	88.9%
74.7	118.2%	89.1%
78.1	124.0%	89.4%

Table 25d. Vertical Large-Diameter Tube Data: Gravity-Stable, 150 GOR, 1700 psig

Run Time, hr	CO_2 inj., HC PV	Oil Prod., HC PV
0.0	0.0%	0.0%
1.1	2.0%	0.7%
1.1	2.1%	3.3%
6.3	11.6%	9.3%
6.3	11.6%	9.3%
14.9	27.7%	16.9%
15.2	28.3%	17.1%
24.2	45.0%	28.8%
24.4	45.3%	29.1%
31.2	57.9%	39.1%
31.4	58.3%	39.4%
38.3	71.2%	49.5%
38.5	71.5%	49.9%
46.7	86.7%	60.6%
46.9	87.1%	60.9%
55.8	103.6%	71.1%
56.2	104.3%	71.6%
62.8	116.5%	80.8%
63.0	117.0%	81.1%
71.9	133.5%	90.6%
72.2	134.1%	90.9%
74.8	138.7%	93.9%
79.2	147.0%	97.9%
80.1	148.7%	98.0%

Table 25e. Vertical Large Diameter Tube Data: Upward-Flow, 150 GOR, 1400 psig

Run Time, hr.	CO_2 inj., HC PV	Oil Prod., HC PV
0.0	0.0%	0.0%
2.0	10.8%	7.9%
2.3	12.7%	8.8%
10.4	56.8%	29.7%
11.0	60.1%	30.9%
19.3	105.2%	44.9%
19.9	108.6%	45.8%
25.2	137.2%	49.2%
26.1	142.0%	51.1%
26.3	143.3%	52.2%
30.3	165.0%	58.5%
30.3	165.0%	58.5%
31.0	168.8%	60.6%

Table 25f. Horizontal Large-Diameter Tube Data: Gravity-Stable,150 GOR, 1400 psig

Run Time, hr	CO_2 inj., HC PV	Oil Prod., HC PV
0.0	0.0%	0.0%
7.2	14.1%	7.0%
7.7	15.1%	7.3%
15.8	30.8%	13.1%
16.2	31.6%	13.5%
28.4	55.4%	23.3%
29.6	57.8%	23.7%
45.1	88.0%	25.9%
65.6	128.1%	27.1%

Table 26. Conditions and Results of Three CO_2-Assisted Gravity Drainage Experiments

Experiment No.:	**1**	**2**	**3**
Core Porosity	0.068	0.066	0.066
Core Permeability, md	15.4	12.7	12.7
Initial Oil Saturation	0.47	0.102	0.191
Oil Type (GOR)	400	150	150
Temperature, °F	150	150	150
Pressure, psig	1,650	1,543	1,320
CO_2 Injection Rate, cm^3/hour	20	10	2
Oil Recovery @ 1.2 PV CO_2 Inj.	0.76	0.51	0.115
Oil Recovery @ 2 PV CO_2 Inj.	0.78	0.57	0.148
Residual Oil Saturation	0.09	0.03	0.100

Table 27. Dimensions and Petrophysical Properties of Core Used in the Injectivity Experiments

Core No.	1	2	3	4
Core Type	Berea	Berea	Fractured Carbonate	Reservoir Sandstone
Diameter, cm	3.81	1.27	3.68	3.61
Length	5.39	7.44	7.65	7.65
Porosity	0.21	0.37	0.05	0.12
Initial Water Saturation	100	650	315	35

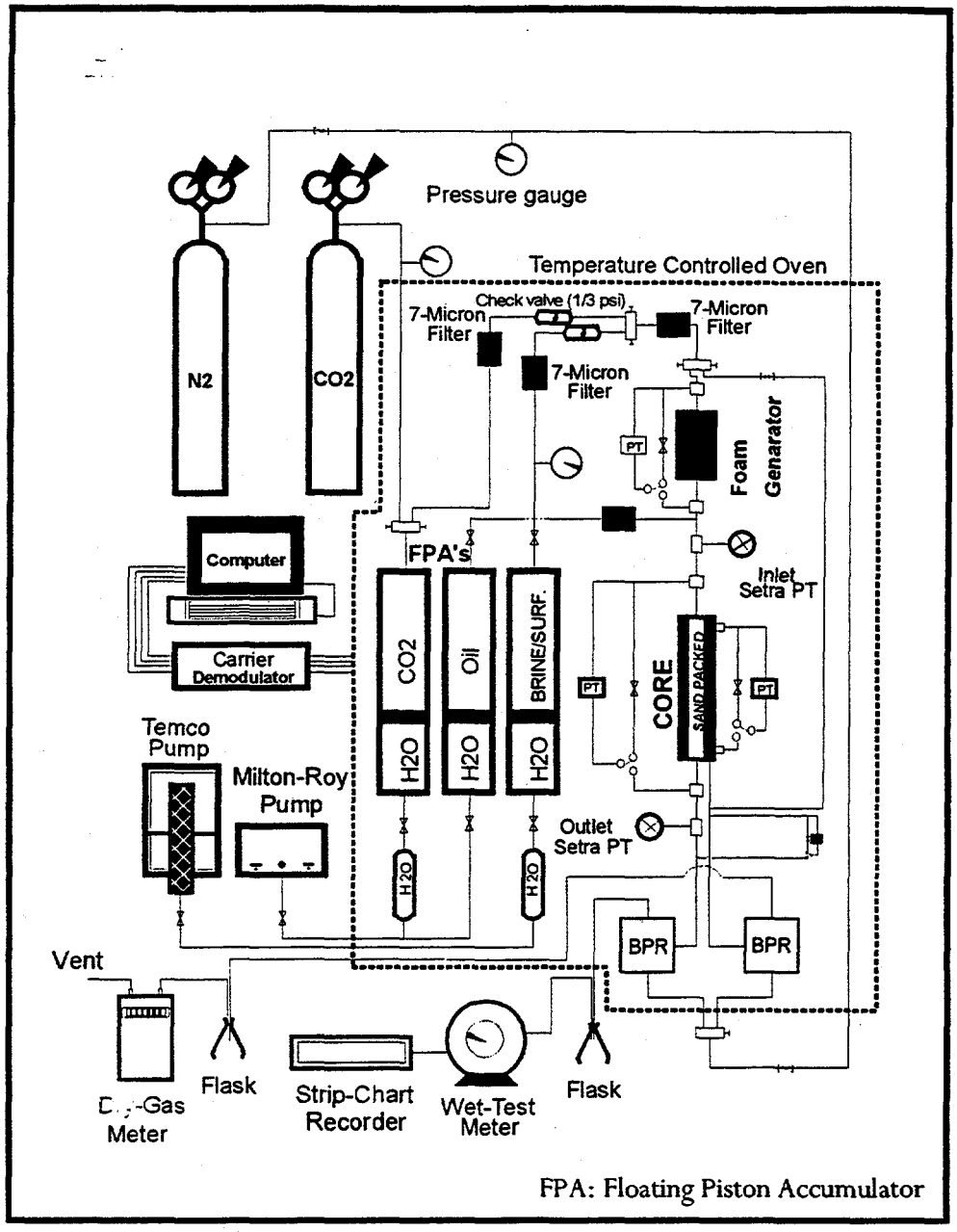

Fig. 1. Schematic diagram of the coreflood apparatus used for selective mobility measurements.

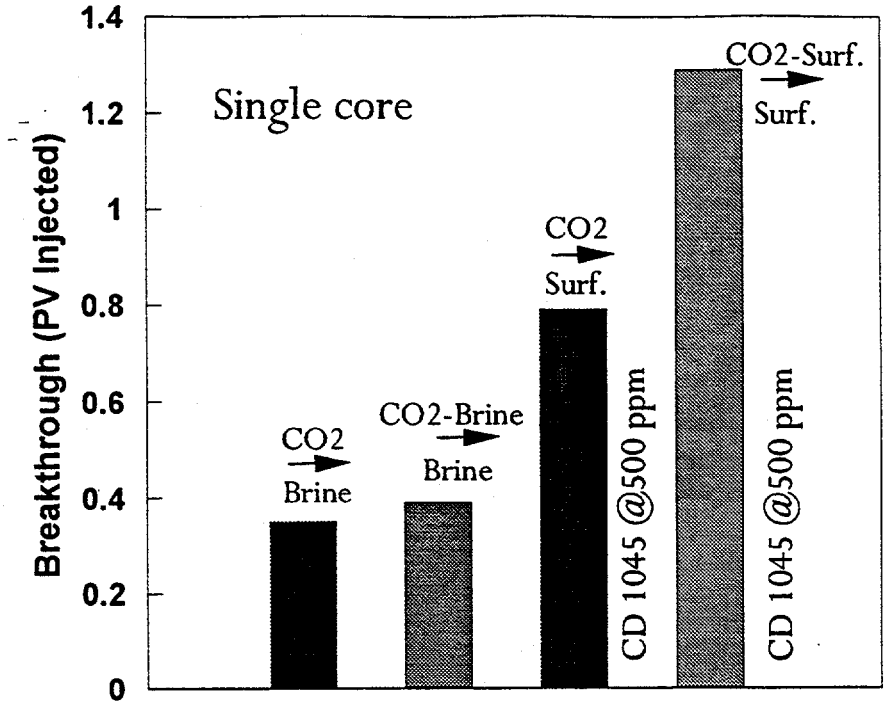

Fig. 2. CO_2 breakthrough (PV injected) in absence of oil.

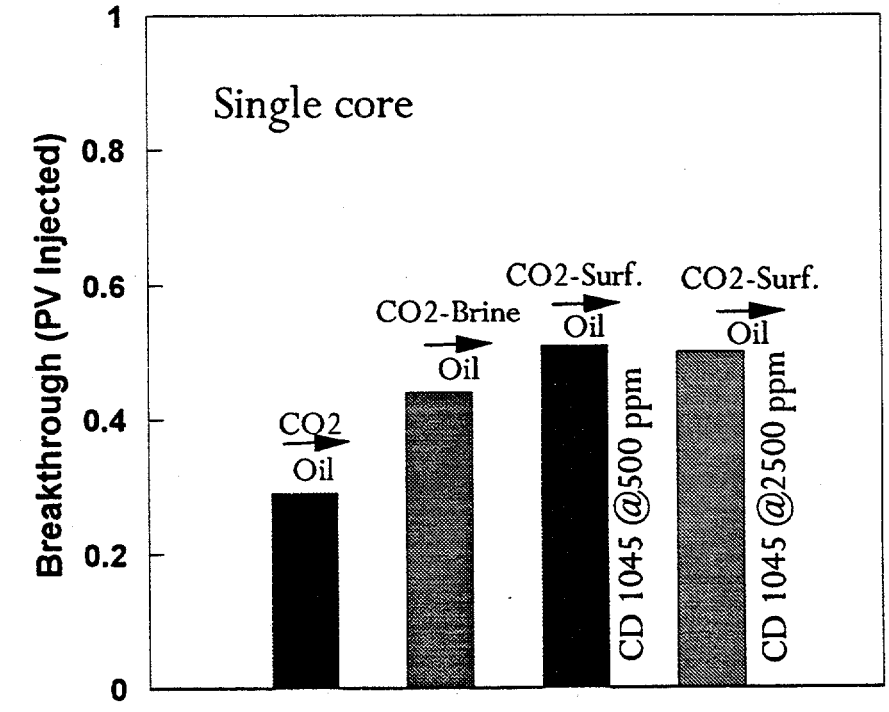

Fig. 3. CO_2 breakthrough (PV injected) in the presence of oil.

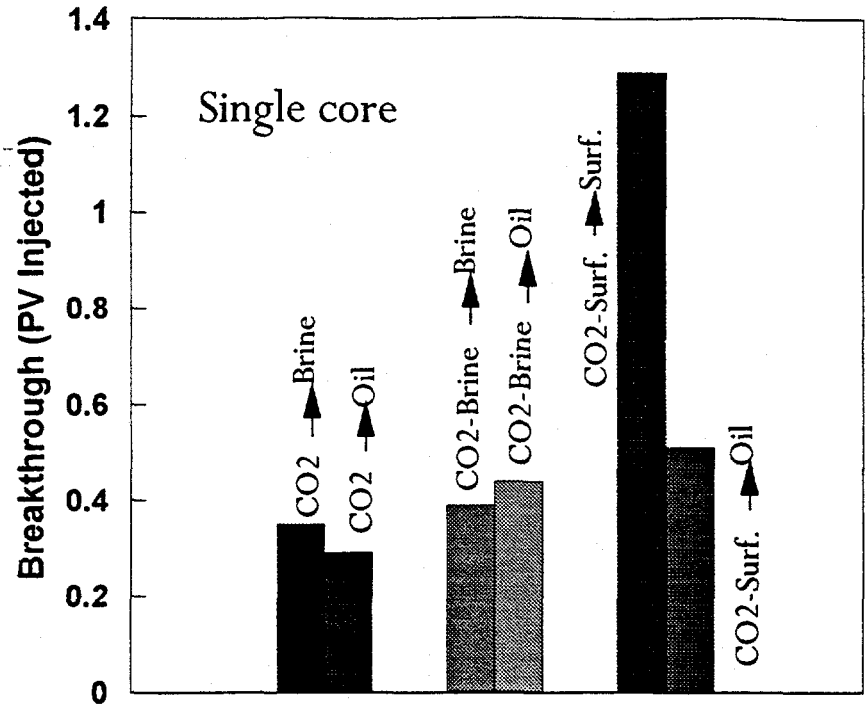

Fig. 4. CO_2 breakthrough (PV injected) for single core experiments with and without the presence of oil.

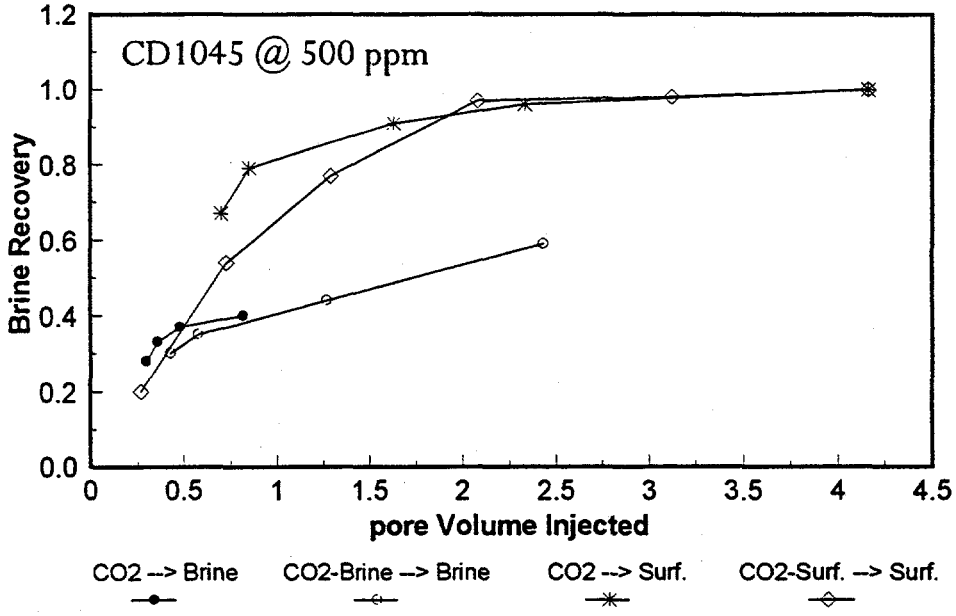

Fig. 5. Single core recovery curves in the absence of oil.

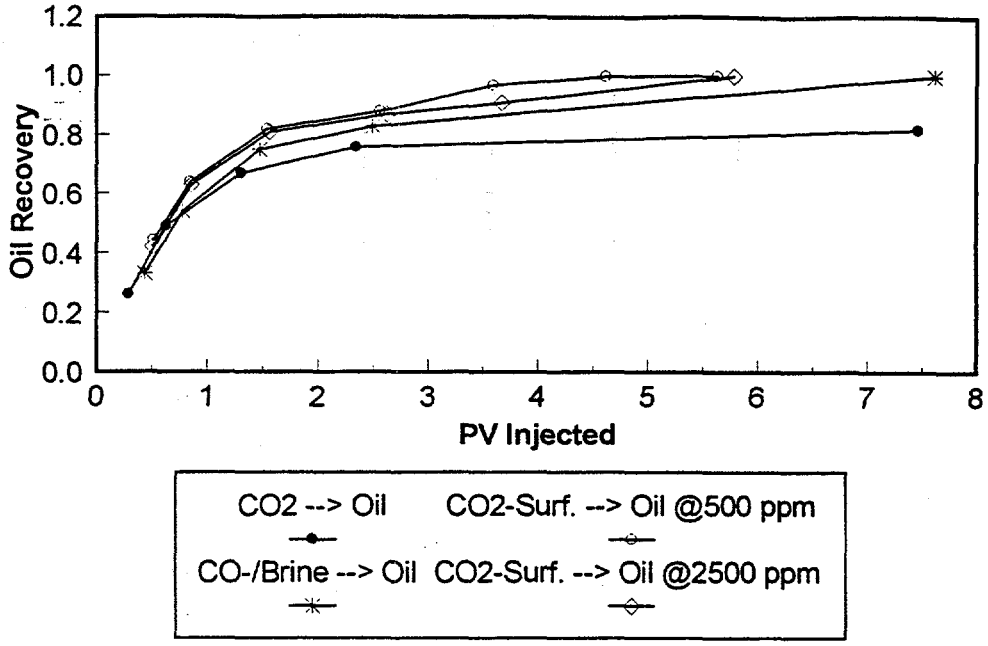

Fig. 6. Single core recovery curves in the presence of oil.

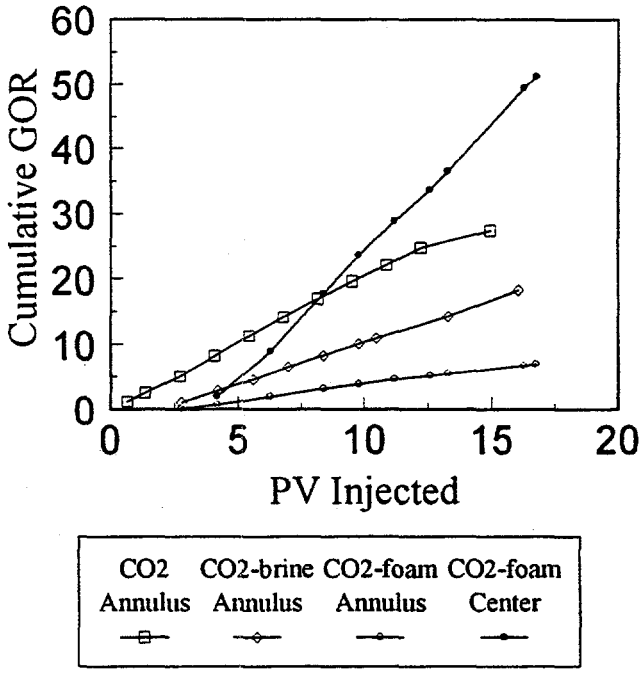

Fig. 7. GOR observed from different permeability regions in capillary isolated composite core.

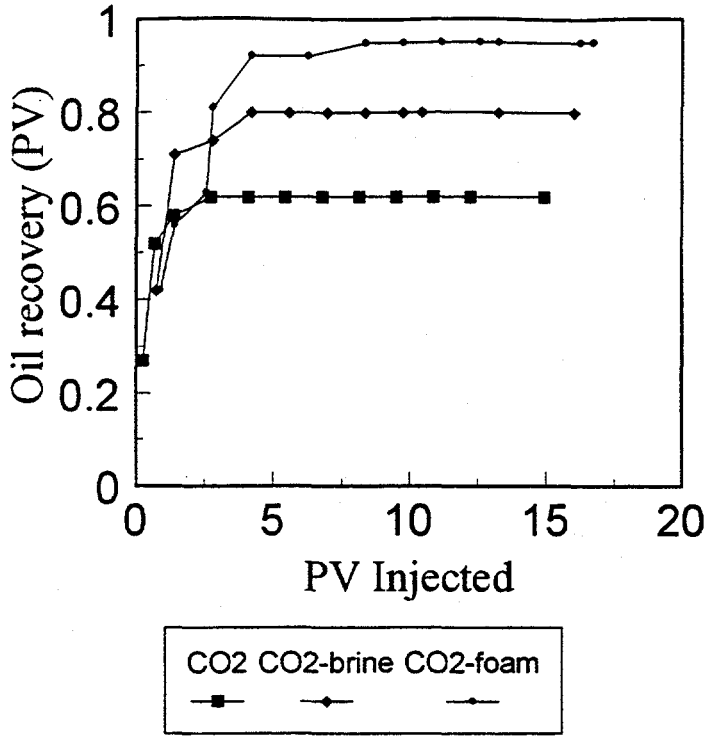

Fig. 8. Oil recovery from high permeability (annulus) region in capillary isolated composite core.

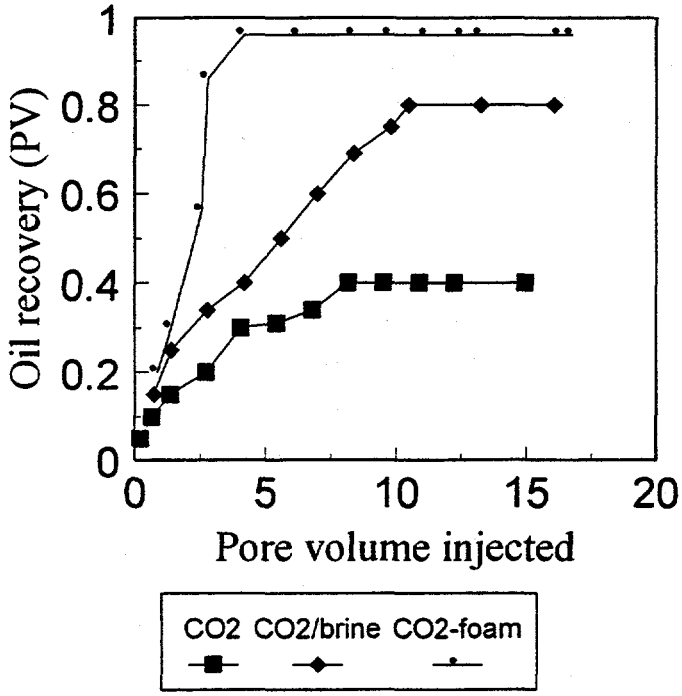

Fig. 9. Oil recovery from low permeability (center) region in capillary isolated composite core.

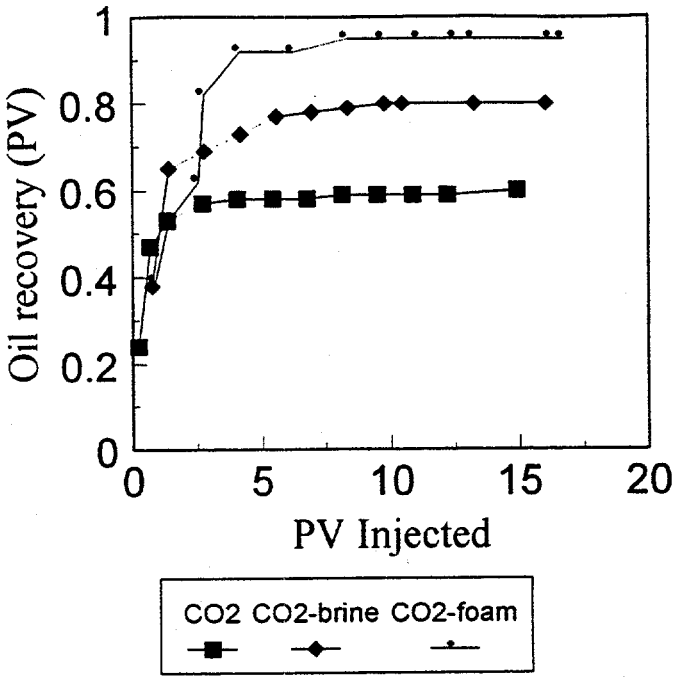

Fig. 10. Total oil recovery in capillary composite core.

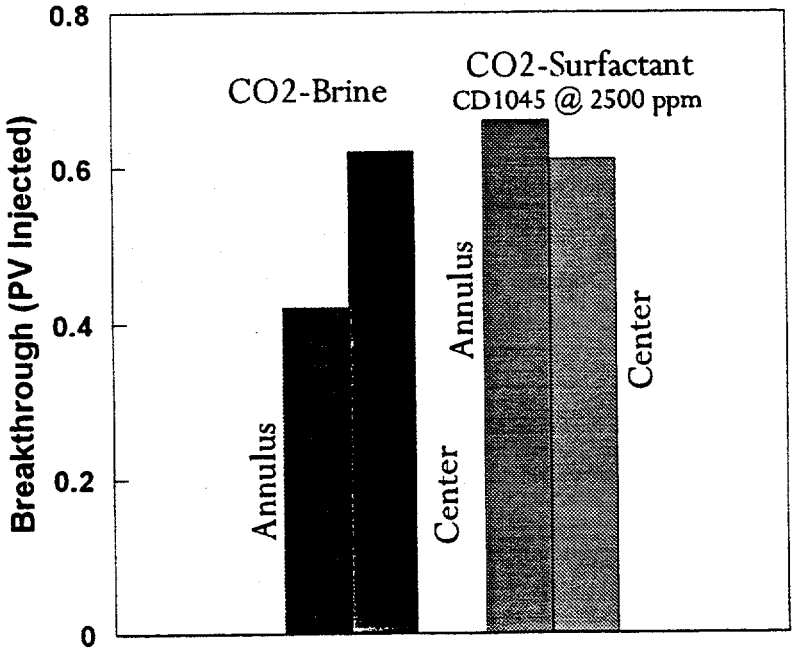

Fig. 11. CO_2 breakthrough (PV injected) in two regions of composite core without oil present.

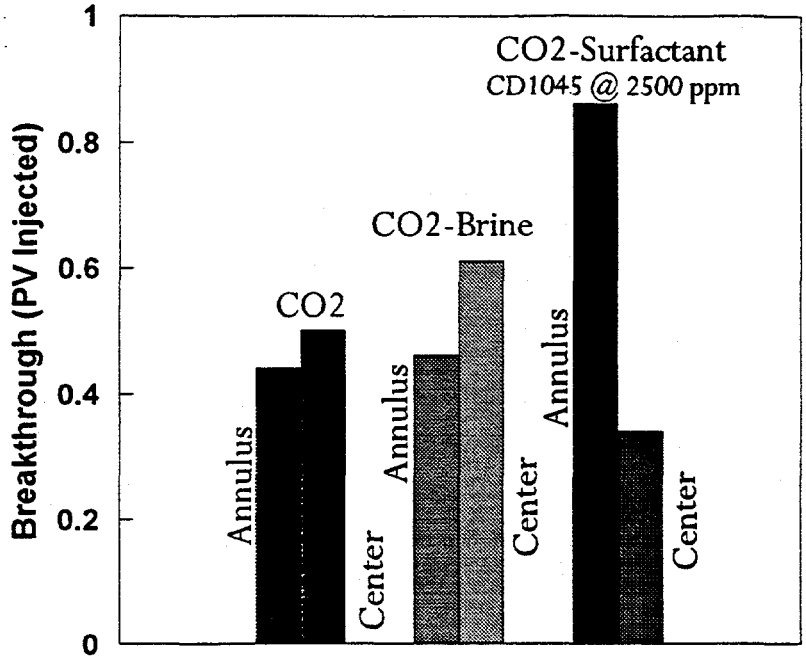

Fig. 12. CO_2 breakthrough (PV injected) in two regions of composite core with oil present.

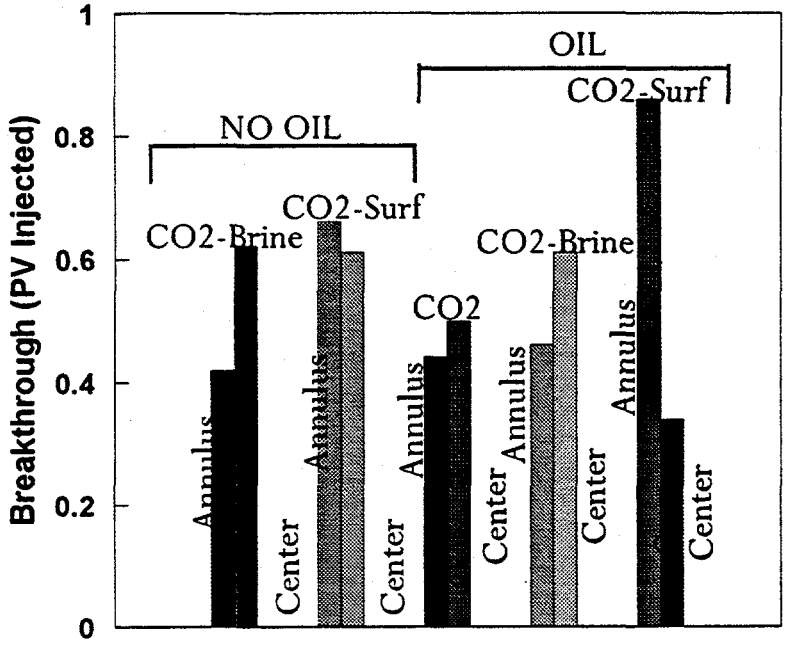

Fig. 13. A comparison of breakthrough (PV injected) for five composite core experiments.

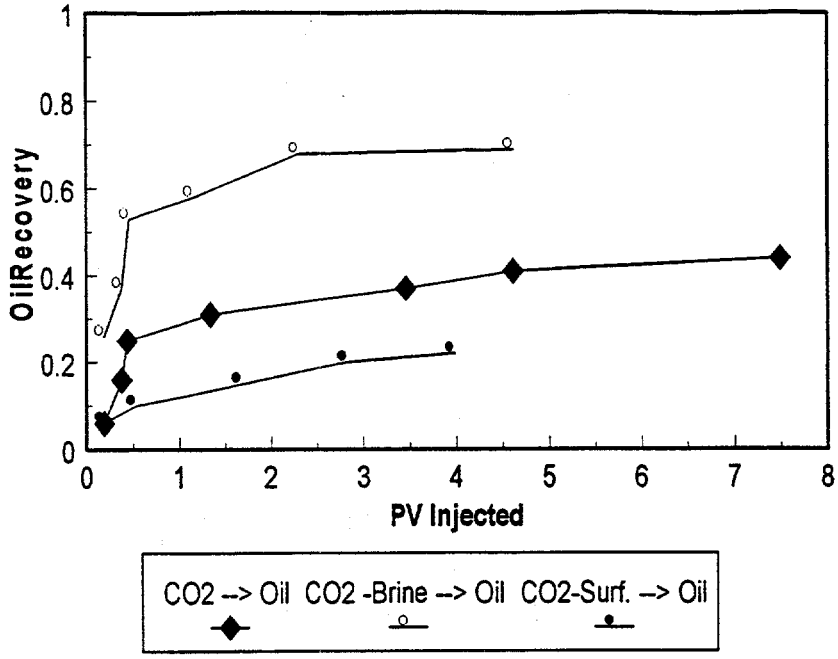

Fig. 14. A comparison of oil recovery from the high permeability region (annulus).

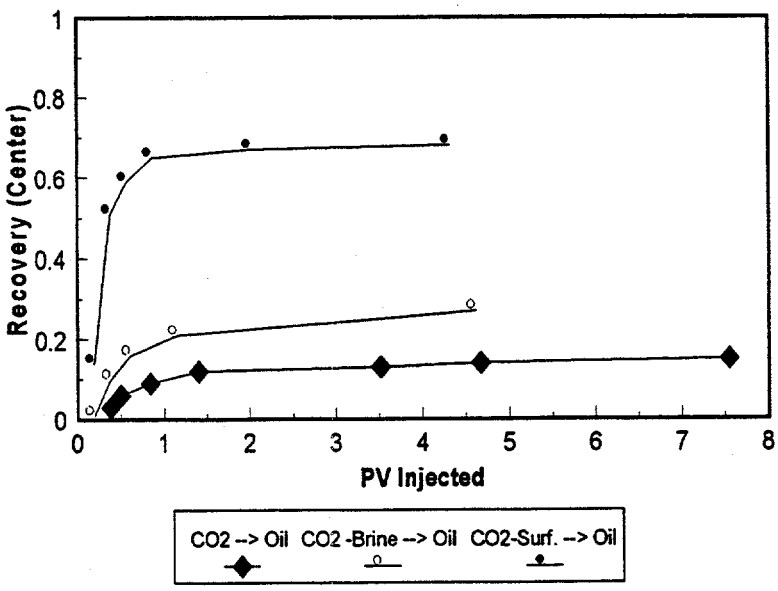

Fig. 15. A comparison of oil recovery from the low permeability region (center).

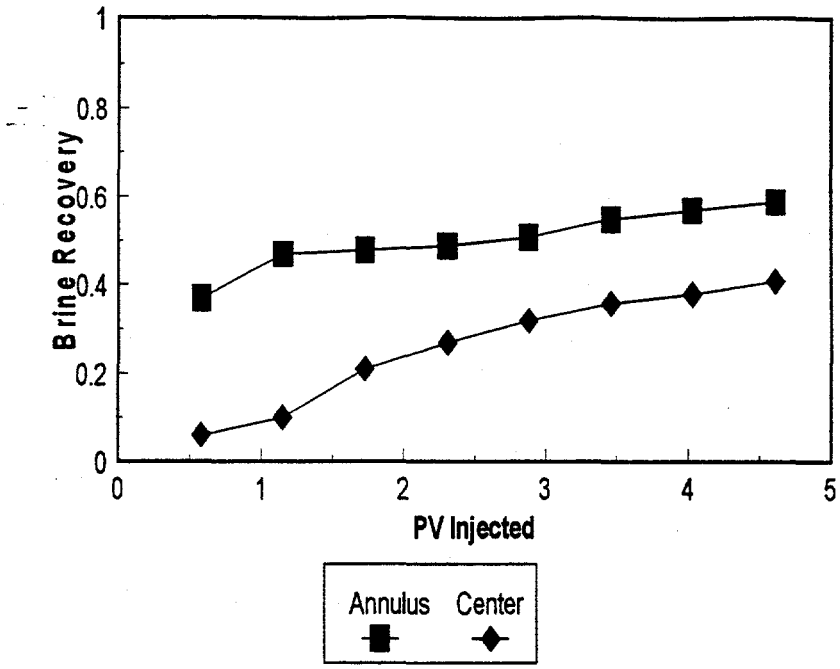

Fig. 16. Recovery curves for both high and low permeability regions. Core was saturated with brine solution.

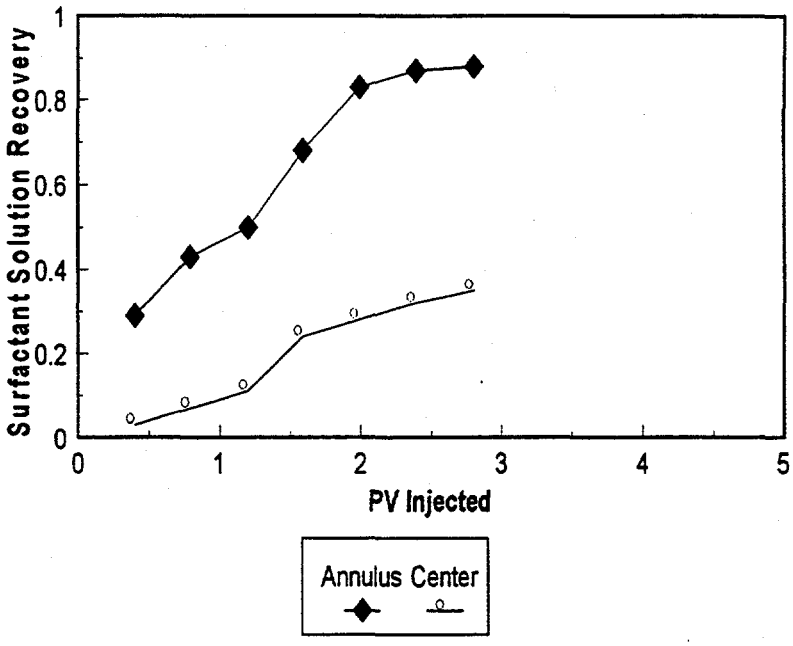

Fig. 17. Recovery curves for both high and low permeability regions. Core was saturated with oil to residual brine.

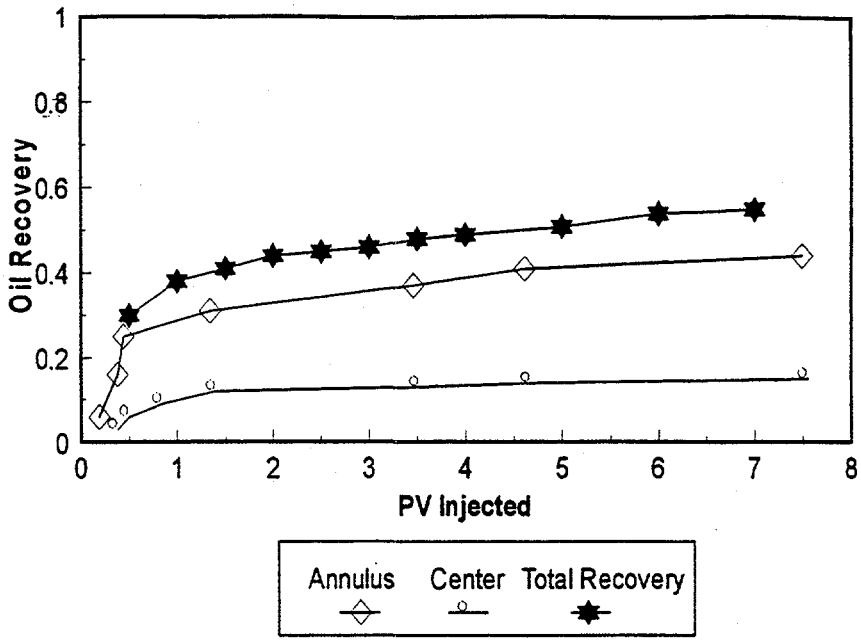

Fig. 18. Oil recovery as a function of PV of CO_2 injected, for both high and low permeability regions.

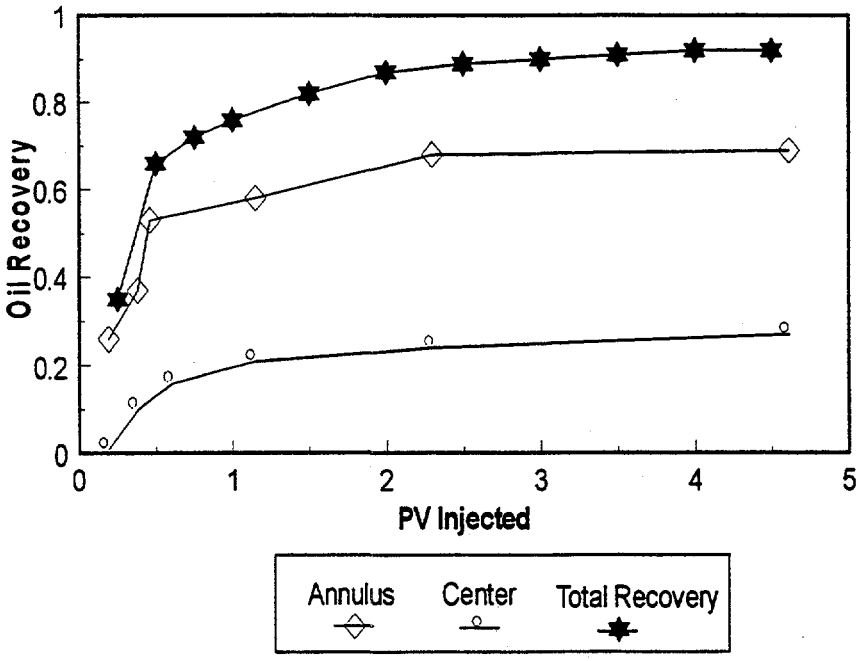

Fig. 19. Oil recovery as a function of PV of CO_2-brine injection, for both high and low permeability regions.

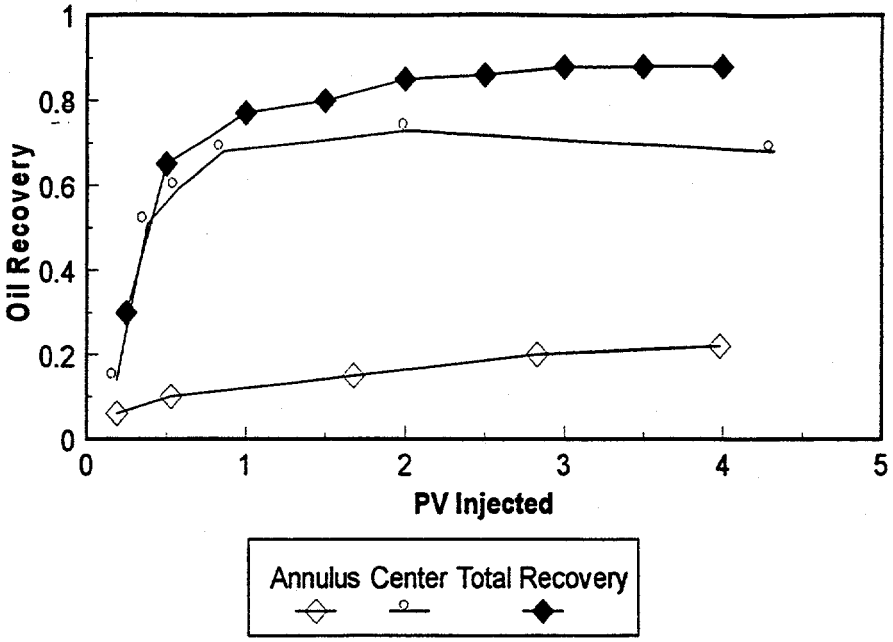

Fig. 20. Oil recovery as a function of PV of CO_2-surfactant injected, for both high and low permeability regions.

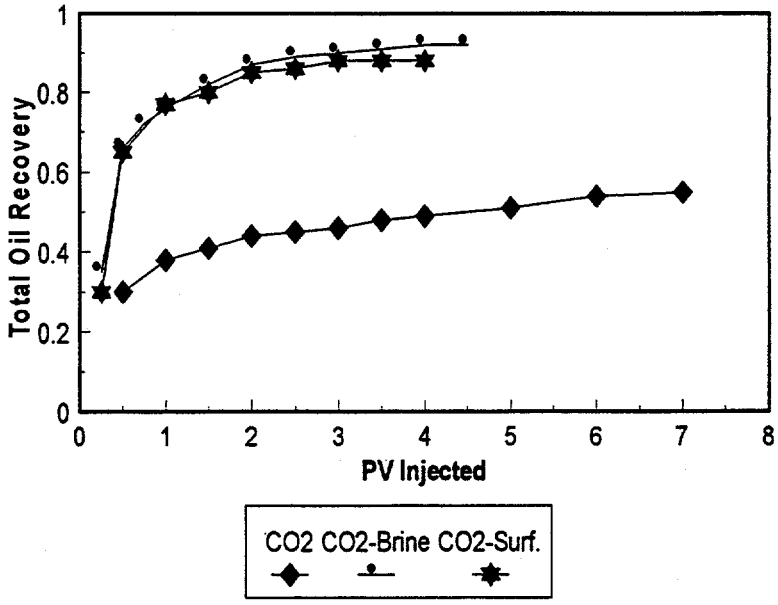

Fig. 21. Total oil recovery from both the high and low permeability regions.

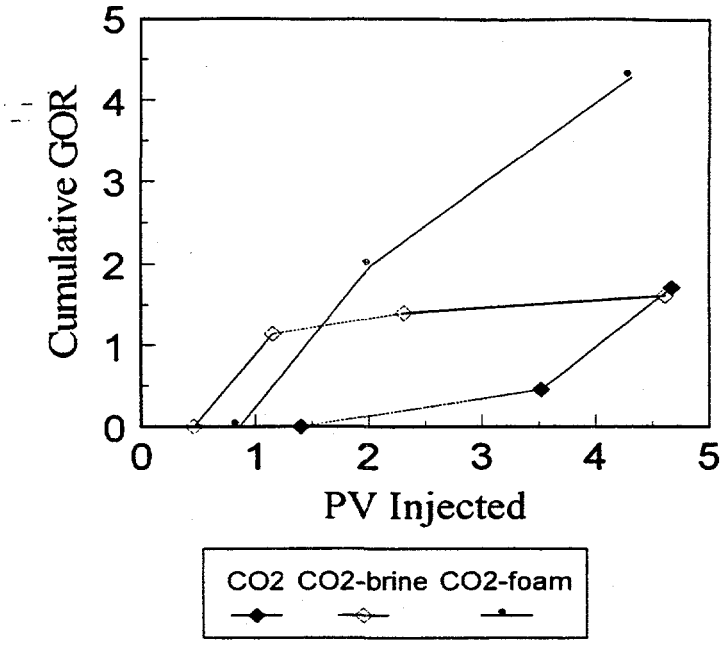

Fig. 22. GOR observed from low permeability (center) region in a capillary contact composite core.

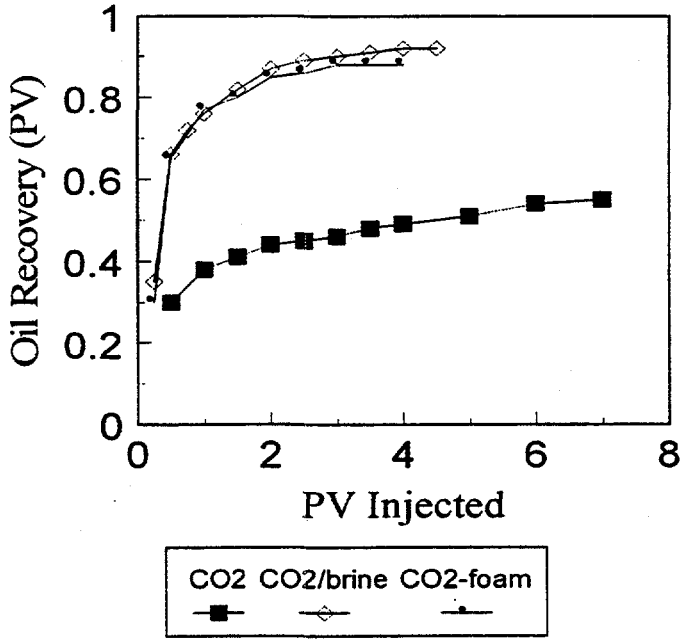

Fig. 23. Total oil recovery in a capillary contact composite core.

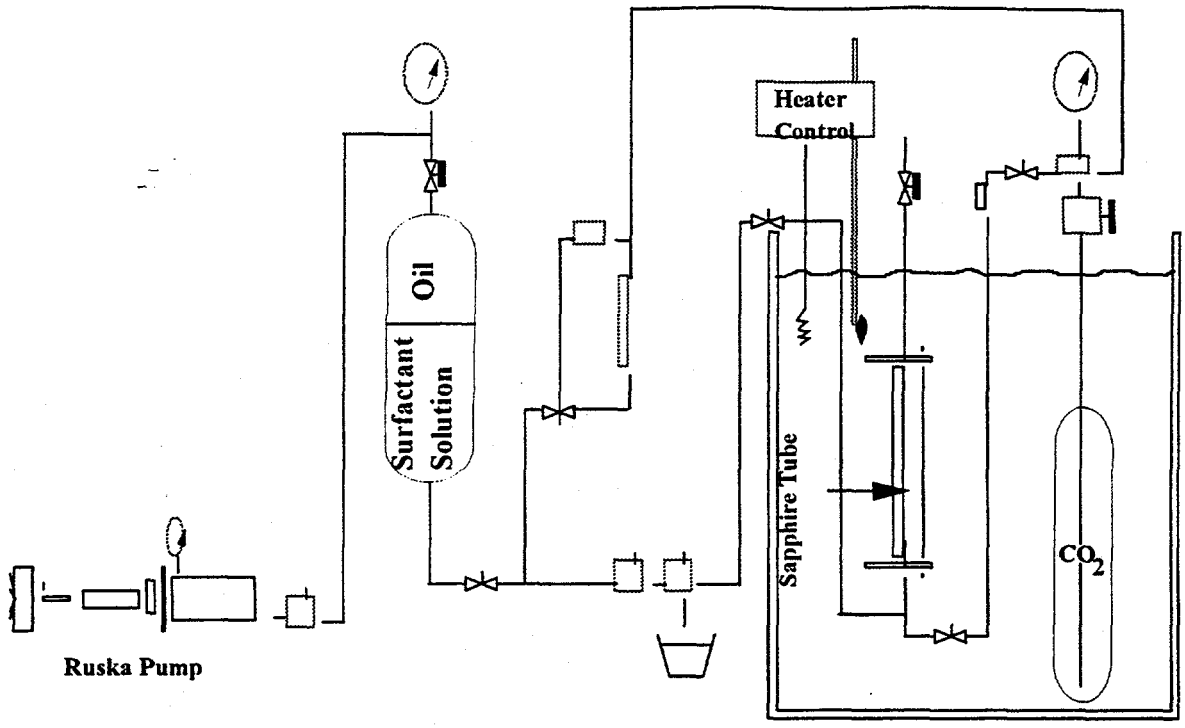

Fig. 24. Foam-durability apparatus.

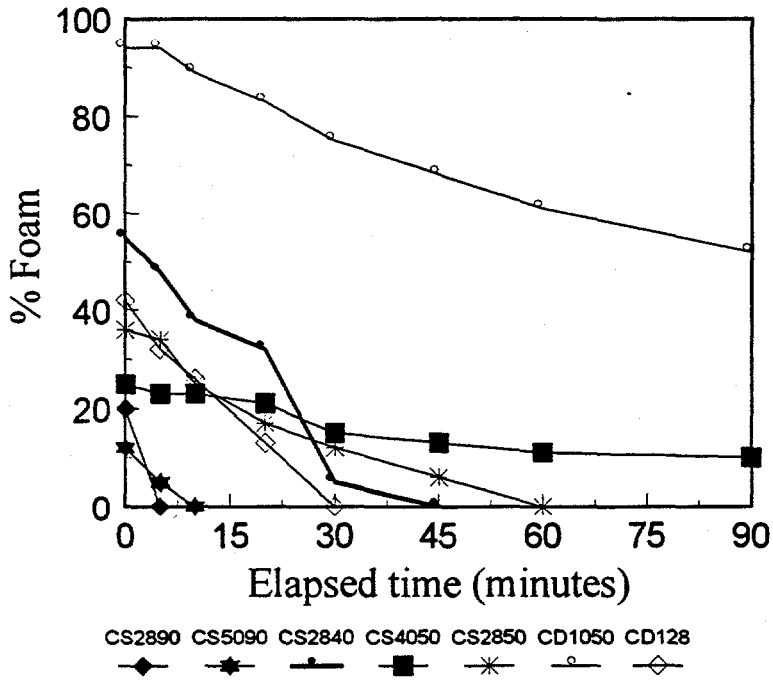

Fig. 25. Decay of CO_2-foam with tested surfactant systems.

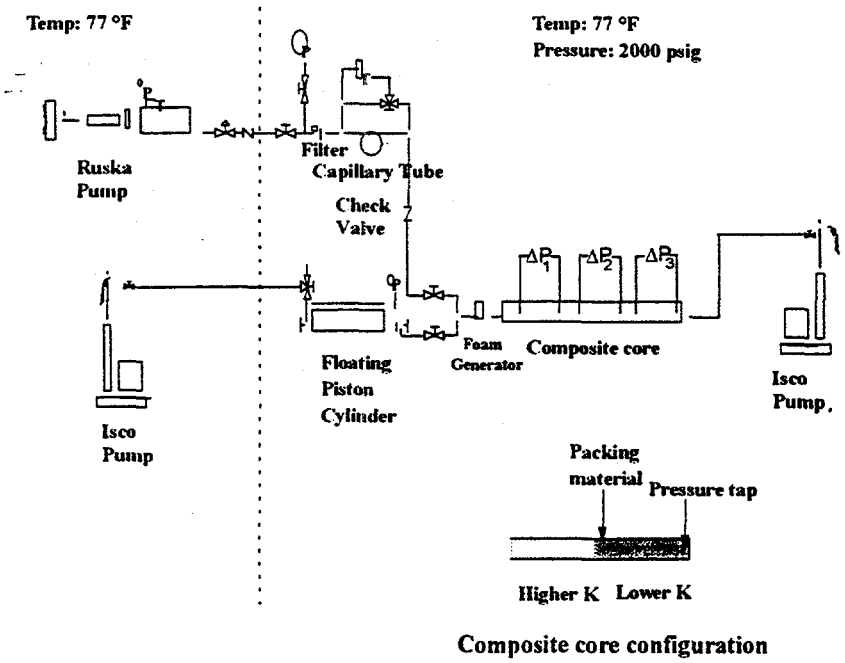

Fig. 26. Schematic of the mobility measurement experimental setup for a series composite core.

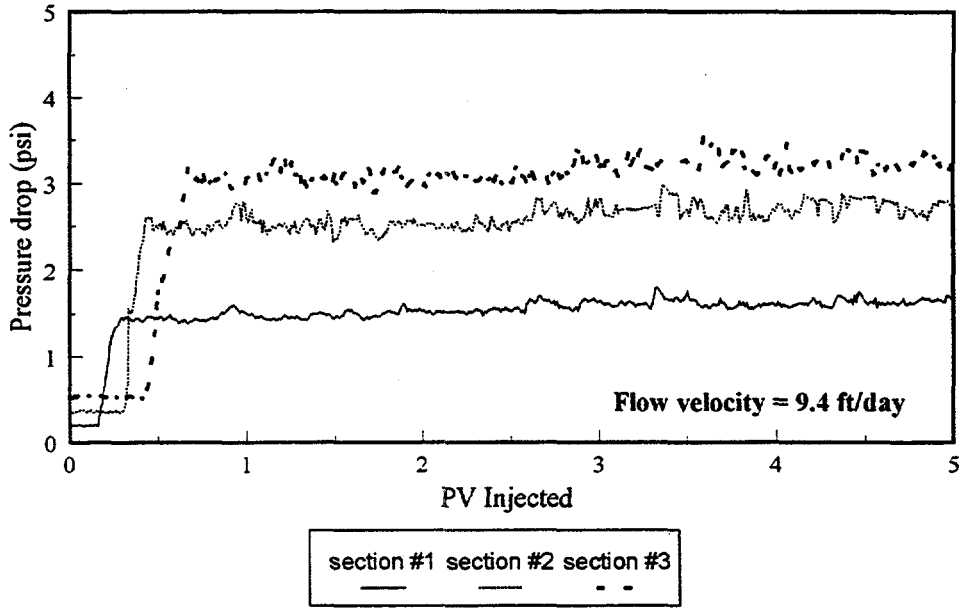

Fig. 27. Pressure profile of 0.25 wt% CD128.

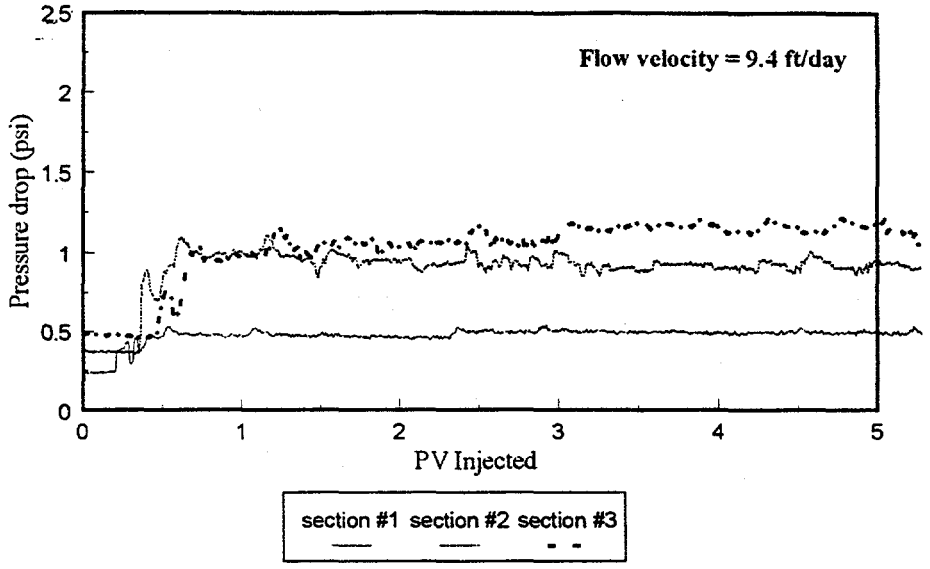

Fig. 28. Pressure profile of mixed surfactant CS2890.

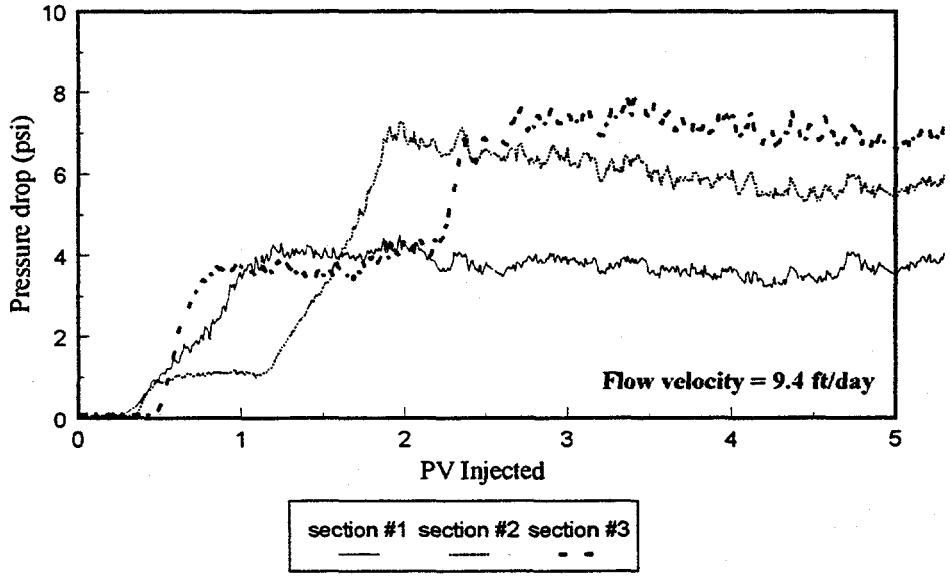

Fig. 29. Pressure profile of mixed surfactant CS2840.

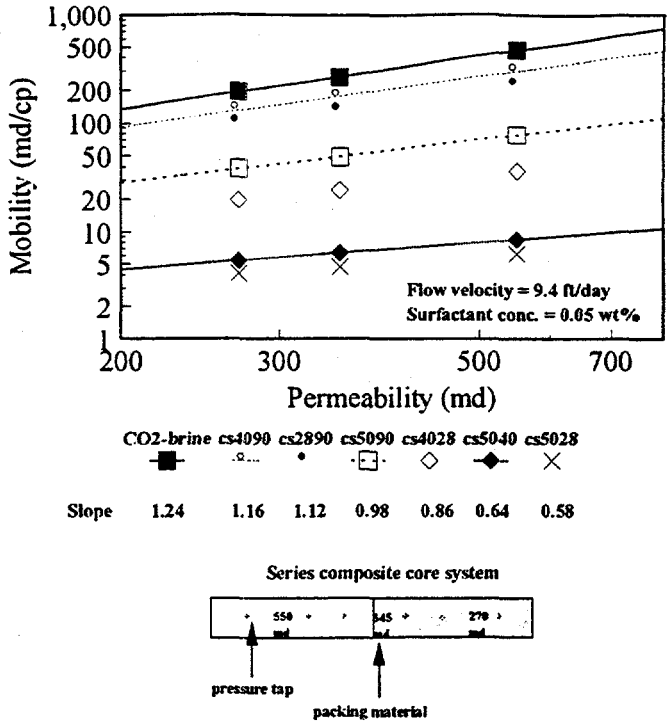

Fig. 30. Mobility dependence on permeability in a series composite core for single surfactant systems.

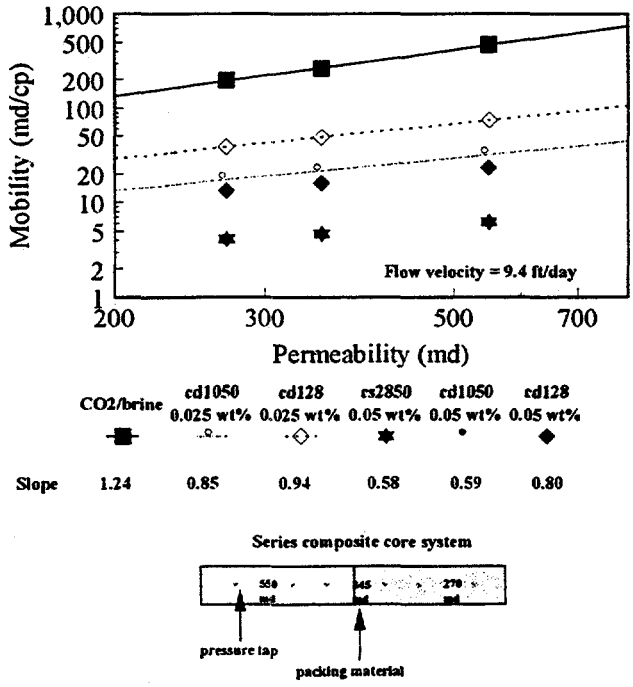

Fig. 31. Mobility dependence on permeability in a series composite core for mixed surfactant systems.

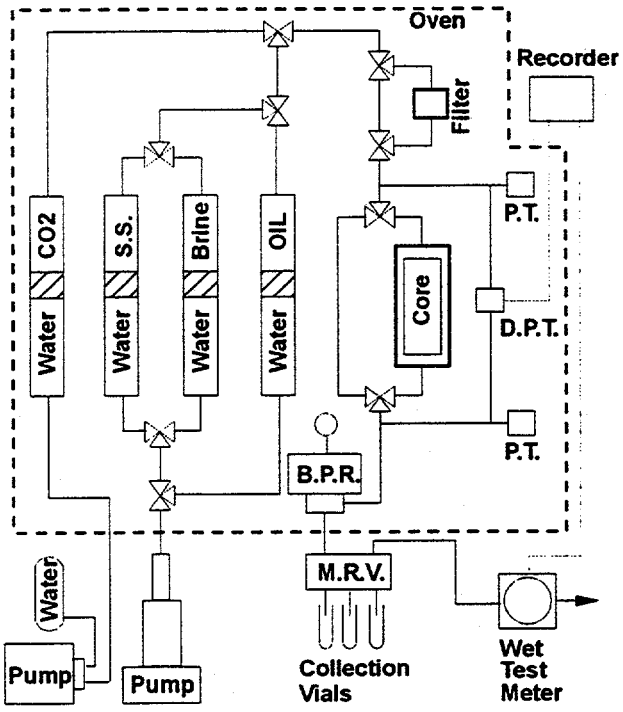

Fig. 32. Schematic of the foam test apparatus.

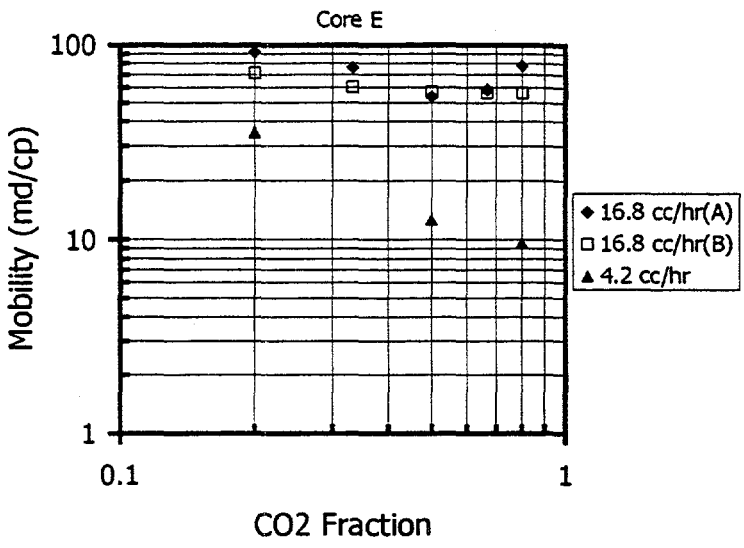

Fig. 33. Total mobility of CO_2-brine versus CO_2 fraction for flow rates of 4.2 and 16.8 cm^3/hr (Core E).

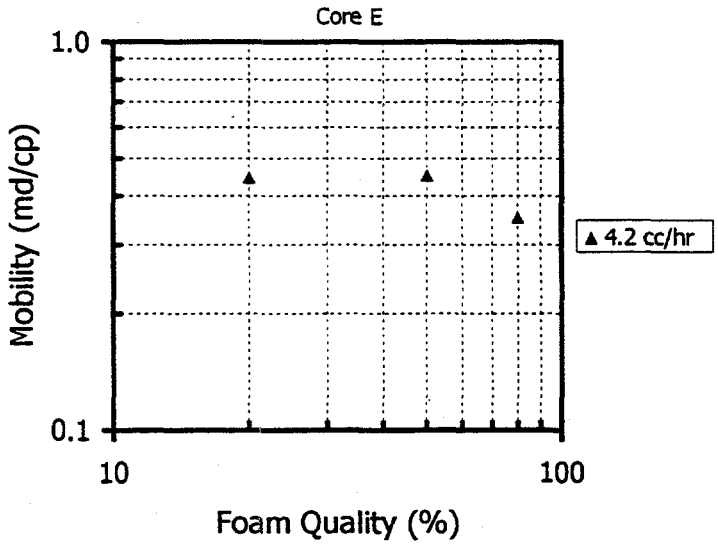

Fig. 34. Foam mobility versus foam quality for Core E at 4.2 cm^3/hr.

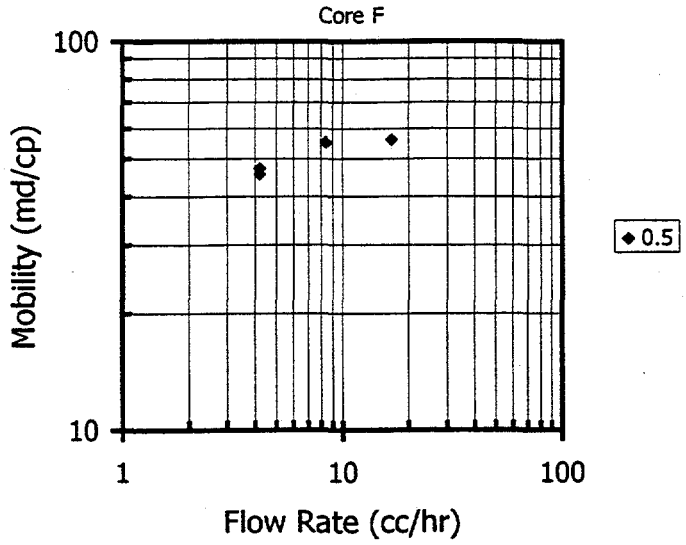

Fig. 35. Total mobility of CO_2-brine versus total flow rate for CO_2 fraction of 0.5 (Core F).

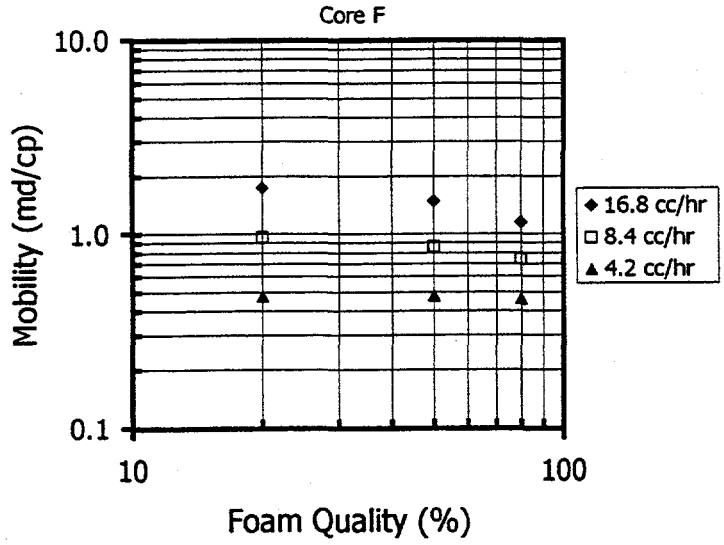

Fig. 36. Foam mobility versus foam quality for total flow rates of 4.2, 8.4, and 16.8 cm^3/hr (Core F).

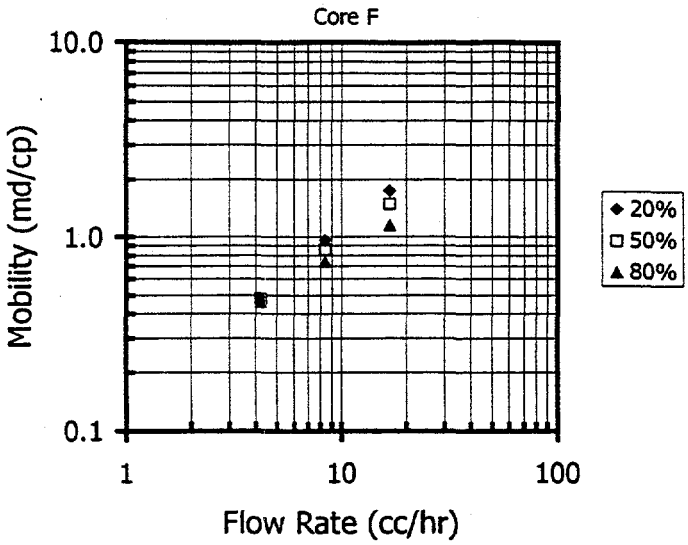

Fig. 37. Foam mobility versus total flow rates for foam qualities of 20, 50, and 80% (Core F).

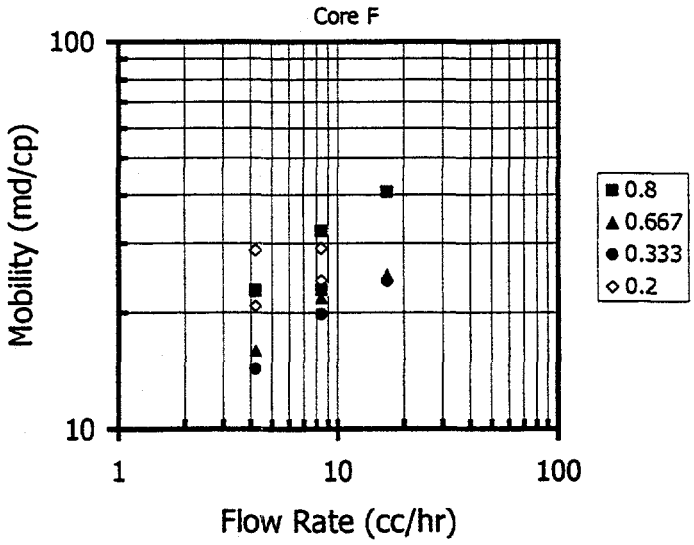

Fig. 38. Total mobility of CO_2-brine versus total flow rates for of CO_2 fractions of 0.8, 0.667, 0.333, and 0.2 (Core F).

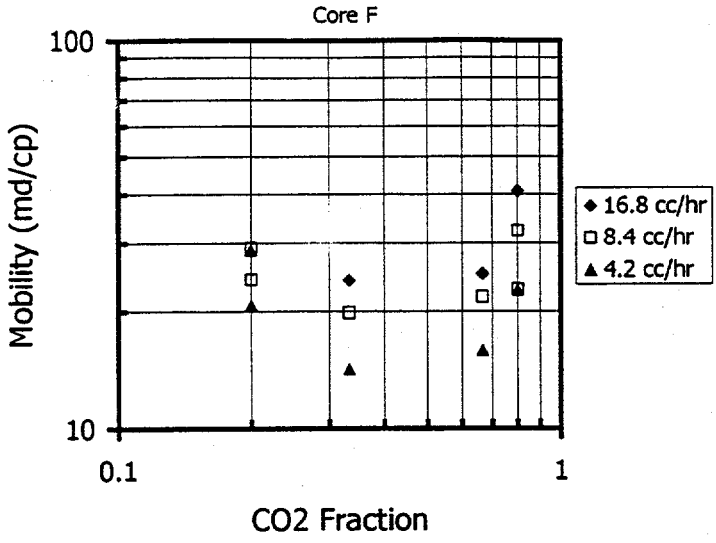

Fig. 39. Total mobility of CO_2-brine versus CO_2 fractions for total flow rates of 16.8, 8.4, and 4.2 cm^3/hr (Core F).

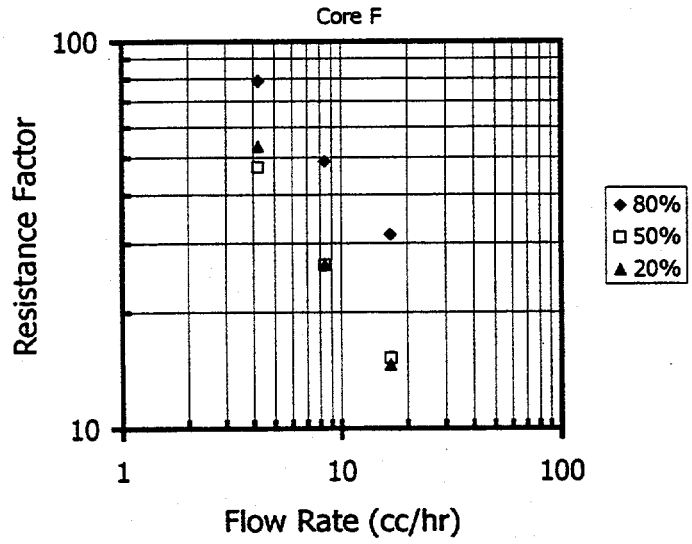

Fig. 40. Foam resistance factor versus total flow rates for foam qualities of 20, 50, and 80% (Core F).

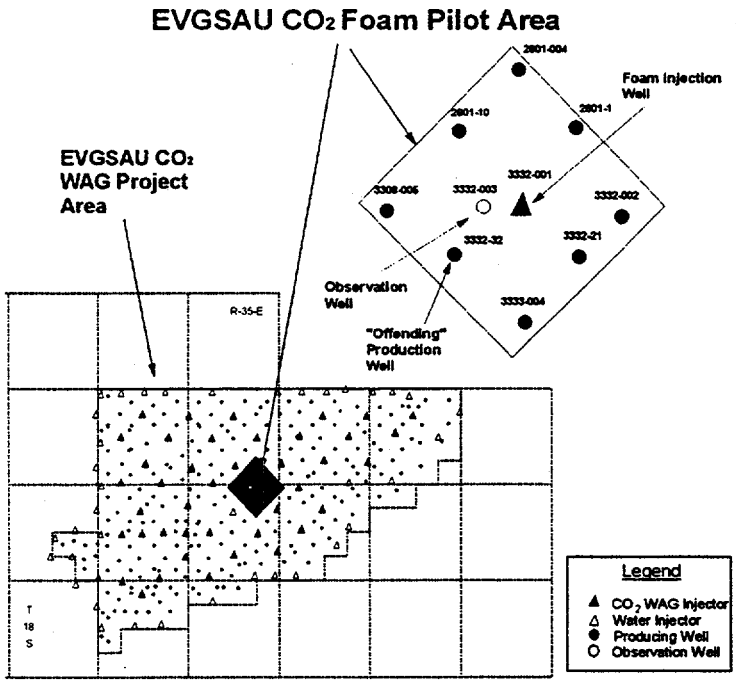

Fig. 41. Location of the EVGSAU CO_2 foam pilot area.

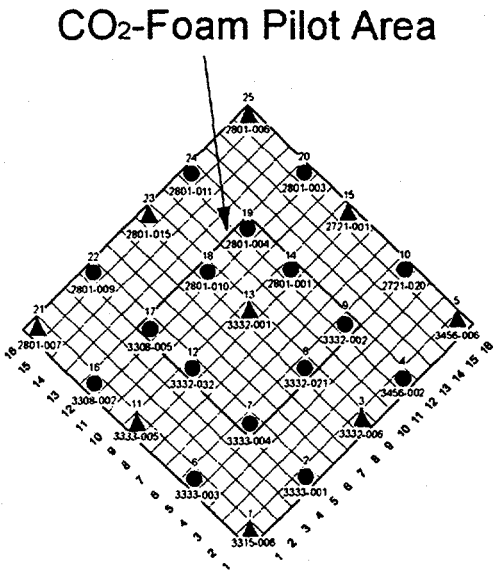

Fig. 42. The layout of the wells in the history model with solid circles as producers and solid triangles as injectors. The CO_2-foam pilot area is an inverted nine-spot pattern with eight producers and one injection well in the center.

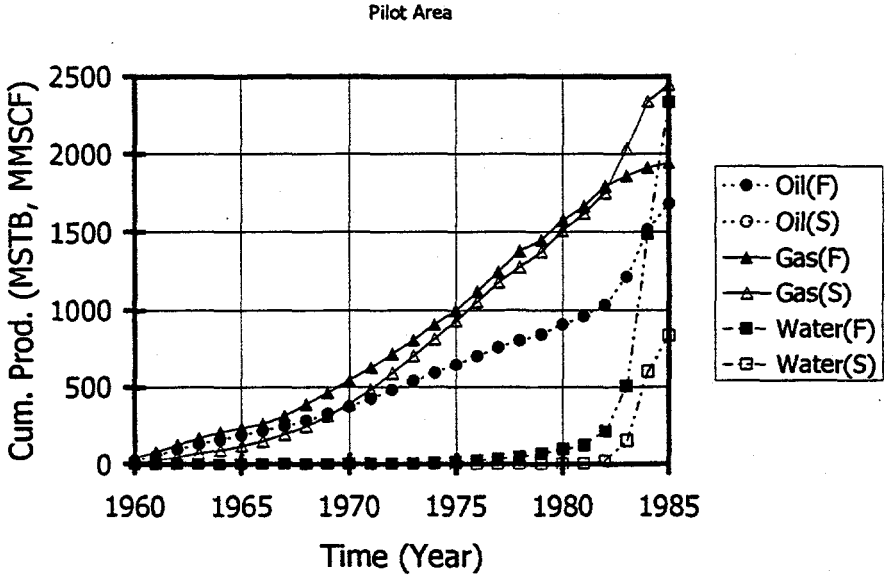

Fig. 43. Simulated and field data of the total cumulative production from the eight producers in the foam pilot area for the primary and waterflood periods (1959-1985).

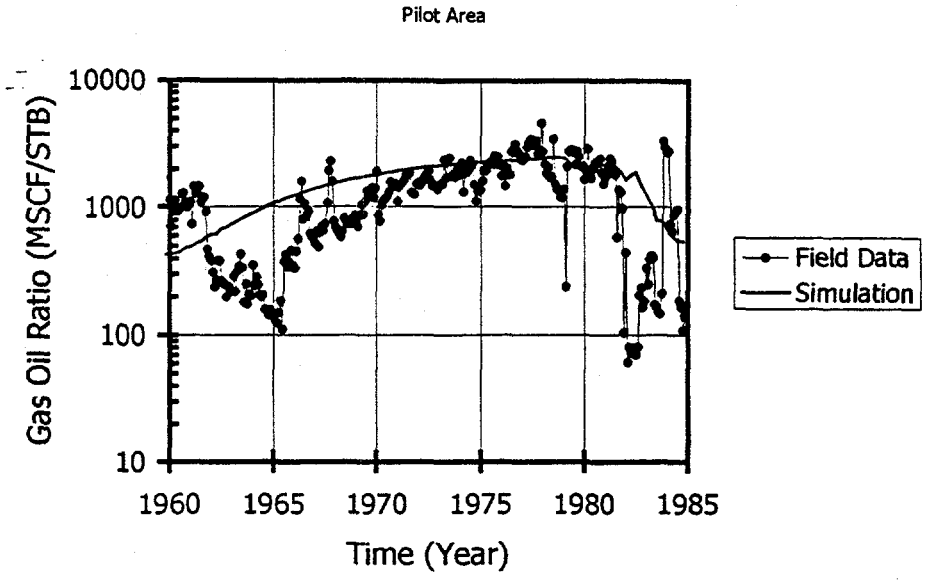

Fig. 44. Simulated and field data of the total instantaneous gas-oil ratio from the eight producers in the foam pilot area for the primary and waterflood periods (1959-1985).

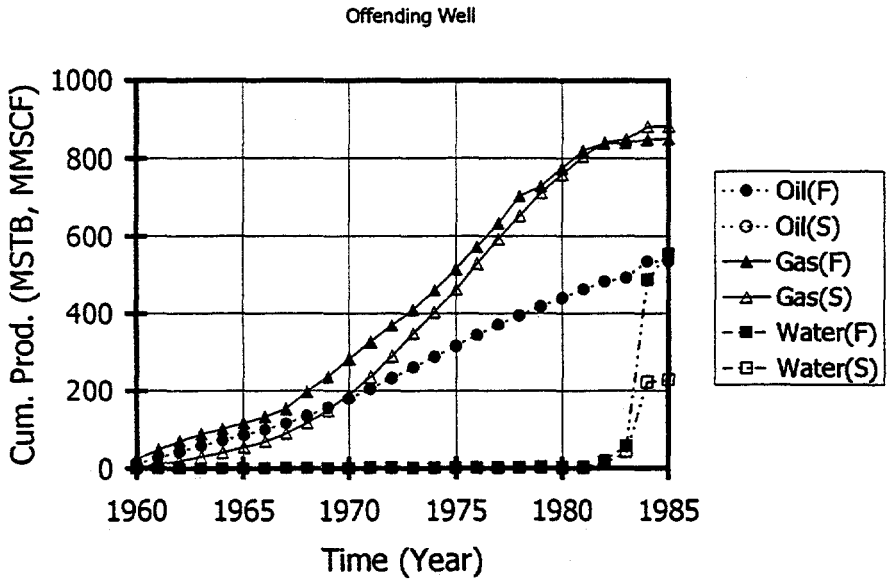

Fig. 45. Simulated and field data of the cumulative production from the offending well for the primary and waterflood periods (1959-1985).

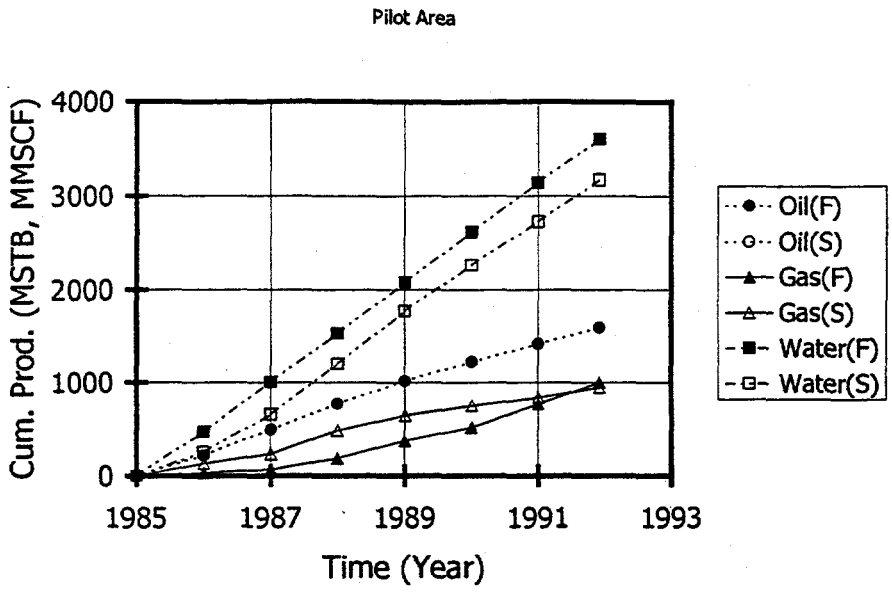

Fig. 46. Simulated and field data of the total cumulative production from the eight producers in the foam pilot area for the CO_2-flood period (1985-1992).

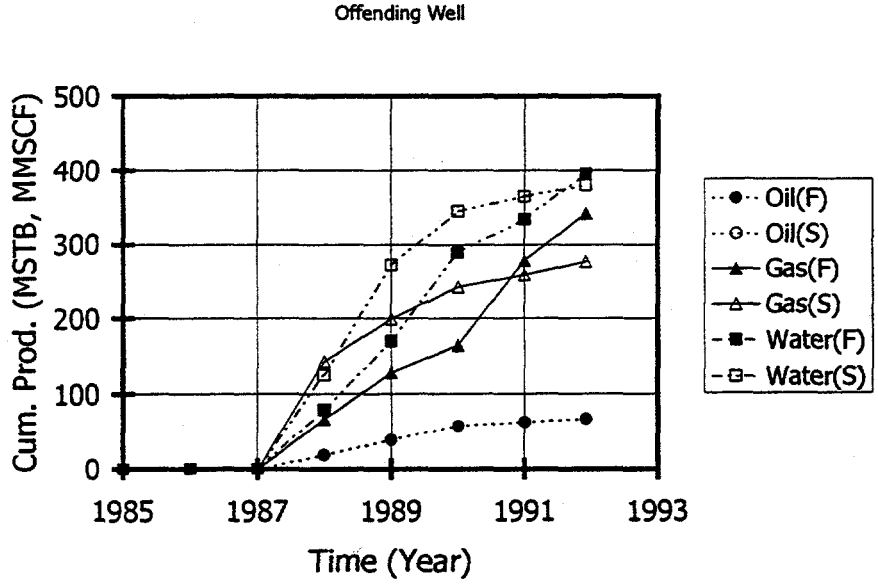

Fig. 47. Simulated and field data of the cumulative production from the offending well for the CO_2-flood period (1985-1992).

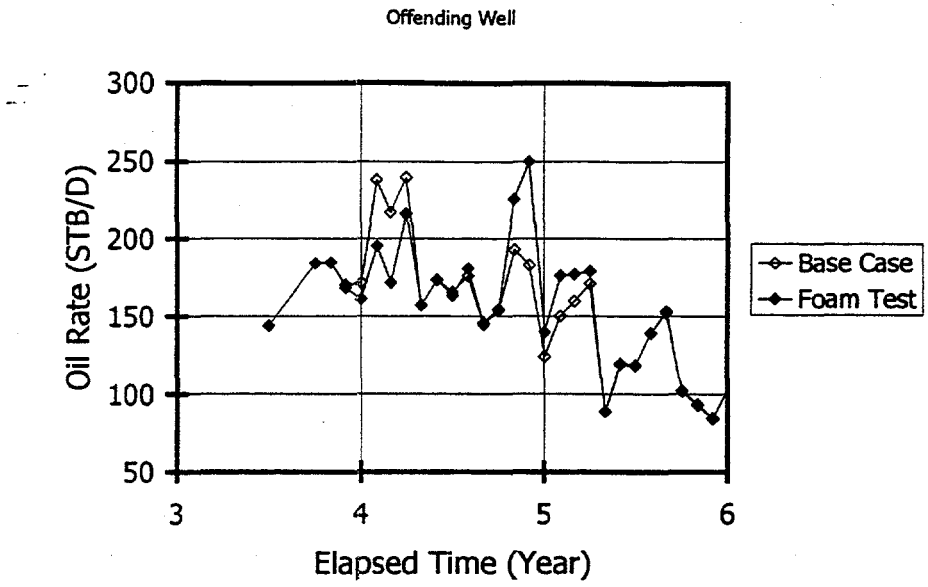

Fig. 48. Comparison of the oil rate history of the offending well between the foam test and the base case.

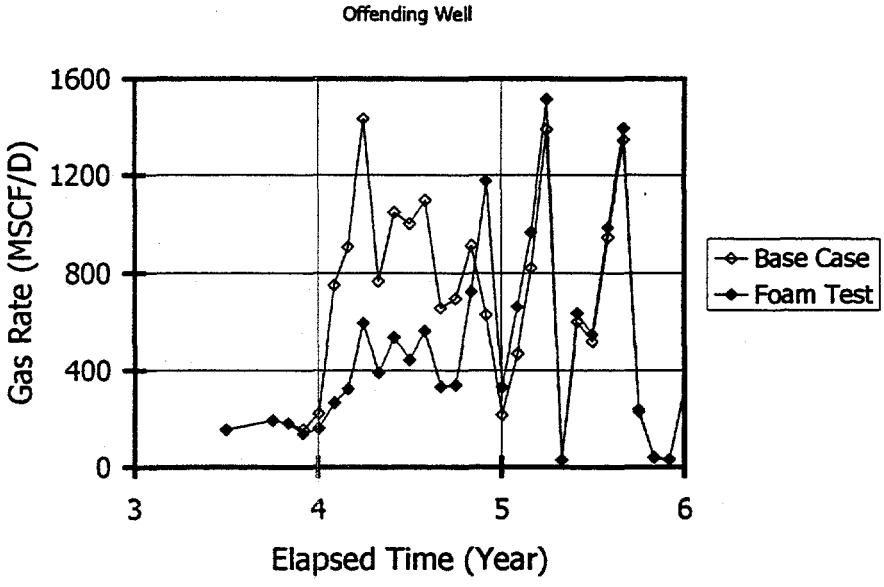

Fig. 49. Comparison of the gas rate history of the offending well between the foam test and the base case.

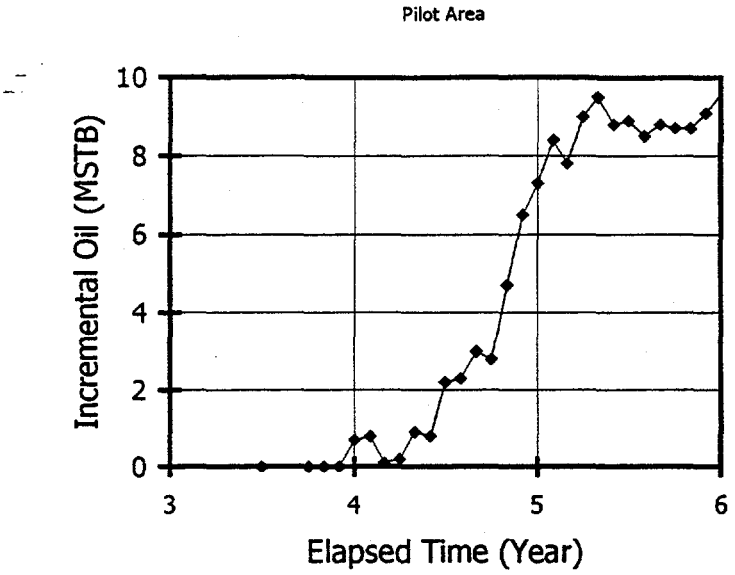

Fig. 50. Total incremental oil recovery of the eight producers in the foam pilot area from the foam test.

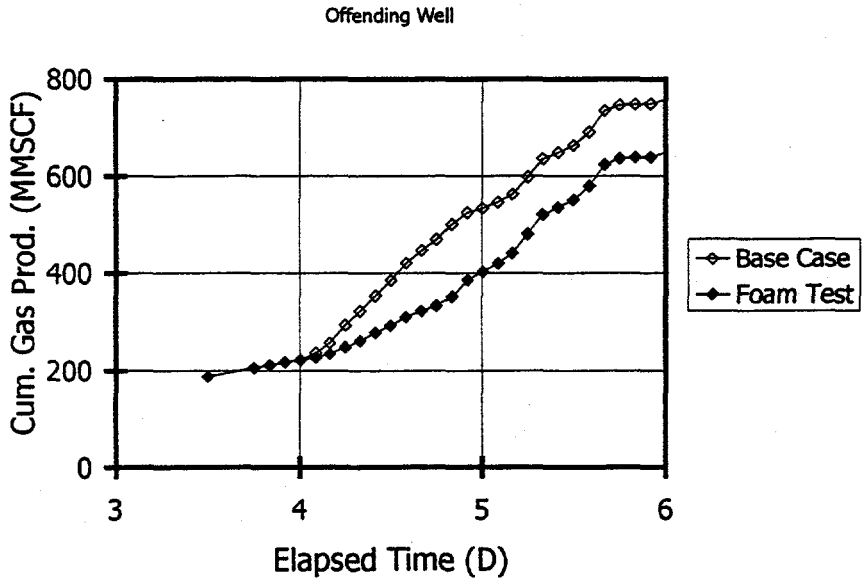

Fig. 51. Comparison of the instantaneous gas oil ratio of the offending well between the foam test and the base case.

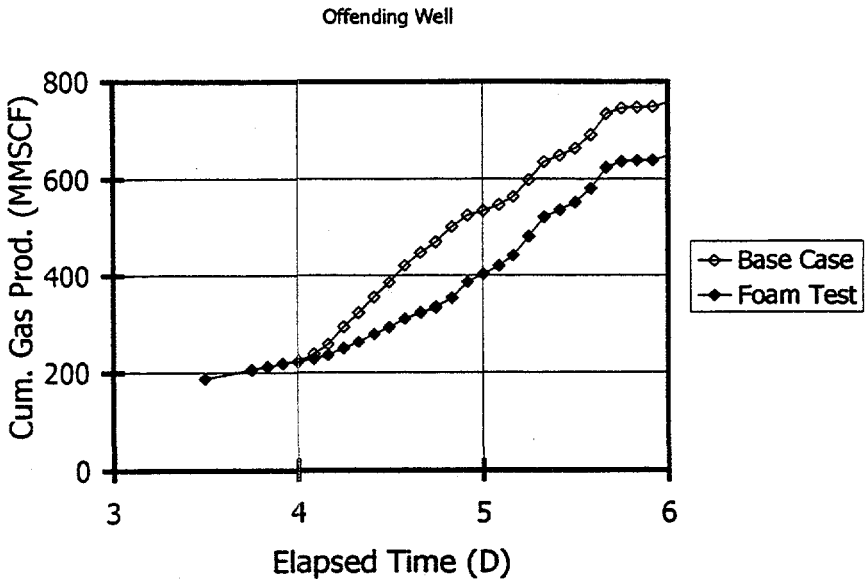

Fig. 52. Comparison of the cumulative gas production history of the offending well between the foam test and the base case.

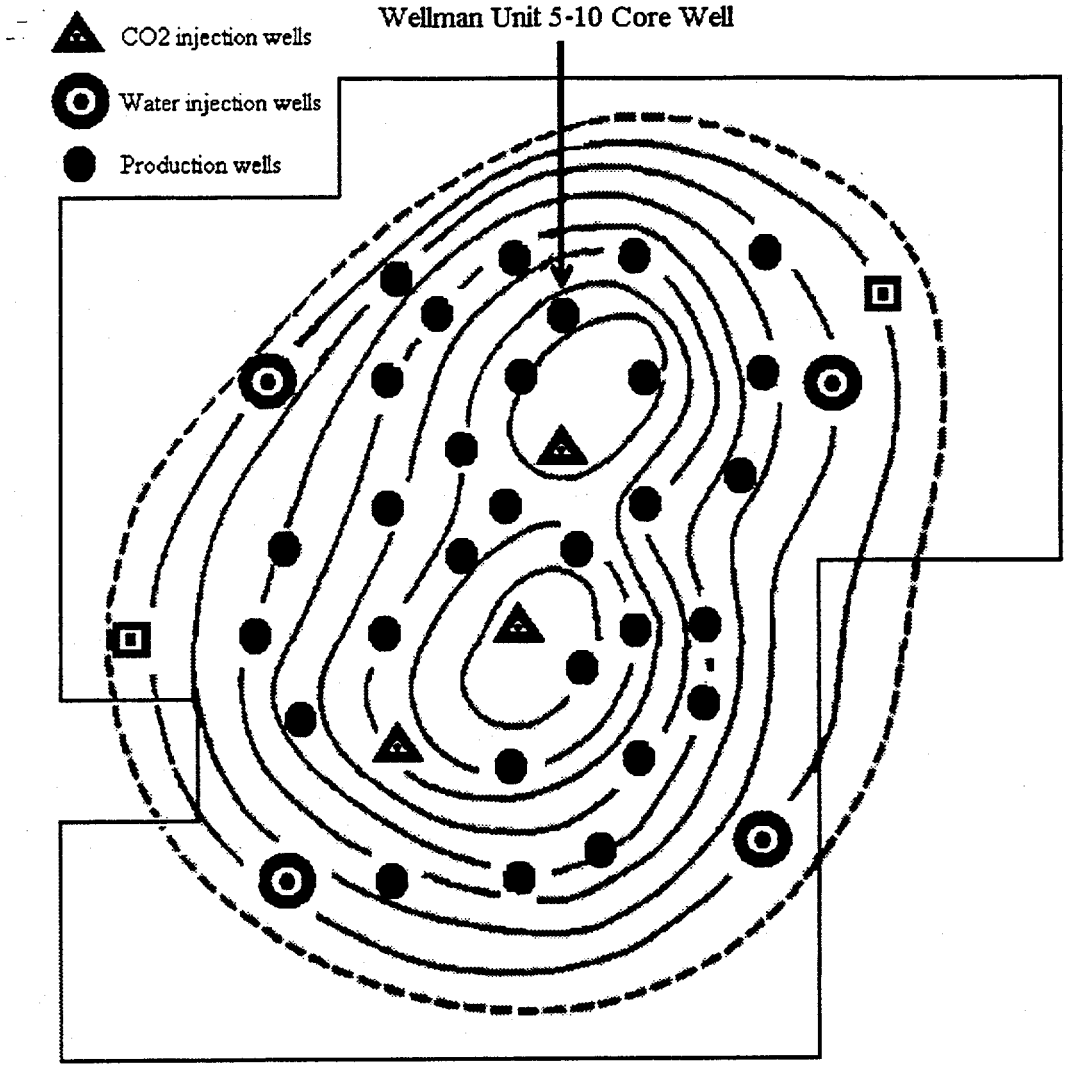

Fig. 53. Wellman Unit Wolfcamp reef structure map.

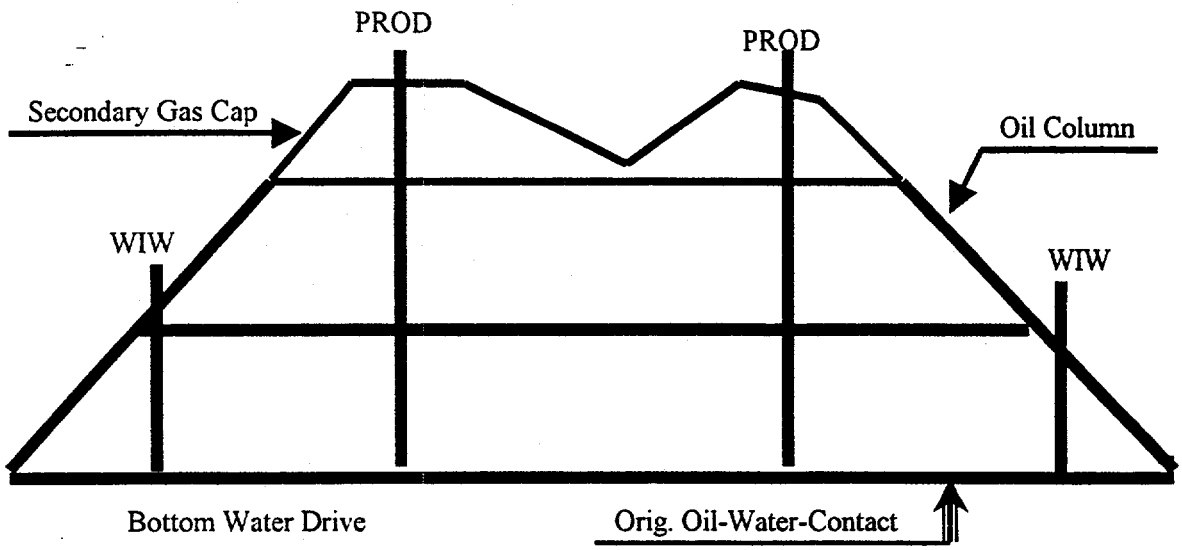

(a) Start of CO_2 flood (1983).

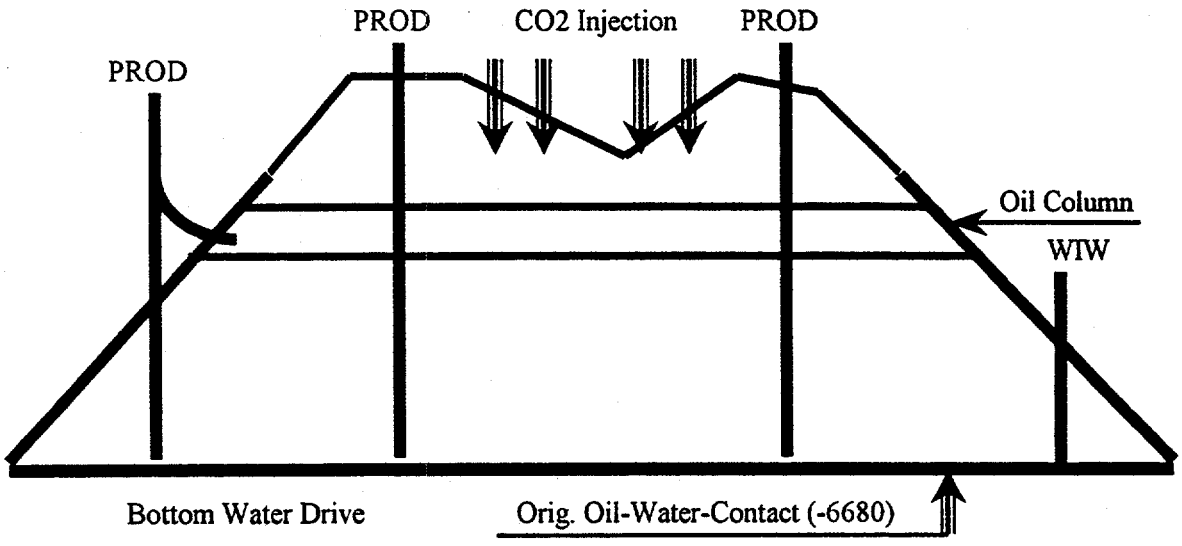

(b) Current condition

Fig. 54. CO_2 flood in Wellman field.

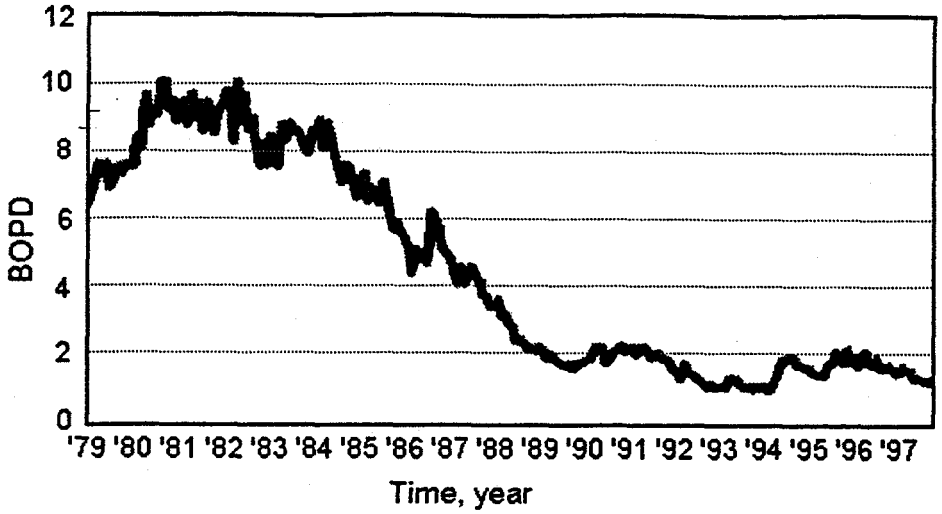

Fig. 55. Historical oil production for the Wellman Unit.

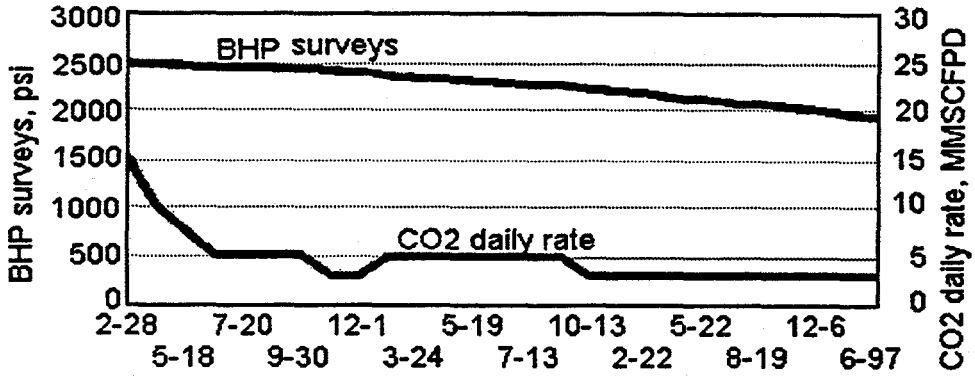

Fig. 56. Wellman Unit BHP surveys from Feb. 1996 to Dec. 1997.

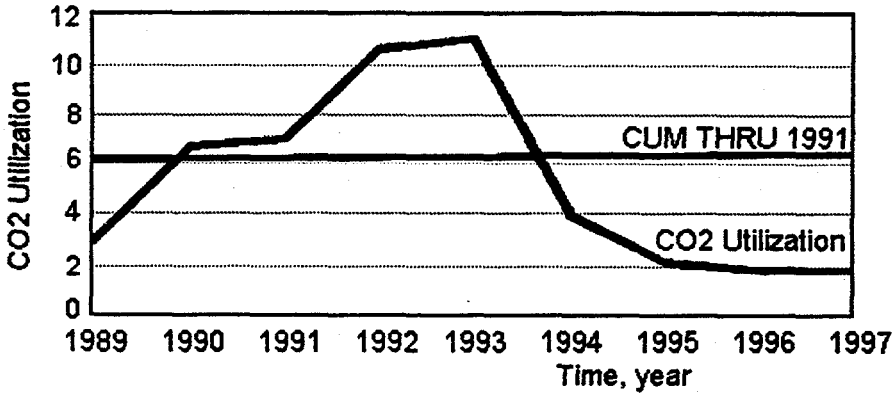

Fig. 57. Wellman Unit annual CO_2 utilization.

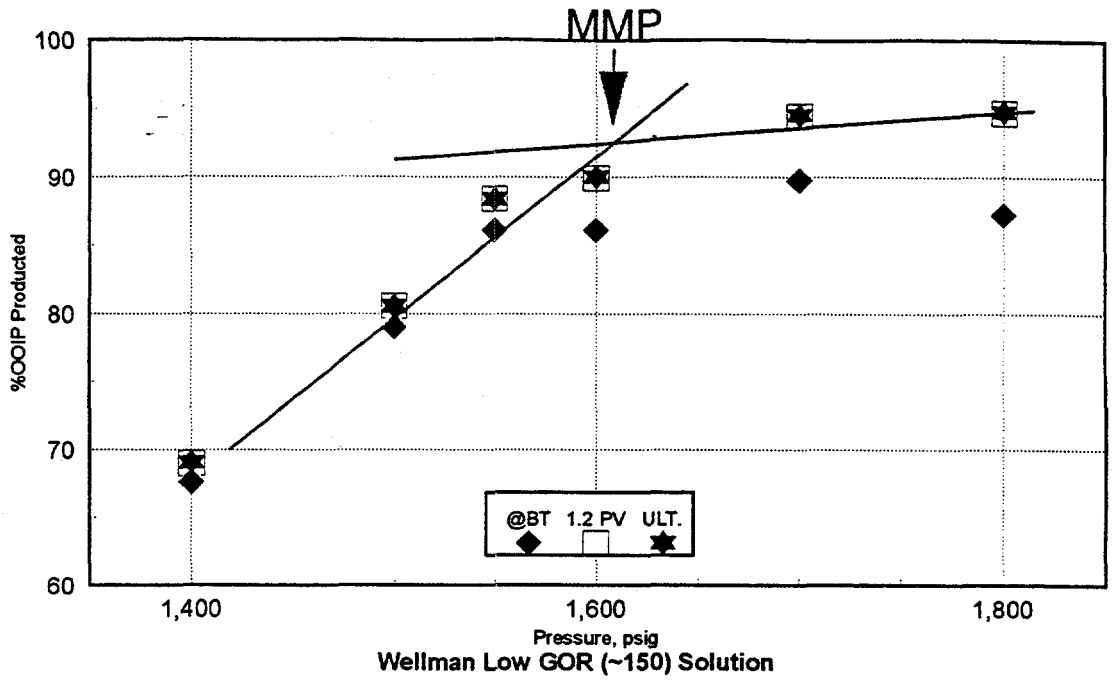

Fig. 58. Recovery vs. pressure slim tube tests for 150 GOR reservoir fluid.

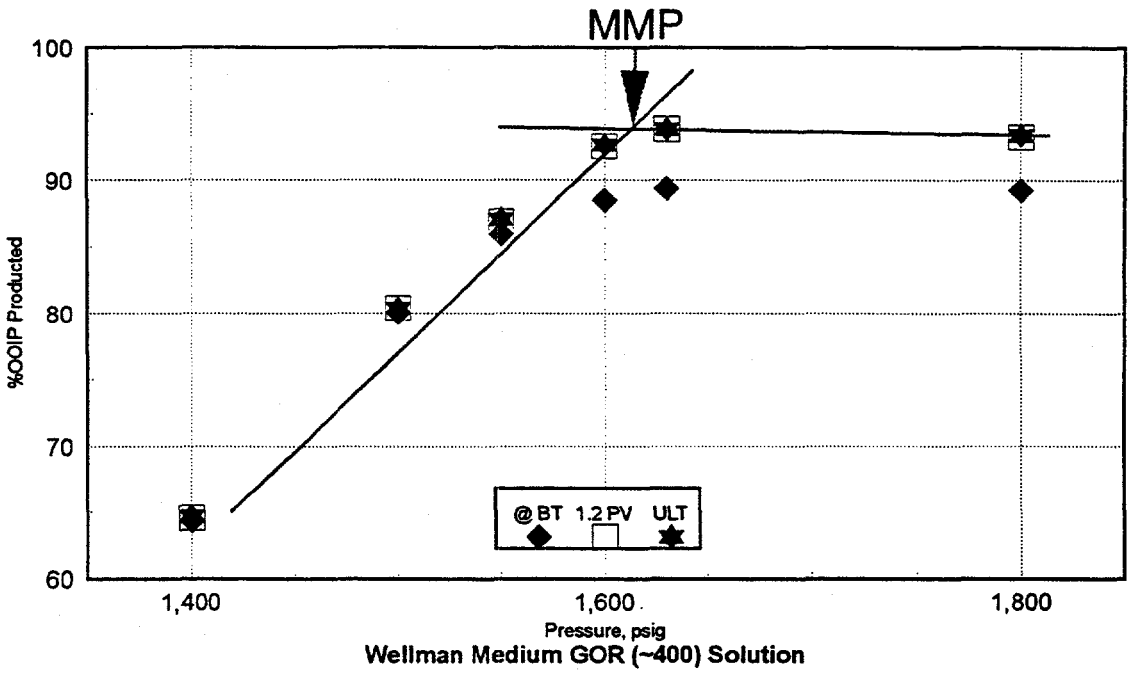

Fig. 59. Recovery vs. pressure slim tube tests for 400 GOR reservoir fluid.

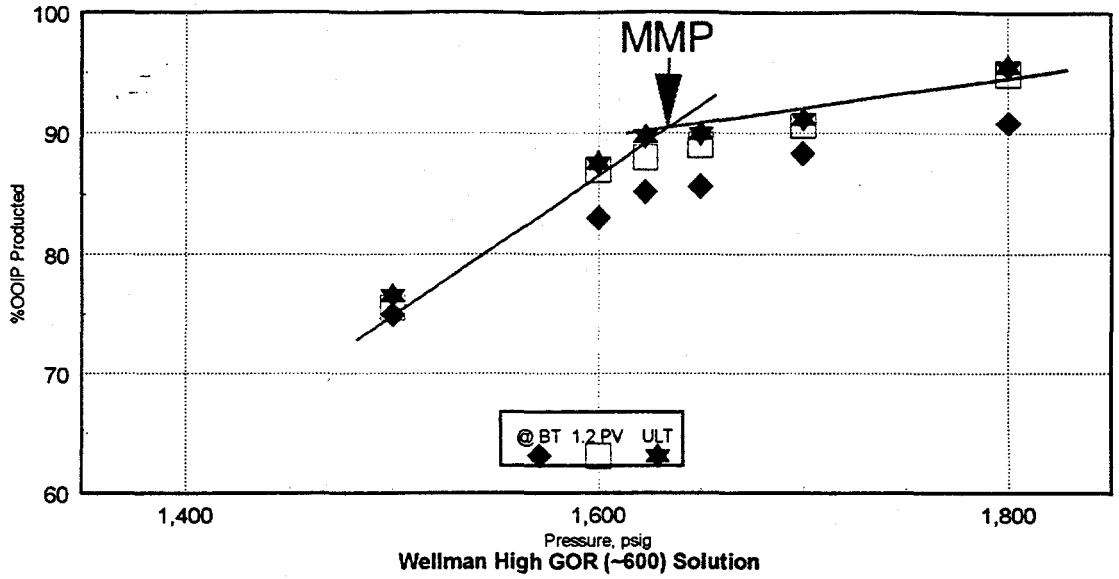

Fig. 60. Recovery vs. pressure slim tube tests for 600 GOR reservoir fluid.

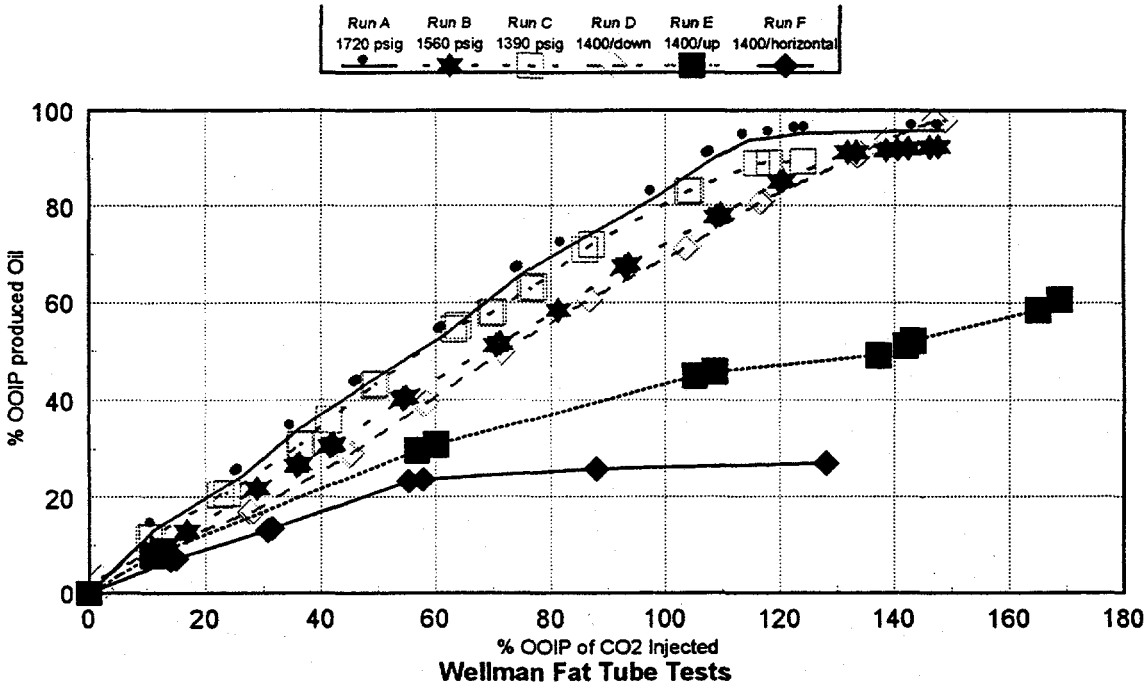

Fig. 61. Recovery curve for six large-diameter tube tests.

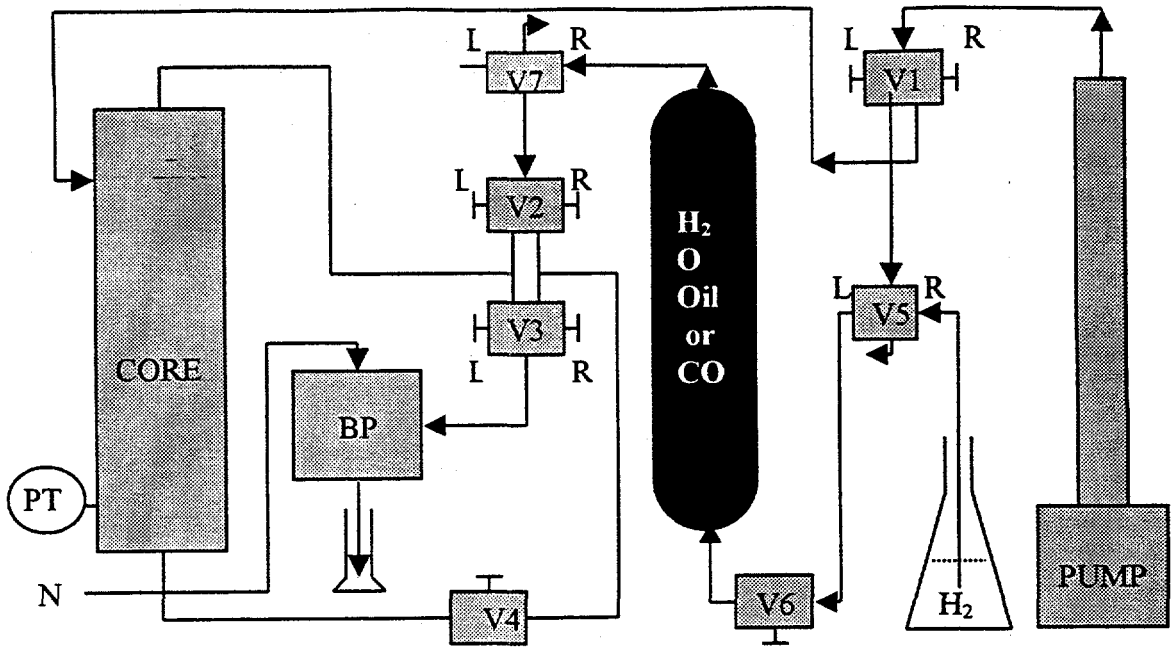

(a) A schematic diagram of the experimental setup.

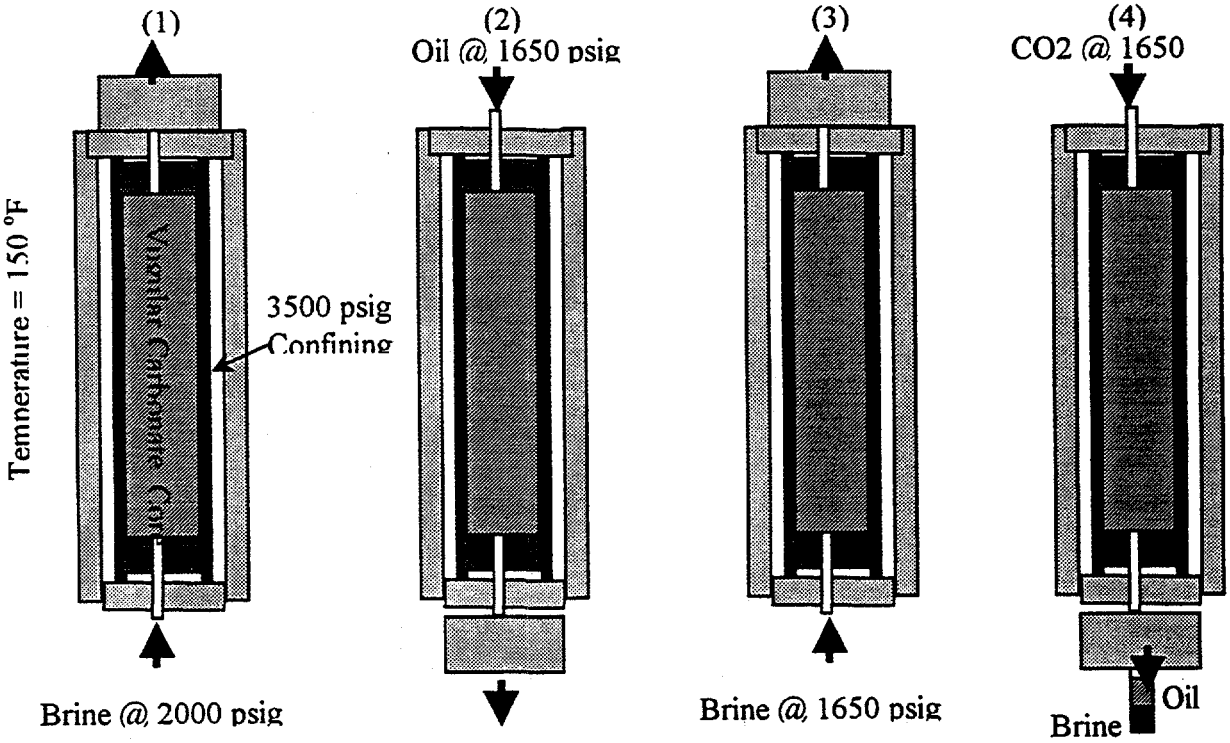

(b) A schematic diagram of the core holder and procedure.

Fig. 62. A schematic diagram of experimental setup for CO_2-assisted gravity drainage.

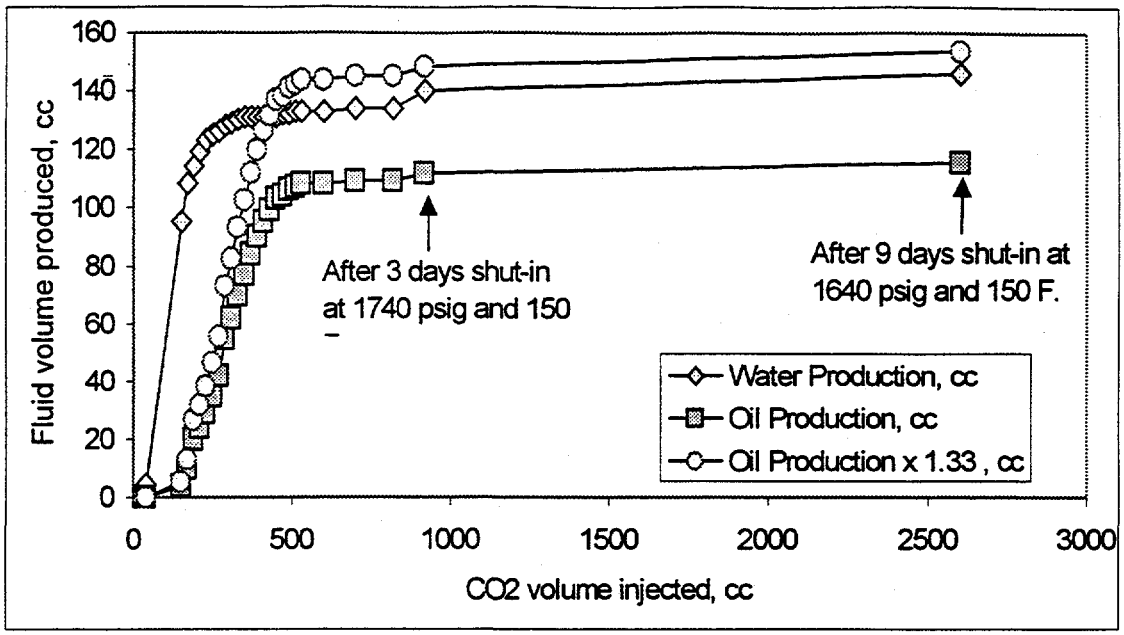

Fig. 63. Fluid production vs. CO_2 throughput during CO_2-assisted gravity drainage at a pressure of 1650 psig.

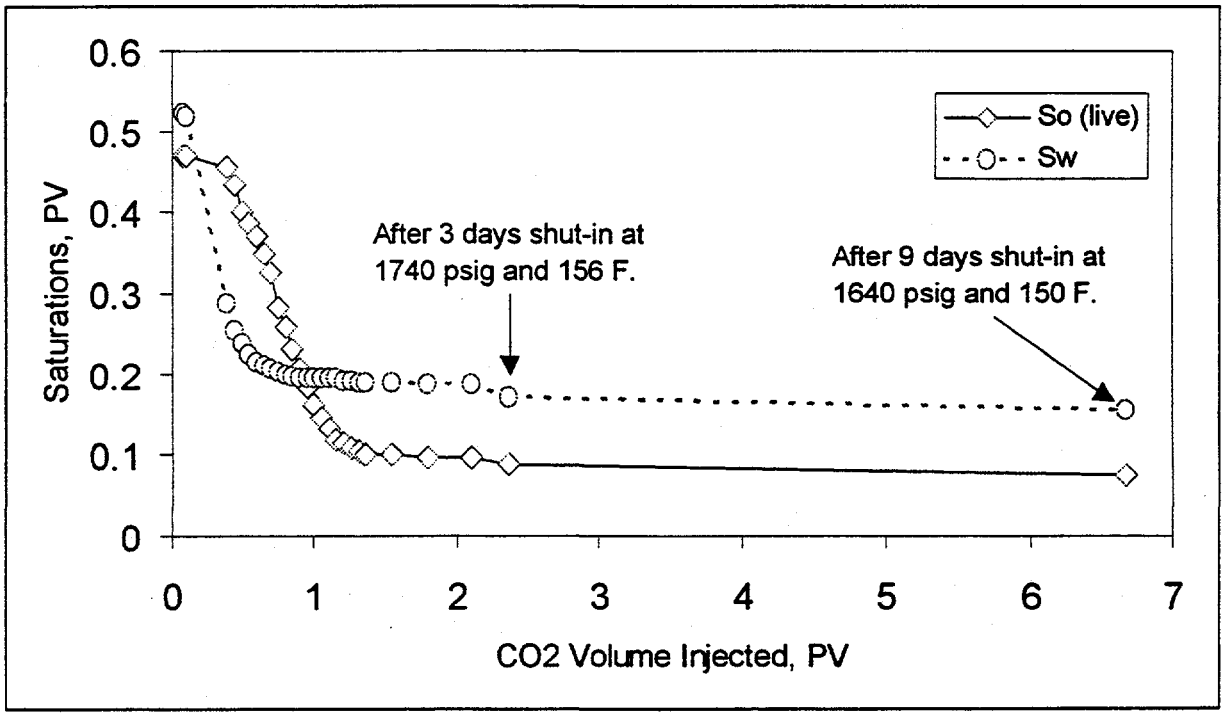

Fig. 64. Changes in fluid saturations in the Wellman Unit whole core during CO_2-assisted gravity drainage at a pressure of 1650 psig.

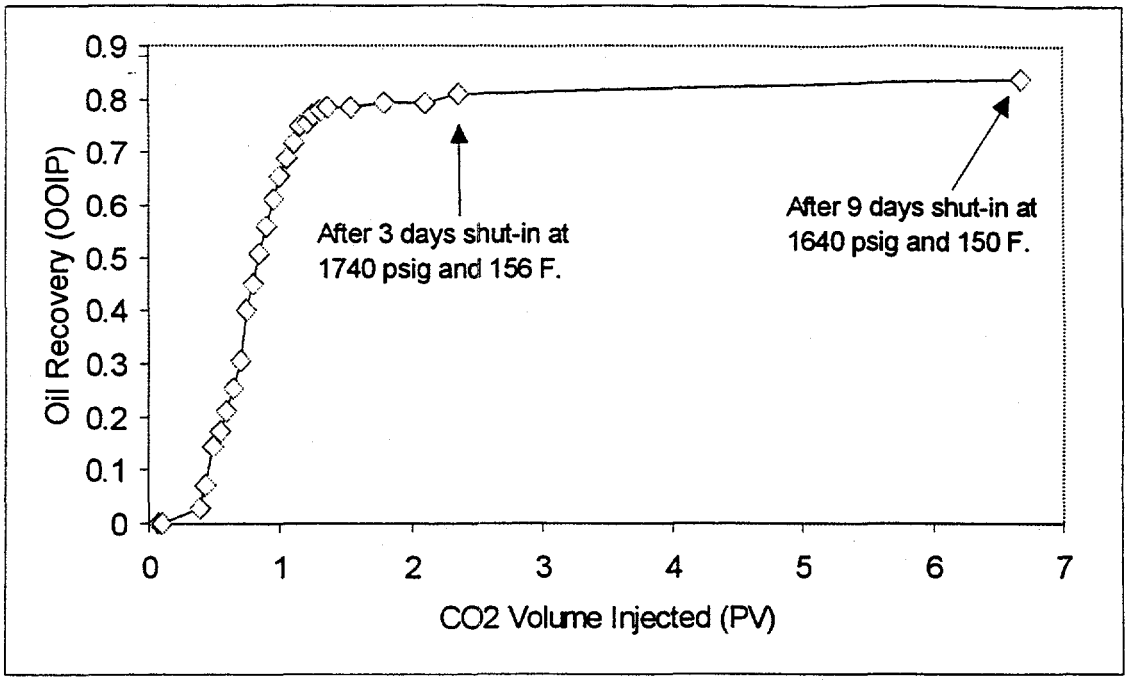

Fig. 65. Oil recovery from the Wellman Unit whole core during CO_2-assisted gravity drainage at a pressure of 1650 psig

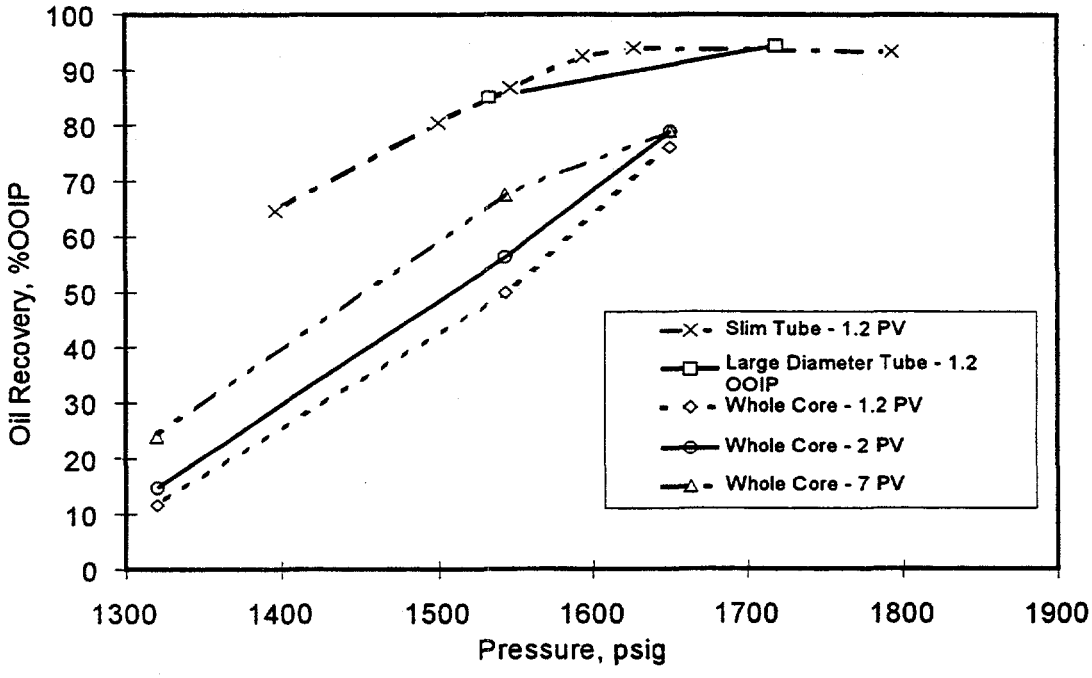

Fig. 66. Comparison of oil recoveries from CO_2-assisted gravity drainage large-diameter tube and slim tube experiments.

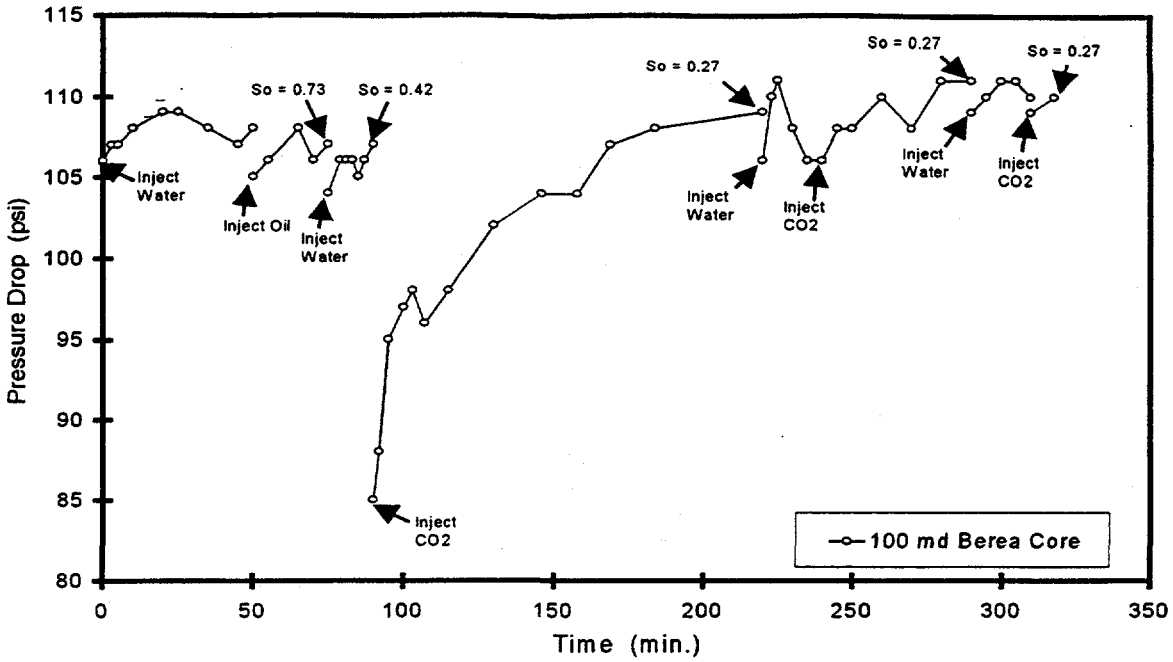

Fig. 67. Recorded pressure drop during WAG injection for a 100 md Berea Core.

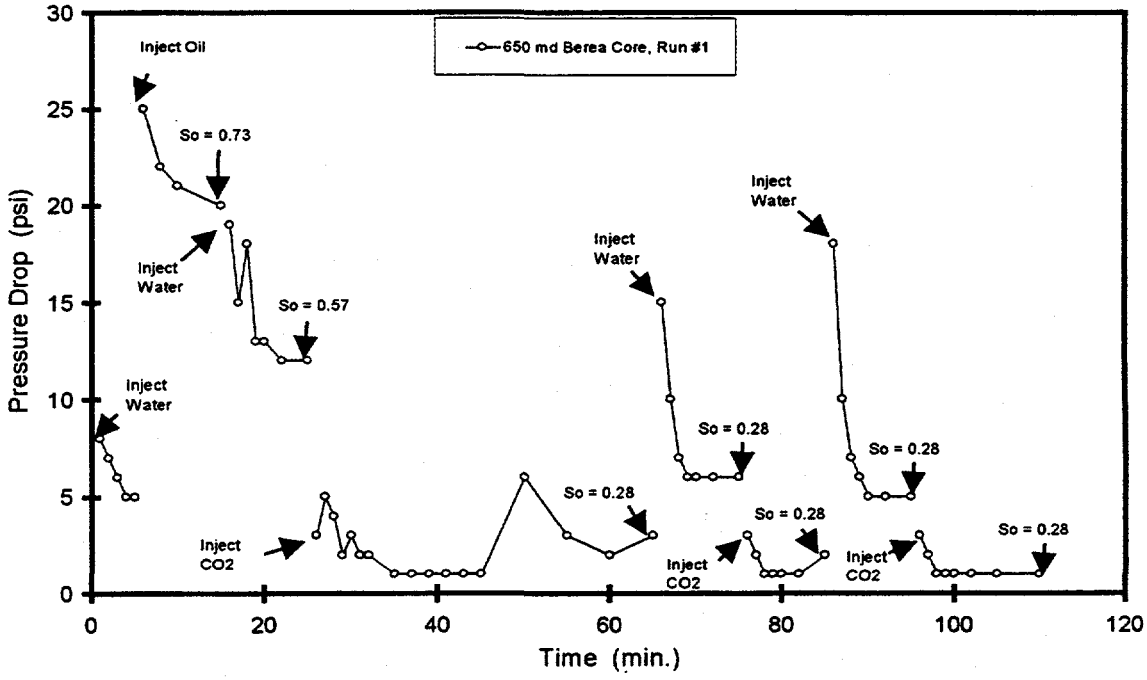

Fig. 68. Recorded pressure drop during WAG injection for a 650 md Berea Core, Run #1.

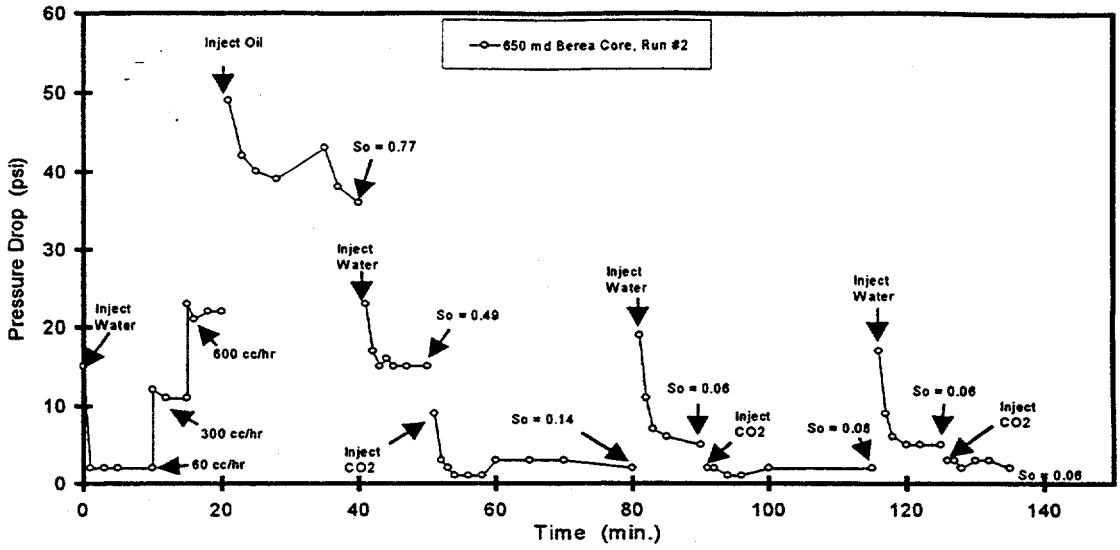

Fig. 69. Recorded pressure drop during WAG injection for a 650 md Berea Core, Run #2.

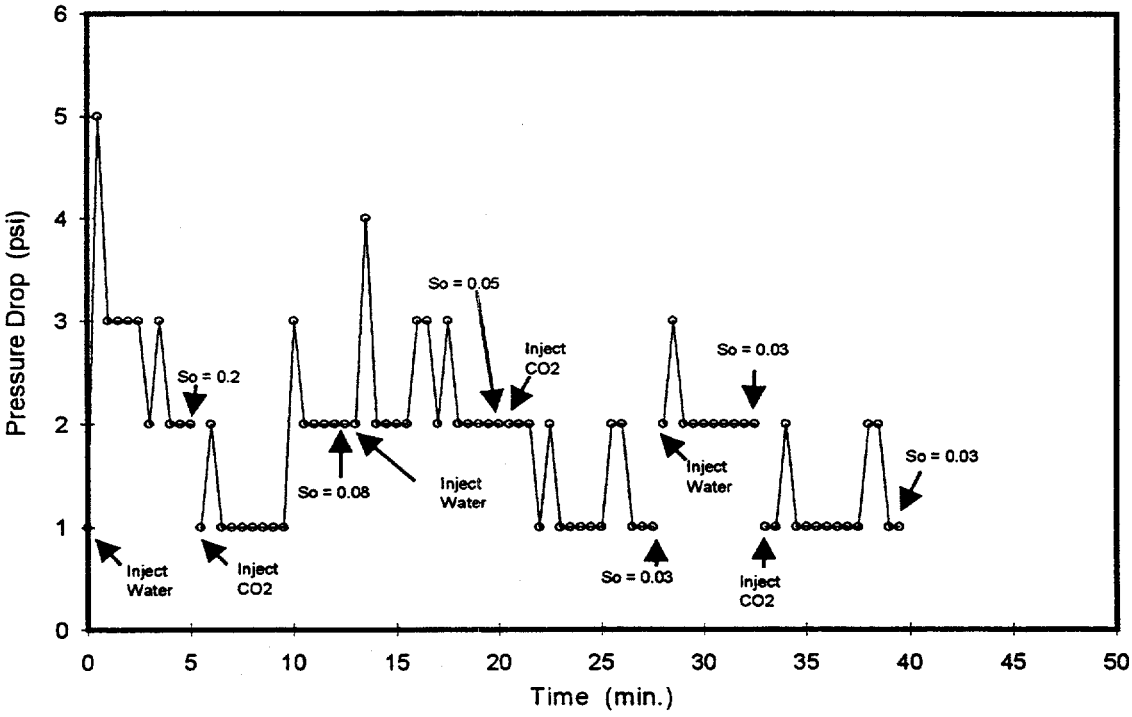

Fig. 70. Recorded pressure drop during WAG injection for a 315 md carbonate reservoir core plug.

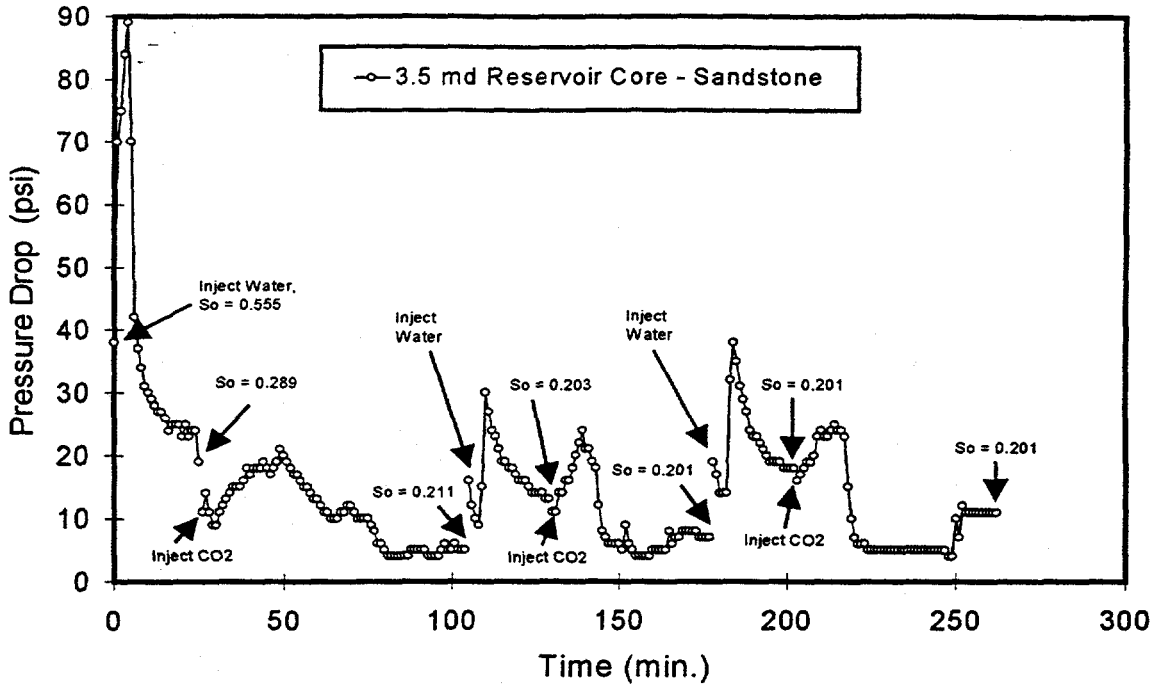

Fig. 71. Recorded pressure drop during WAG injection for a 3.5 md sandstone reservoir core plug.